THE MECHANISM OF HYDROPHILIC AND HYDROPHOBIC COLLOIDAL SILICON DIOXIDE TYPES AS GLIDANTS

MECHANISMUS DER WIRKUNG HYDROPHILER UND HYDROPHOBER HOCHDISPERSER KIESELSÄURE ALS FLIEßREGULIERUNGSMITTEL

DISSERTATION

der Fakultät für Chemie und Pharmazie
der Eberhard-Karls-Universität Tübingen
zur Erlangung des Grades eines Doktors
der Naturwissenschaften

2005

vorgelegt von

STÉPHANE JONAT

Tag der mündliche Prüfung   22. April 2005

Dekan   Prof. Dr. S. Laufer

1. Berichterstatter   Prof. Dr. P. C. Schmidt

2. Berichterstatter   Prof. Dr. T. Vandamme

Kommissionsmittglieder   Prof. Dr. J.-Y. Pabst

Meinen Mitbewohnern, die mir ans Herz gewachsen sind, danke ich für ihre Freundschaft, für das dreijährige, sehr angenehme und lustige Zusammenleben, für die zahlreichen deutschen Korrekturen und für das Zuhören bei Probevorträgen. Zusammen mit den „13 Typen" haben sie dazu beigetragen, dass ich mich während meiner Zeit im kleinen Tübingen in der Mitte des Schwabenlandes sehr wohl gefühlt habe.

Un grand merci à mes amis français, qui malgré la distance et les frontières, ont toujours été présent dans mes moments de joie tout comme dans mes moments de doute. Votre amitié m´est précieuse.

Enfin, ma dernière pensée revient à mes parents sans qui ce travail n'aurait jamais abouti. Merci pour votre présence, votre serviabilité, votre confiance et votre soutien à toute épreuve.

"Il est extrêment rare que la montagne soit abrupte de tous les côtés !"

André Gide

"Il est extrêment rare que la montagne soit abrupte de tous les côtés !"

André Gide

RESÜMEE

Hochdisperse Kieselsäure vom Typ AEROSIL® 200 (Degussa AG, Düsseldorf) wird seit langem zur Verbesserung der Fließfähigkeit von Tablettiermischungen in der Pharmazie eingesetzt. Ein Nachteil dieses Typs ist sein geringes Schütt- und Stampfgewicht sowie die Staubbildung während der Anwendung. Seit kurzem werden mit AEROSIL® 200 VV und AEROSIL® R 972 V zwei verdichtete Typen angeboten, die deutlich höhere Schütt- und Stampfgewichte aufweisen und bei der Verarbeitung wesentlich weniger stauben. Während AEROSIL® 200 VV hydrophil ist und sich bezüglich seiner chemischen Eigenschaften nicht vom AEROSIL® 200 unterscheidet, handelt es sich bei AEROSIL® R 972 V um ein obenflächenbehandeltes Produkt, das hydrophobe Eigenschaften aufweist.

Das Ziel der Arbeit ist der Vergleich neuer AEROSIL®-Typen mit dem bisher verwendeten AEROSIL® 200 hinsichtlich der Wirkung als Fließregulierungsmittel, der Auswirkungen auf den Tablettiervorgang und die Eigenschaften der resultierenden Tabletten.

Als Modellsubstanzen werden drei bekannte pharmazeutische Tablettierhilfsstoffe eingesetzt:

eine mikrokristalline Cellulose (Avicel® PH 101), ein α-Lactose-Monohydrat (Tablettose® 80) und eine teilhydrolysierte Stärke (Starch 1500®). Der Anteil an AEROSIL® in allen Mischungen beträgt 0,5 Gew.-%. Um den Einfluss der Mischbedingungen auf die Fließfähigkeit zu untersuchen, wurden fünf unterschiedliche Mischungen ausgewählt.

Die Fließfähigkeit der Mischungen wird mit der Sieb-Kegel-Methode, dem Förderband und der Ringscherzelle untersucht. Bei moderaten Mischbedingungen ist die Wirkung von hydrophobem AEROSIL® als Fließregulierungsmittel dem hydrophilen Typ überlegen. Dieser Effekt gleicht sich bei Anwendung intensiverer

Mischbedingungen teilweise aus. Um die Unterschiede zu erklären, wird die Oberfläche von Mischungen aus Avicel® PH 101 und AEROSIL® mittels rasterelektronenmikroskopische Aufnahmen und X-Ray Photoelectron Spectroscopy untersucht und die Adhäsionskraft mittels Atomic Force Microscopy bestimmt. Die unterschiedlichen Fließeigenschaften der Mischungen sind von der Verteilung der AEROSIL®-Agglomerate auf der Oberfläche des Hilfsstoffes abhängig. Diese Verteilung wird durch die Natur des AEROSIL® beeinflusst. Die hydrophoben Agglomerate lassen sich leichter als die hydrophilen Agglomerate zerteilen und erreichen ihre optimale Größe und Belegung bereits nach schonender Mischung. Diese bessere Verteilung führt zu einer Abnahme der Adhäsionskraft in der Mischung. Es besteht eine gute Korrelation zwischen dem Böschungswinkel als Maß für die Fließfähigkeit und den mittels Atomic Force Microscopy gemessenen mittleren Adhäsionskräften. Die makroskopisch festgestellte Verbesserung der Fließfähigkeit durch verschiedene AEROSIL®-Typen kann also auf partikulärer Ebene bestätigt werden.

Der Einfluss von AEROSIL® auf die Kompressionsparameter und die Tabletteneigenschaften hängen von der Natur des AEROSIL®-Types und von der Verformbarkeit des Hilfsstoffes ab. Die Unterschiede können mit der Ryskewitch – Duckworth Gleichung quantifiziert werden. Bei der Tablettierung ternärer Mischungen mit Magnesiumstearat als dritter Komponente eliminiert der AEROSIL®-Zusatz den negativen Effekt von Magnesiumstearat auf die Tablettenhärte, ohne seine guten Schmiereigenschaften zu beeinträchtigen.

Hydrophile verdichtete AEROSIL®-Typen sind bessere Fließregulierungsmittel als ihre nicht verdichteten Pendants, weil sie einfacher zu handhaben sind, bessere Fließfähigkeit bedingen und die gleichen Tablettiereigenschaften zeigen. Hydrophobe AEROSIL®-Typen ergeben die stärkste Verbesserung der Fließfähigkeit, führen aber zu einer starken Abnahme der Tablettenhärte bei schlecht bindenden Materialien, wie Starch 1500®. Dennoch stellen sich die hydrophoben AEROSIL®-Typen als gute Alternative für die Tablettierung von plastischen Substanzen, wie Avicel® PH 101, und sprödbrüchigen, wie Tablettose® 80, dar.

CONTENTS

ABBREVIATIONS

approx.	approximately
DIN	Deutsche Industrie Norm
e.g.	exempli gratia
et al.	et alii
i.e.	id est
M	mixture
N	Newton
No	number
Pa	Pascal
Ph. Eur.	Pharmacopea Europea
r.H.	relative humidity
s.d.	standard deviation
s.e.	standard error
W/O	water in oil
wt%	weight in percent

Notes:

Error bars in figures represent the 95% confidence interval of the mean.

Parts of this thesis have been presented:

as research papers:
Jonat, S.; Hasenzahl, S.; Drechsler, M.; Albers, P.; Wagner, K. W. and Schmidt, P. C.
"Investigation of compacted hydrophilic and hydrophobic colloidal silicon dioxides as glidants for pharmaceutical excipients"
Powder Technol. **141,** 31-43 (2004)

Jonat, S.; Hasenzahl, S.; Gray, A. and Schmidt, P. C.
"Mechanism of glidants: Investigation of the effect of different colloidal silicon dioxide types on powder flow by atomic force and scanning electron microscopy"
 J. Pharm. Sci. **93**, 2635-2644 (2004)

Jonat, S.; Hasenzahl, S.; Gray, A. and Schmidt, P. C.
*"Influence of compacted hydrophobic and hydrophilic colloidal silicon dioxide on tableting properties of pharmaceutical excipient*s"
Drug Dev. Ind. Pharm., accepted for publication

Jonat, S.; Gray, A.; Albers, P. and Schmidt, P. C.
"Investigation of the glidant properties of compacted colloidal silicon dioxide by X-ray photoelectron spectroscopy"
Eur. J. Pharm. Biopharm., review process

as oral communications:
Jonat, S.; Hasenzahl, S.; Drechsler, M. and Schmidt, P. C.
"Einsatz verdichteter hochdisperser Kieselsäuren als Fließregulierungsmittel bei der Herstellung von Tabletten"
GVC VDI- Gesellschaft Verfahrenstechnik - Chemieingenieurwesen, Baden-Baden (2003)

Jonat, S.; Hasenzahl, S.; Gray, A.; Albers, P. and Schmidt, P. C.

"*Investigation of the glidant properties of compacted hydrophilic and hydrophobic colloidal silicon dioxide*"

International meeting on pharmaceutics, biopharmaceutics and pharmaceutical technology, Nuremberg (2004)

Jonat, S.; Hasenzahl, S.; Gray, A.; Albers, P. and Schmidt, P. C.

"*Wirkung von hydrophober und hydrophiler hochdisperser Kieselsäure als Fließregulierungsmittel*"

DPhG Doktorandentagung, Freudenstadt (2004)

Schmidt, P. C.; Hasenzahl, S.; Gray, A.; Albers, P. and Jonat, S.

"*Zum Mechanismus der Wirkung hochdisperser Kieselsäure als Fließregulierungs-mittel*"

GVC VDI- Gesellschaft Verfahrenstechnik - Chemieingenieurwesen, Braunschweig (2004)

Jonat, S.; Hasenzahl, S.; Gray, A. and Schmidt, P. C.

"*Einfluss hochdisperser Kieselsäure auf die Fließeigenschaften und die Tablettierung von Avicel$^®$ PH 101*"

GVC VDI- Gesellschaft Verfahrenstechnik - Chemieingenieurwesen, Tübingen (2005)

as posters:

Jonat, S.; Hasenzahl, S.; Gray, A.; Albers, P. and Schmidt, P. C.

"*Investigation of the glidant properties of compacted hydrophilic and hydrophobic colloidal silicon dioxide*"

European conference on drug delivery and pharmaceutical technology, Sevilla (2004)

Gray, A.; Hasenzahl, S.; Derchsler, M.; Jonat, S. and Schmidt, P. C.

"*Colloidal silicon dioxide: new variations for improved products performance*"

European conference on drug delivery and pharmaceutical technology, Sevilla (2004)

Schmidt, P. C.; Hasenzahl, S.; Gray, A.; Albers, P. and Jonat, S.

"*Investigation of the glidant properties of compacted hydrophilic and hydrophobic colloidal silicon dioxide*"

Jahrestagung der polnischen pharmazeutischen Gesellschaft, Breslau (2004)

Fox, P.; Jonat, S.; Gray, A.; Schmidt, P. C. and Hasenzahl, S.

"*Investigation of the effect of different colloidal silicon dioxide types and mixing on powder flow by secondary electron and atomic force microscopy*"

AAPS annual meeting and exposition, Baltimore (2004)

CHAPTER 1

INTRODUCTION

In the pharmaceutical industry powders are widely used as intermediates as well as final products. In the manufacture of tablets or in the filling of capsules a volumetric dosing is predominant. Considering the dosing and weight accuracy required by the pharmacopeias, it becomes evident that mastering the flowability of powders is of the utmost importance. The development of free flowing powder mixtures is, therefore, a basic requirement for successful production. In fact, most of the filler/binders used in pharmaceutical formulations are not free flowing, hence small amounts of glidants are incorporated into the mixtures to improve the flow properties of the powders.

Glidants used in pharmacy include talc, colloidal silicon dioxide, calcium phosphates and to a certain extent various metallic stearates. Several groups have investigated the addition of glidants to a variety of powders and noted that silica-type glidants are the most efficient because of their small particle size (Lieberman and Lachman 1989, Ritschel and Bauer-Brandel 2004).

AEROSIL® 200 is a hydrophilic highly disperse colloidal silicon dioxide that is commonly used to improve flowability. This conventional colloidal silicon dioxide has low bulk and tapped densities and can produce dust if handled improperly. Furthermore, it requires considerable storage space and is relatively complicated to process. In order to improve the handling of colloidal silicon dioxide, special mechanical processes were developed for the homogeneous compaction of colloidal silicon dioxide. As a result, two new products have been recently introduced: AEROSIL® 200 VV, which is especially designed for the pharmaceutical industry, and AEROSIL® R 972 V. AEROSIL® 200 VV is hydrophilic and chemically identical to AEROSIL® 200. It differs from conventional colloidal silicon dioxide only in its higher tapped density and its larger secondary agglomerates. The compacted product

AEROSIL$^{®}$ R 972 V is hydrophobic, a result of dimethyl silyl groups chemically bound to the silica surface.

The aims of this study are threefold. The first objective is to compare the compacted hydrophilic and hydrophobic products to their non-compacted hydrophilic counterparts in terms of their effect on flowability and water absorption of typical tableting excipients. The study aims to discover whether the compaction process or the modification of the structure through hydrophobic treatment can influence the flow regulating effect of AEROSIL$^{®}$. To date, only limited information is available concerning what occurs on a particulate level during powder flow; the development of powder mixtures is still carried out by trial-and-error. Therefore, the second aim of the study is to examine the mechanism of glidants on a microscopic level. This will be done by analyzing the surface coverage of AEROSIL$^{®}$ on the excipient's surface and by measuring the interparticulate forces within the powder mixture. Finally, on the basis of these flowability results and the microscopic investigations, the influence of the different colloidal silicon dioxide types on the tableting properties of typical tableting excipients will be investigated.

CHAPTER 2

COLLOIDAL SILICON DIOXIDE

AS GLIDANT IN PHARMACEUTICAL POWDER MIXTURES

2.1 Colloidal silicon dioxide

2.1.1 Manufacture of AEROSIL®

Hydrophilic AEROSIL®

AEROSIL® is a highly disperse or colloidal silicon dioxide (also referred to as fumed silica) manufactured by the hydrolysis of chlorosilanes in a hydrogen/oxygen flame:

$$2H_2 + O_2 \rightarrow 2H_2O$$

$$\underline{SiCl_4 + 2H_2O \rightarrow SiO_2 + 4HCl}$$

$$2H_2 + O_2 + SiCl_4 \rightarrow SiO_2 + 4HCl$$
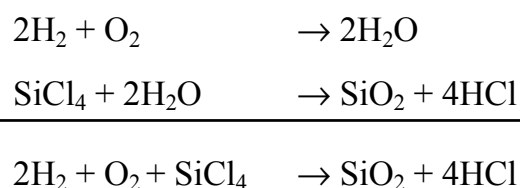
Figure 2.1 depicts schematically the manufacture of AEROSIL®. Gaseous $SiCl_4$ reacts in a gas flame burner (1000°C) with just-formed H_2O to produce silicon dioxide. Hydrochloric acid is the only by-product, and it is removed from the SiO_2 in the separation chamber. The HCl that remains adsorbed onto the colloidal silicon dioxide surface is removed in the deacidification chamber by washing with water vapour. The colloidal silicon dioxide product is collected in a silo, tested and packaged.

The concentration of H_2 and O_2, the temperature of the flame and the dwell time of the silica in the burner influence the particle size and size distribution and the surface area of the colloidal silicon dioxide. Upon production, colloidal silicon dioxide is hydrophilic, containing silanol (-Si-OH) and siloxane (-Si-O-Si-) groups on its surface.

Silanes such as methyltrichlorosilane or trichlorosilane can also be used, either alone or in combination with tetrachlorosilane, as precursor materials.
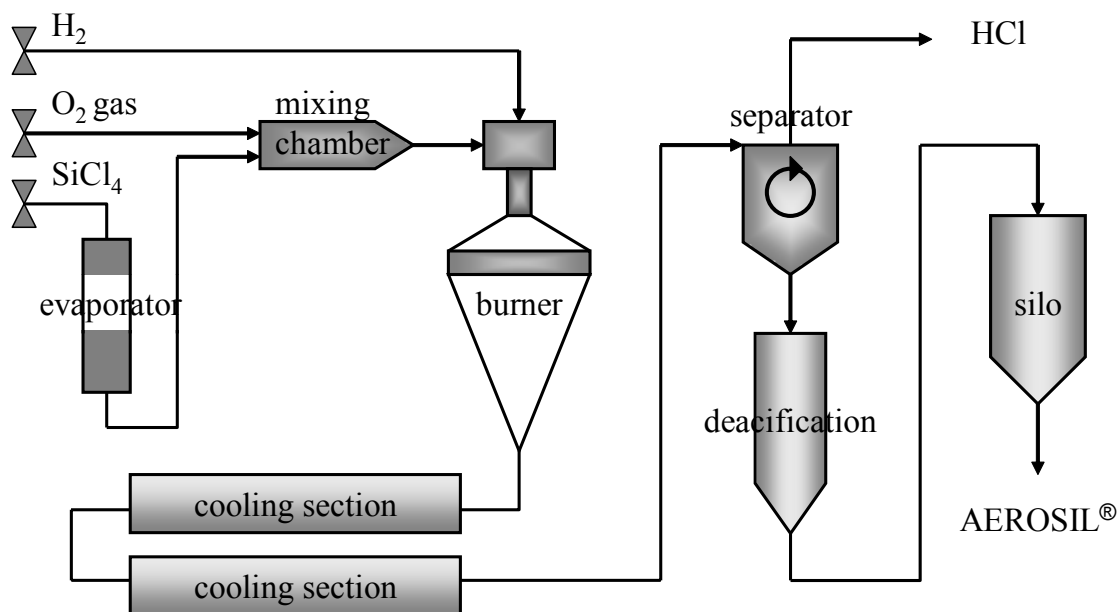
Figure 2.1   Manufacture of hydrophilic AEROSIL®.

Degussa first patented this procedure in 1942 and production of AEROSIL® was begun on a large scale in the 1950s. The process has been continuously developed further since then. The raw materials used are exclusively of chemical origin and are very pure, thus allowing AEROSIL® to meet the requirement of pharmacopoeia monographs for colloidal silicon dioxide with no restrictions (Technical bulletin Degussa 2003).

Hydrophobic AEROSIL®

The silanol groups of the "in statu nascendi" AEROSIL®, i.e freshly formed hydrophilic AEROSIL®, can react with organosilicon compounds to form hydrophobic AEROSIL®. Freshly prepared hydrophilic AEROSIL® is treated immediately after the deacidification step. The hydrophobic AEROSIL® formed is designated "R" for repellent.

Through hydrophobic treatment, the density of silanol groups per nm² decreases from approx. 2 for hydrophilic AEROSIL® to approx. 0.75 for the hydrophobic types.

Tetrachlorosilane

Flame $O_2 + H_2$

Hydrophilic AEROSIL®

Silane

Hydrophobic AEROSIL®
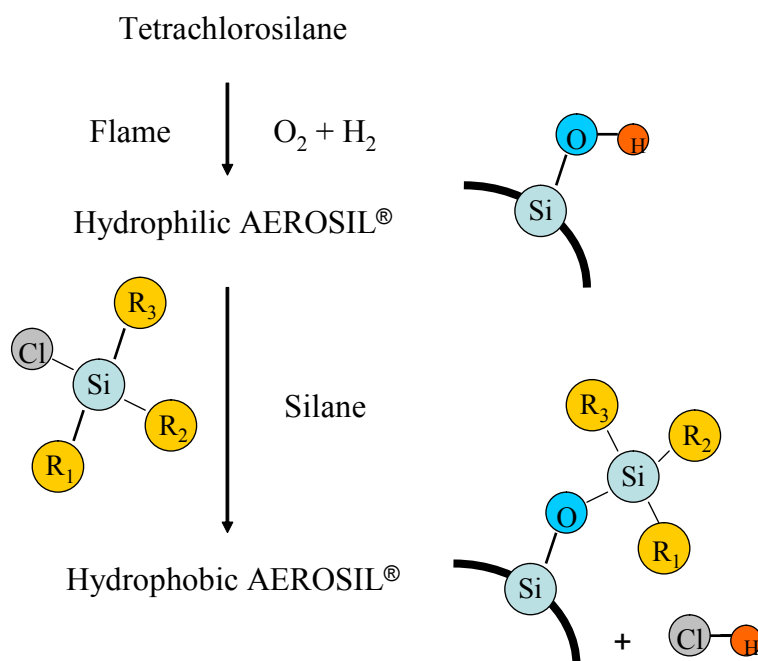
Figure 2.2   *Hydrophobic treatment of AEROSIL®.*

Compaction process

Conventional colloidal silicon dioxide has low bulk and tapped densities. The tapped density is typically only 50-60 g/L. To increase the bulk and tapped densities and thus improve the handling of AEROSIL®, special mechanical processes were developed and patented by Degussa. The compacted products, characterized by the suffix "V" or "VV", have tapped densities in the range of 90-120 g/L. The compaction process is gentle and homogeneous and does not affect the other physico-chemical characteristics of the product.

2.1.2 Properties of AEROSIL®

AEROSIL® is a fine, white, light and amorphous powder consisting of primary particles in the nanometer range (10-40 nm), resulting in a very large specific surface area (from 50-400 m^2/g). The primary particles are not isolated but are fused together in relatively stable chain-like aggregates, which in turn form larger agglomerates in the micrometer range (Figure 2.3).

| Primary particles | Aggregates | Agglomerates |
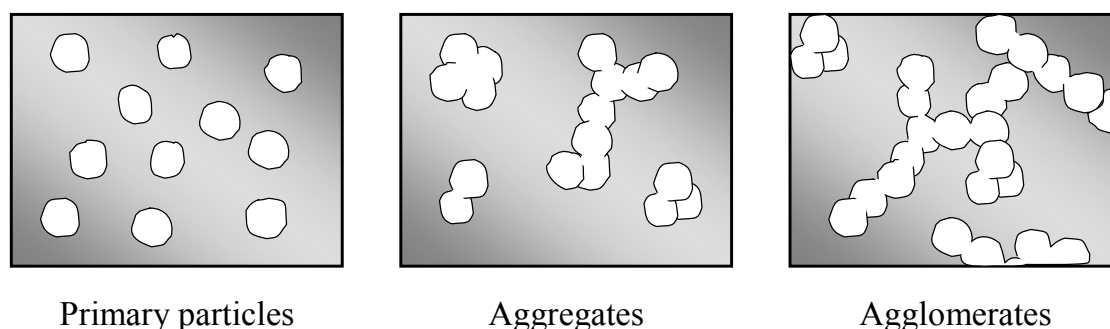
Figure 2.3   Primary particles, aggregates and agglomerates of AEROSIL®.

The physical and chemical properties of AEROSIL® can be varied within wide limits depending on the process parameters. The properties of the AEROSIL® used in this study are listed in Table 2.1.

Table 2.1   Physicochemical properties of hydrophilic and hydrophobic colloidal silicon dioxide types used in this study.

	AEROSIL® *200*	*AEROSIL®* *200 VV*	*AEROSIL®* *130 V*	*AEROSIL®* *R 972 V*	*AEROSIL®* *R 974 V*
Average primary particle size (nm) [a]	12	12	16	16	12
BET surface area (m^2/g) [b]	206	201	138	111	176
Bulk density (g/cm^3) [b]	0.050	0.119	0.104	0.094	0.089
Tapped density (g/cm^3) [b]	0.054	0.134	0.118	0.115	0.105
Silanol group density (nm^{-2}) [a]	approx. 2	approx. 2	approx. 2	approx. 0.75	approx. 0.75
Behavior towards water	hydrophilic	hydrophilic	hydrophilic	hydrophobic	hydrophobic

[a] Typical values

[b] Batch record, ex-plant

AEROSIL® 130 and AEROSIL® 200 are the starting materials for the synthesis of AEROSIL® R 972 and AEROSIL® R 974, respectively (Technical bulletin Degussa 2003).

2.1.3 Applications of AEROSIL®

AEROSIL® is widely used in the pharmaceutical field for its glidant activity. AEROSIL® is incorporated into solid dosage forms in a concentration of between 0.2 and 1.0 wt% to improve the flow properties of cohesive powders and granulates. When applied to tableting operations, AEROSIL® improves flow into the hopper and the die cavities of the tablet press. AEROSIL® increases the tablet weight, decreases the unit weight variation and minimizes the tendency of powder or granule components to separate or segregate due to excessive vibrations (Technical informations Degussa 2001, 2002). For powder-filled capsules, addition of AEROSIL® ensures a high accuracy of metering and a uniform distribution of active ingredients (Lieberman and Lachman 1989). Table 2.2 lists important studies on AEROSIL® as a flow promoting agent.

Table 2.2   Review of studies dealing with AEROSIL® as glidant.

Authors	AEROSIL® types	Concen-tration [%]	Excipients	Methods
Tawashi (1963)	not mentioned*	0.01-2.0	starch, lactose, magnesium carbonate, titan dioxide, zink and magnesium oxide	packing volume and rate
Czetsch-Lindenwald (1963)	AEROSIL® R 972	0.5	starch	flowabilty
Czetsch-Lidenwald and Asker (1966)	AEROSIL® R 972 and 200	0.1-10.0	starch, titan dioxide	capsule filling
Gstirner and Pick (1967)	AEROSIL® R 972 and 200	0.05-10.0	zink oxide	range of dispersion of flow
Gstirner and Pick (1969)	AEROSIL® R 972 and 200	0.05-10.0	zink and magnesium oxide, titan dioxide, magnesium carbonat, talk, starch, lactose, diatomaceous earth	water uptake
List and Müller (1972)	AEROSIL® 200	0.1-0.3	lactose, sodium chloride	flowability, scanning electron microscopy
Nürnberg (1972)	AEROSIL® 200	1 and 5	lactose	tableting parameters

York (1975)	AEROSIL® 200	0.25-4.0	α-lactose monohydrate, calcium hydrogen phosphate	tensile strength and annular shear cell measurement
Lerk et al (1977)	AEROSIL® 200	0.1-0.4	STA-Rx 1500	tableting parameters
Lerk and Bolhuis (1977)	AEROSIL® 200	0.1-0.4	STA-Rx 1500	crushing strength, wettability
Ragnarsson et al. (1979)	AEROSIL® 200	0.5	sodium chloride	tableting parameters
Staniforth and Ahmed (1986)	not defined	2	Avicel® PH 101	work of failure
Rowe (1988)	not defined	2	Avicel® PH 101	solubility parameter
Ohta et al. (2003)	AEROSIL® 200 AEROSIL® 50	-	Avicel® PH 101, Tablettose 80®	Carr index, adhesion force microscopy
Meyer and Zimmermann (2004)	AEROSIL® 200, OX 50, R 805, 300, R 812	0.2	Cerestar	tensile strength tester, SEM
Zimmerman et al. (2004)	AEROSIL® OX 50, 200, 300, 380, R 805, R 972, R 812	0.2	Cerestar	tensile strength tester, SEM
van Veen et al. (2005)	AEROSIL® 200	0.2-2.0	Emcocel® 90M, Prosolv SMCC® 90	tableting parameters

* Most likely AEROSIL® 200.

Tawashi (1963) first reported that addition and intimate mixing of AEROSIL® to powders and granules markedly influenced the packing volume and the flow properties of the blend. He stated that the AEROSIL® concentration for optimum flowability was identical with the concentration required to build a continuous monolayer of AEROSIL® particles around the individual particles of the powder. Electron microscopy investigations performed by List and Müller (1972) showed, on the contrary, that glidants covered the surface area not in a particulate manner but in agglomerates, which filled up the unevenesses.

Hydrophobic and hydrophilic AEROSIL[®] types were first compared in the 1960s. Czetsch-Lindenwald (1965) reported that AEROSIL[®] R 972 improved the flowability of tablet granulates and that the flow enhancement of starch was greater upon addition of hydrophobic AEROSIL[®] as compared to the hydrophilic type. Czetsch-Lidenwald and Asker (1966) studied capsule filling and found that AEROSIL[®] was the most effective glidant, and the hydrophobic type yielded the best results. Gstirner and Pick (1967, 1969) evaluated the effect of hydrophobic and hydrophilic AEROSIL[®] types on the flowability of zinc oxide and also their influence on the water absorption of various powders. The results showed that AEROSIL[®] R 972 enhanced the flowability of zinc oxide and reduced the water uptake of powders to a greater extent than did the hydrophilic type AEROSIL[®] 200 at concentrations between 0.05 to 10.0%.

When compared with other glidants, AEROSIL[®] was judged to be the most effective by Lidenwald and Asker (1966). This was confirmed by York (1975), who used powder failure equipment, i.e. annular shear cell and tensile tester, to study the effect of three glidants and found the following order of efficiency: fine silica > magnesium stearate > purified talc.

With regards to tableting, Nürnberg (1972) observed an increased strength in lactose tablets upon addition of 1% AEROSIL[®], and other studies dealt with the influence of AEROSIL[®] on the film formation of magnesium stearate during mixing (Lerk et al. 1977, Lerk and Bolhuis 1977, Ragnarsson et al. 1979, Rowe 1988, Staniforth and Ahmed 1986).

Recently, Meyer and Zimmermann (2004) and Zimmerman et al. (2004) investigated different "nanomaterials", including hydrophobic and hydrophilic AEROSIL[®], as flow regulators in dry powders, while Van Veen et al. (2005) compared the compaction properties of silicified microcrystalline cellulose to a mixture of microcrystalline cellulose and AEROSIL[®] 200. Finally, Ohta et al. (2003) studied the effect of the geometric structure of several glidants on the flow properties of a pharmaceutical powder mixture.

Beside its glidant activity, hydrophilic AEROSIL[®] has found numerous other applications in the pharmaceutical field as shown in Table 2.3.

Table 2.3   Applications of hydrophilic colloidal silicon dioxide in pharmacy (Fiedler 1996, Technical bulletin Degussa 2003).

Solid Pharmaceutical Forms		
Dosage form	**Functions**	**Typical concentration in use (%)**
Coated tablets	• speeds up drying • prevents tablet cores from sticking together • improves texture • stabilizes pigments suspensions	10-15 (solid formulations) 0.5-2.0 (pigment suspension)
Semi-Solid Pharmaceutical Forms		
Dosage form	**Functions**	**Typical concentration in use (%)**
Ointments, gels, creams and pastes	• viscosity increasing agent • emulsion stabilizer • suspending agent • dispersing agent • improves storage and thermal stability	5-10
Suppositories, sticks	• viscosity control • keeps active ingredients more evenly distributed • increases temperature and storage stability	0.5-2
Transdermal therapeutic systems	• viscosity controlling agent • sustained release of active ingredients • increases storage and temperature stability	1-5
Liquid Pharmaceutical Forms		
Dosage form	**Functions**	**Typical concentration in use (%)**
Suspensions, aerosols	• prevents sedimentation or formation of hard sediments • prevents clogging of spray nozzles • increases storage and temperature stability	0.5-3

Hydrophobic AEROSIL® types are superior to hydrophilic AEROSIL® in several pharmaceutical applications, including stabilization and improvement of the flow properties of hygroscopic substances, control and reduction of the release of active substance from tablets, capsules, ointments, suppositories and patches, and improvement of the thermal stability of W/O emulsions.

2.2   Powder mixtures

2.2.1   Properties of powders

A cohesive powder behaves like an imperfect solid. Sometimes it flows like a liquid or can be compressed like a gas. The mechanical behavior of powders or granulates depends directly on prestressing history. This can be demonstrated by a simple tilting test of storage containers (Tomas 2004). Depending on how to fill the container, tilt it and bring it back, different shapes of the bulk surface will be generated, as depicted in Figure 2.4. Solids or parcels and fluid products are comparatively easier to handle.
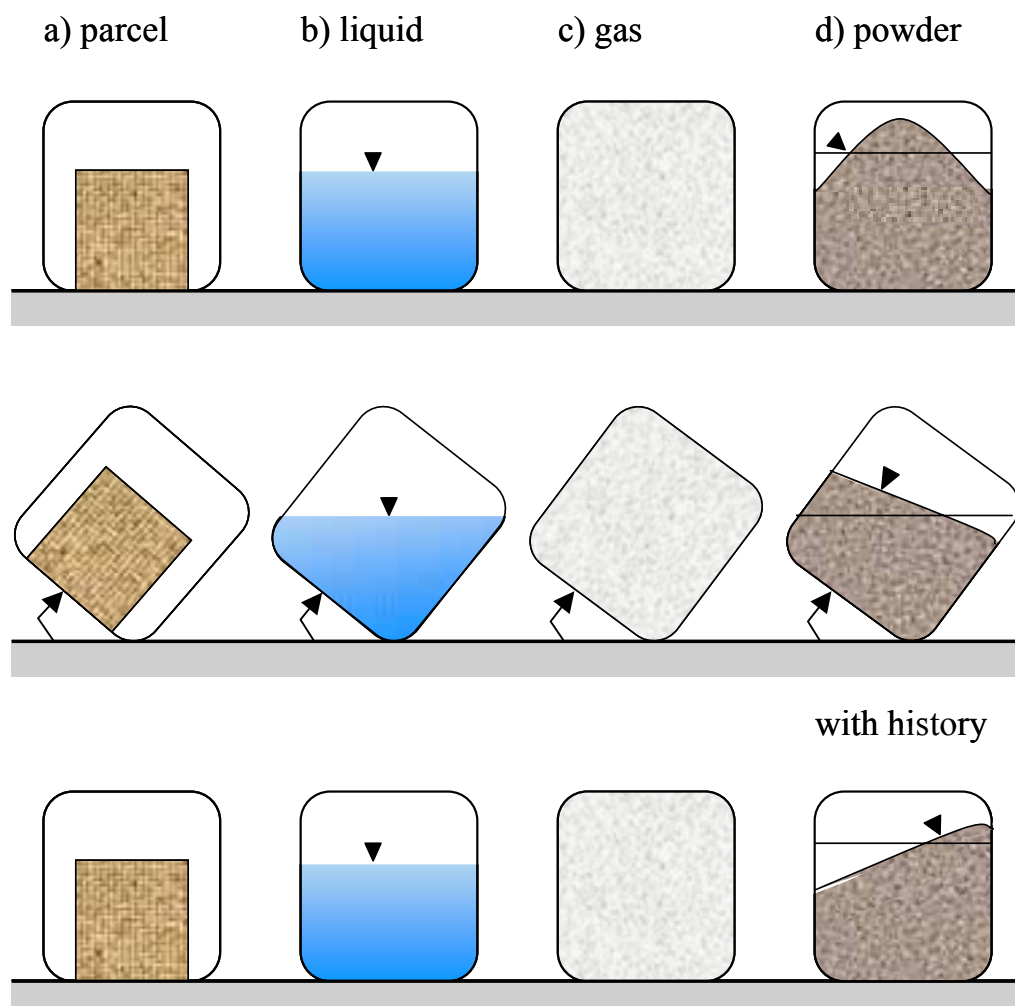
Figure 2.4   *Storage in containers – mechanical behaviour of solid, liquid, gas and bulk solid. Picture taken from Tomas (2004).*

Flowability of powders

The assignment of a given powder to flow or not is primarily determined by the ratio of interparticle forces and gravity. Whereas, gravity is usually relied upon to cause the powder to flow, the cohesion force prevents them from flowing. The ratio of interparticle force to the gravitational force is inversely proportional to the square of the particle diameter. For most organic materials, at particle diameters smaller than 30 µm, the cohesive forces exceed the particle weight. Therefore, small particles stick more strongly together.

The cohesive forces acting between particles are also dependent on their surface roughness (particles with rough surfaces flow better than smooth particles), the particle size distribution, the packing density and consequently the number of contacts between particles (the higher the number of contacts, the higher the cohesion forces) and external factors such as temperature and relative humidity of the air (Podczeck 1998). Techniques used for the determination of interparticle forces include the vibration method, the centrifuge technique, the impact separation method and atomic force microscopy.

In pharmaceutical industry, glidants are incorporated into powders in order to improve their flowability. To understand how these substances act, a consideration of the forces acting in powders is required, and will now be discussed.

2.2.2   Forces acting in powders

Force of gravity

The force of gravity (F_G) acting on a particle of volume V and of solid density ρ is given by:

$$F_G = \rho \, V \, g$$

Interparticle forces

The interparticle forces include forces due to liquid bridges, electrostatic or Coulomb forces, capillary forces and van der Waals forces. At short interparticle distances, which are relevant for the flow properties (below 50 nm down to the contact distance of around 0.4 nm), the van der Waals forces are significantly higher than the Coulomb forces. For a given interparticle distance, for all radii of the particles, the van der Waals forces are greater than the capillary forces. In non-hygroscopic materials, liquid bridges are observed to a marked extent only at relative humidities above 60%. Therefore, in dry powders, the van der Waals forces are the prevailing interparticle forces.

Three different types of intermolecular interactions are summarized under the name van der Waals forces. The Keesom-orientation force is due to the interaction between rotating permanent dipoles, while the Debye induction force describes the interaction between a permanent and an induced dipole. The London dispersion force, due to the interaction between two induced dipoles, contributes most to the van der Waals force (Podczeck 1996).

Different procedures to calculate the free energy of the van der Waals force interaction between macroscopic bodies have been developed. The interaction between two spheres of radii R_1 and R_2 and the interaction between a sphere and a wall are of specific importance (Figure 2.5).

The corresponding van der Waals forces F_{vdW} are obtained according to:

$$F_{vdW} = \frac{-d\omega}{dH}$$

where ω is the interaction potential and H is the interparticle distance (Visser 1995).

$$\omega = -\frac{A}{6H}\ \frac{R_1 R_2}{R_1 + R_2}$$

sphere-sphere

$$\omega = -\frac{AR}{6H}$$

ω: interaction potential

H: interparticle distance

A: Hamaker constant

sphere-wall
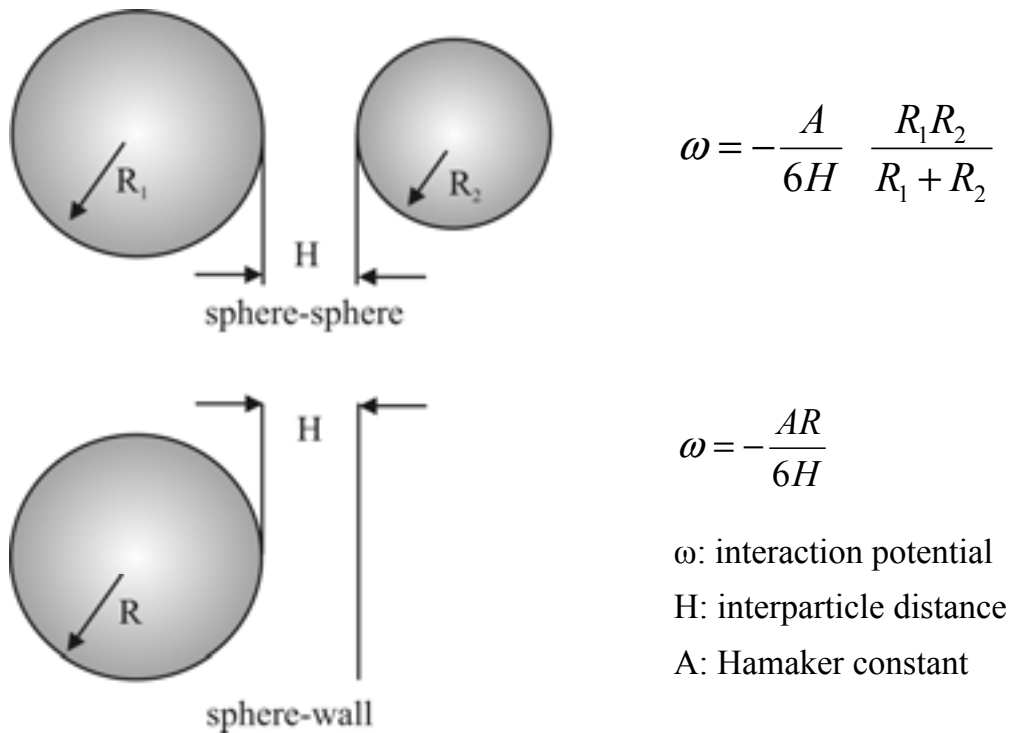
Figure 2.5   Van der Waals potentials for different geometries of the interacting macroscopic bodies.

Rumpf (1974) observed that the interactive particle forces determined experimentally are always significantly smaller than the forces calculated on the basis of ideal geometries. He explained this discrepancy by the assumption that surface roughness increases the distance between the interacting particles.

2.2.3   Binary powder mixtures consisting of AEROSIL® and a filler/binder

Due to their particle size in the nanoscale range, the primary particles of AEROSIL® always tend to form highly porous aggregates/agglomerates. If they are added to a filler/binder, they always swim on top according to the difference in specific density. During the mixing, the agglomerates of AEROSIL® are degraded into smaller fragments or even to their primary particles, and AEROSIL® is distributed on the surface of the filler/binder particles. The mixing time and the mixer type can, therefore

influence the size of the agglomerates and the homogeneity of the mixture and as a result the flowability. Several groups have investigated the importance of the mixing process by comparing different types of mixers, different excipients and varying drug contents to achieve an optimum mixing time (Otsuka et al. 1993, Schweiger et al. 1997, De Villiers and Van der Watt 1994). The mixing efficiency is influenced by the physical properties of the mixture components (e.g. flow properties, density, water content, wettability, particle size, particle shape, and surface roughness) and by the mixing principle, the mixing time and the apparatus used (Poux et al. 1991). Sindel et al. (1998) examined the homogeneity of a mixture of colloidal silicon dioxide and lactose by measuring the angle of repose and by determining the variance of the colloidal silicon dioxide content. At the optimum mixing time, a significant reduction of the angle of repose was found.

The AEROSIL$^{®}$ particles are strongly adhered on the surface of the bigger filler/binder particles of the mixture. Due to the strength of this bonding, they behave like surface roughness, that is to say, the adhered glidant particle increases the minimum contact distance of two filler/binder particles. In addition the contact area between the two particles is reduced. In consequence the van der Waals forces are reduced allowing the gravitational forces to prevail.

Rumpf (1974) first introduced the "sphere-wall" model to explain the reduced adhesion forces acting between rough surfaces. To allow more realistic conclusions about the glidant action in a powder mixture, a sphere-sphere model of the van der Waals interaction was developed. In this central one-particle contact model, a particle of the glidant with a radius (r_f) is assumed to be adsorbed at the surface of a larger particle with a radius (R_1). Even in the adsorbed state, there is a small distance, called contact distance about $D = 4 \times 10^{-10}$ m between the two particles. The center of the small particles lies on the line connecting the centers of the two bigger particles (Figure 2.6).
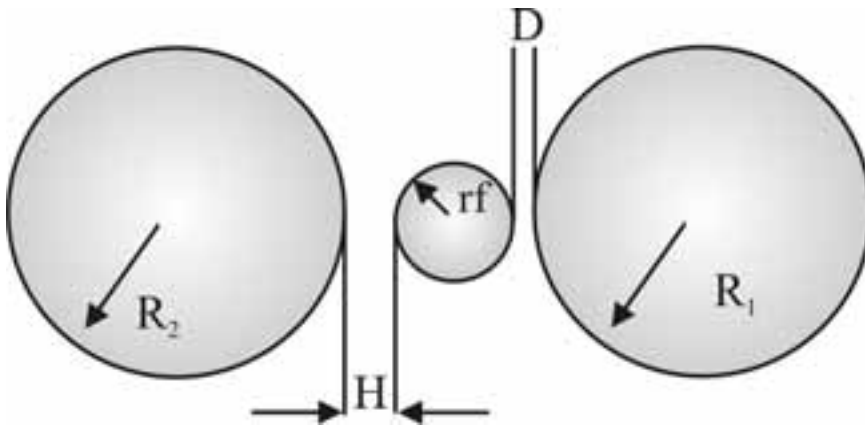
Figure 2.6   Sphere-sphere contact model of the van der Waals interaction with rf <<
              R_1 and R_2.

The presence of the small sphere representing a glidant particle results in a significant
reduction of the net van der Waals forces given by the following equations:

$$F_{vdW} = -\frac{A}{6}\left[\frac{R_1 rf}{H^2(R_1 + rf)} + \frac{R_1 R_2}{(H + D + 2rf)^2(R_1 + R_2)}\right]$$

where,   H: interparticle distance

              D: contact distance

              A: Hamaker constant

              rf: radius of the glidant particle

              R_1 and R_2: radii of the spheres

This model was further developed into a non-central one-particle contact model by
Zimmermann et al. (2004) or into a three-point contact model according to Meyer
(2003).

Beside the theory dealing with the reduction of particle attraction forces, a second
theory describing a ball bearing type of action was proposed to model glidant action.
Glidants form a monoparticle layer on the powder or granulate particles causing them
to roll over one another. The rough surface is thus smoothed out, reducing the
frictional and adhesive forces that operate between the surfaces.

2.2.4 Tableting of binary powder mixtures

Tablets are still the most frequently orally applied dosage form. Considering the dosis and weight accuracy required by the pharmacopeias, the flowability of the powder is of utmost importance in the tablet production. The flow into the hopper and the die cavities of the tablet press must be free and constant, in order to reduce a small weight variation and to enable a dosing accuracy. AEROSIL® fulfills this demand in improving the flow of powders. Furthermore AEROSIL® minimizes the tendency of powder or granule components to separate or segregate due to excessive vibrations (Technical information Degussa 2001).

With regards to tableting, the results are contradictory. Nürnberg (1972) observed an increased strength of lactose tablets by addition of 1% AEROSIL®, while van Veen et al. (2004) showed that colloidal silicon dioxide decreased the tablet strength most probably by lowering the interparticle bonding strength between Avicel® PH 101 particles.

2.3   Aim of the thesis

With the introduction of the new compacted hydrophobic and hydrophilic AEROSIL® products, their effects on flowability and water absorption of typical tableting excipients seemed to be an interesting topic. The study should enable a comparison not only between compacted and non-compacted materials but also between hydrophobic and hydrophilic AEROSIL® types. Therefore, three excipients used as filler/binders for direct compression of tablets were selected for their different structures, flow properties and compressibility behavior. These are microcrystalline cellulose (Avicel® PH 101), pregelatinized starch (Starch 1500®) and agglomerated α-lactose-monohydrate (Tablettose® 80). Additionally, to assess how the mixing time and the mixer type influences flowability of the mixtures, different mixers and mixing conditions were chosen. Gentle mixing was obtained in a free-fall mixer, while forced mixing and homogenization milling were achieved in a high speed mixer and in a pin mill, respectively.

To better understand the mechanism of the glidant (ball bearing type of action or surface roughness according to Rumpf), the mixtures were investigated on a microscopic level. The distribution of AEROSIL[®] on the excipient's surface was analyzed using scanning electron microscopy. The qualitative impressions were supported by quantitative X-Ray photoelectron spectroscopy measurements. Additionally, the interparticle forces within the powder mixture were measured using atomic force microscopy.

On the basis of flowability results and the microscopic investigations, the influence of the different hydrophobic and hydrophilic colloidal silicon dioxide types on the tableting properties of the above mentioned three excipients was investigated. The study was based on binary mixtures to show the influence of colloidal silicon dioxide on compression parameters like Heckel plots and residual and ejection forces, tablet properties as radial tensile strength and friability and storage of the tablets at different relative humidities. Moreover, ternary mixtures containing magnesium stearate as a third component were evaluated in order to study the effect of colloidal silicon dioxide on the film formation of magnesium stearate.

CHAPTER 3

INVESTIGATION OF THE EFFECT OF

DIFFERENT COLLOIDAL SILICON DIOXIDE TYPES

ON THE FLOWABILITY OF BINARY POWDER MIXTURES

3.1   Introduction

The first objective of the study is to compare the compacted hydrophilic and hydrophobic AEROSIL® to their non-compacted hydrophilic counterparts in terms of their effect on flowability and water absorption of typical tableting excipients. The study aims to discover whether the compaction process or the modification of the structure through hydrophobic treatment can influence the flow regulating effect of AEROSIL®.

Angle of repose and mass flow rate are certainly the most simple and the most popular tests used for the flowability measurements. In the literature, the angle of repose has been used in approximately 40% of papers attempting to measure powder flow of pharmaceutical excipients (Amidon 1999). Other methods determine the flow characteristics by evaluating the packing properties through bulk density determination such as Carr´s compressibility index (Carr 1965) and Hausner´s ratio (Hausner 1967) or by describing the volume reduction of a powder when subjected to pressure using the Kawakita equation (Lüdde and Kawakita 1966). Lüdde and Kawakita (1966) have shown that one of the constants, namely "a", is theoretically equal to Carr´s compressibility index. Podczeck and Lee-Amies (1996) confirmed this experimentally. Other methods of predicting powder flow include shear cell measurement according to Jenike (Schwedes 1996, Ramachandruni and Hoag 2000) and critical orifice diameter (Lee et al. 2000). More recent sophisticated flow characterization approaches relate to avalanching methods (Lee et al. 2000, Lavoie et al. 2002), vibratory feeder method

(Bhattachar et al. 2004), powder rheometer (Freeman 2004) and multichamber microscale fluid bed (Räsänen et al. 2004).

Amidon et al. (1999) have recommended several procedures for the measurement of flow properties. However, individual tests are not always able to measure small differences in flow between similar powders and to rank their flow properties (Taylor et al. 2000). Thus, the combination of various tests is a better approach to achieve reliable data. Three methods, namely the classical static angle of repose, a dynamic conveyor belt method and the ring shear cell method were chosen to compare the flow-enhancing properties of conventional colloidal silicon dioxide (AEROSIL® 200) to the new compacted hydrophilic and hydrophobic types (AEROSIL® 200 VV and AEROSIL® R 972 V). Different mixing conditions were studied to investigate the influence of the relative humidity, the mixing time and the mixer type using three different tablet excipients: Avicel® PH 101, Starch 1500® and Tablettose® 80. Additional to the angle of repose, poured and tapped densities of binary Avicel® PH 101 mixtures containing AEROSIL® 200, AEROSIL® 200 VV, AEROSIL® 130 V, AEROSIL® R 972 V or AEROSIL® R 974 V were measured to confirm the influence of the chemical nature of colloidal silicon dioxide on the flow enhancement.

3.2   Influence of the mixing process and the colloidal silicon dioxide type

3.2.1   Determination of angle of repose

Avicel® PH 101

The angle of repose of mixtures containing Avicel® PH 101 with various AEROSIL® types was investigated with respect to the mixing time and mixer type (Figure 3.1). As expected, each type of colloidal silicon dioxide clearly improved the flowability of Avicel® PH 101 for all mixtures. According to the classification of Carr (1965), which relates the angle of repose to the flow properties, Avicel® PH 101 showed fair (36°-40°) or passable (41°-45°) flow properties upon addition of 0.5% AEROSIL®.

Figure 3.1   Angle of repose of Avicel® PH 101 containing 0.5% AEROSIL® R 972 V (●), 0.5% AEROSIL® 200 (♦), 0.5% AEROSIL® 200 VV (▲) and without AEROSIL® (■). Error bars indicate a 95% confidence interval of six measurements.

Statistical analyses (ANOVA and Newman-Keuls tests) were used to rank the flow properties of the mixtures (Bolton 1990). Accordingly, AEROSIL® R 972 V has improved the flowability of mixtures 1, 2 and 3 most significantly, followed by AEROSIL® 200 VV and AEROSIL® 200. For mixture 4, there was no statistically significant difference between AEROSIL® 200 VV and AEROSIL® R 972 V. Under these mixing conditions, the two AEROSIL® types improved the flowability to the same extent, whereas AEROSIL® 200 showed the lowest flowability enhancement.

The flowability of mixtures containing AEROSIL® 200 or AEROSIL® 200 VV was strongly influenced by the mixing conditions. Flowability increased with mixing time and energy, reaching an optimum with mixture 4. The results of the ANOVA test for Avicel® PH 101 mixtures with AEROSIL® R 972 V, however, indicated that there were no differences in the angles of repose of mixtures 1, 2, 3 and 4. The flowability increase obtained with 0.5% AEROSIL® R 972 V was influenced neither by the free-fall nor by the high speed mixer. This means that the flowability optimum was obtained directly after gentle mixing (mixture 2), and remained constant until mixture 4. For a homogenization of the mixture with higher mixing energy, a pin mill was used

to mill mixture 4. For all preparations, the resulting mixture 5 showed the highest angle of repose. The poorest flowability was due to the reduction of the particle size (Table 3.1), which increased the adhesion forces between cellulose particles.

Table 3.1   The influence of mixer type and mixing time on the mean particle diameter of Avicel® PH 101, Starch 1500® and Tablettose® 80.

Sample	Avicel® PH 101 (µm)	Starch 1500® (µm)	Tablettose® 80 (µm)
Bulk	48.8	73.3	159.9
Mixture 2	49.5	74.4	149.0
Mixture 4	49.7	75.4	130.6
Mixture 5	28.8	49.5	23.8

Starch 1500®
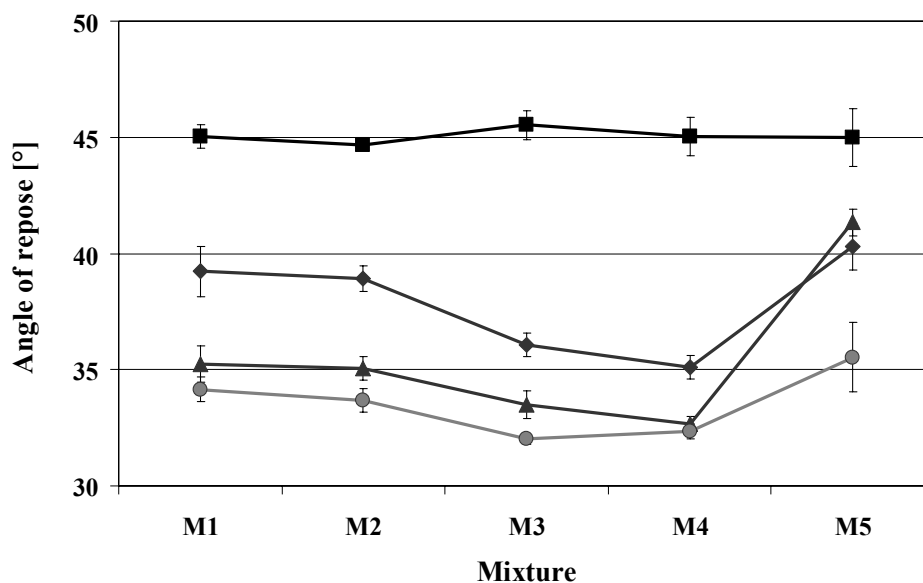
Figure 3.2   Angle of repose of Starch 1500® containing 0.5% AEROSIL® R 972 V (●), 0.5% AEROSIL® 200 (♦), 0.5% AEROSIL® 200 VV (▲) and without AEROSIL® (■). Error bars indicate a 95% confidence interval of six measurements.

The addition of 0.5% colloidal silicon dioxide clearly improved the flowability of Starch 1500® for all mixing conditions. According to the classification of Carr (1965), Starch 1500® became a good (31°-35°) or a fairly good (36°-40°) flowing material (Figure 3.2). From mixture 1 to mixture 4, the angles of repose of AEROSIL® 200,

AEROSIL® 200 VV and AEROSIL® R 972 V mixtures were decreased from 39.2° to 35.1°, from 35.2° to 32.7° and from 34.1° to 32.4°, respectively. The ANOVA results have shown that the highest flowability was obtained with and the mixing conditions had the lowest influence on AEROSIL® R 972 V. As a glidant, hydrophobic AEROSIL® R 972 V seems to be less sensitive with respect to the mixing conditions. Milling reduced the particle of Starch 1500®. In consequence, mixture 5 showed an increase of the angle of repose; i.e. poorest flowability.

Tablettose® 80

Figure 3.3 depicts the angle of repose of Tablettose® 80 mixtures as a function of colloidal silicon dioxide types and the mixing steps. Tablettose® 80 is already a free-flowing material, nevertheless its flowability was further improved upon addition of 0.5% AEROSIL®. Furthermore, for all mixtures, the angle of repose increased with increasing mixing energy, whereby the milling process led to a dramatic increase (mixture 5).
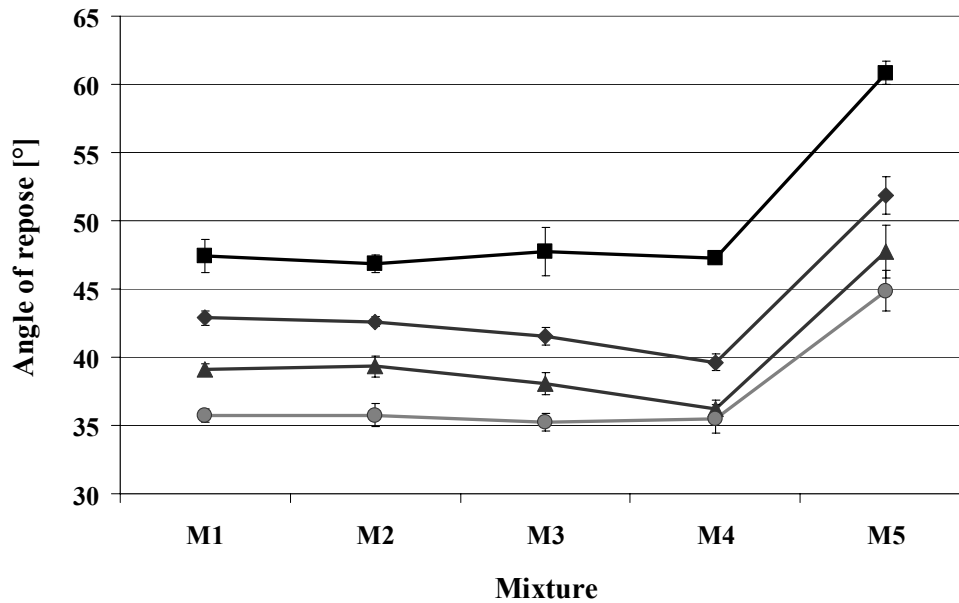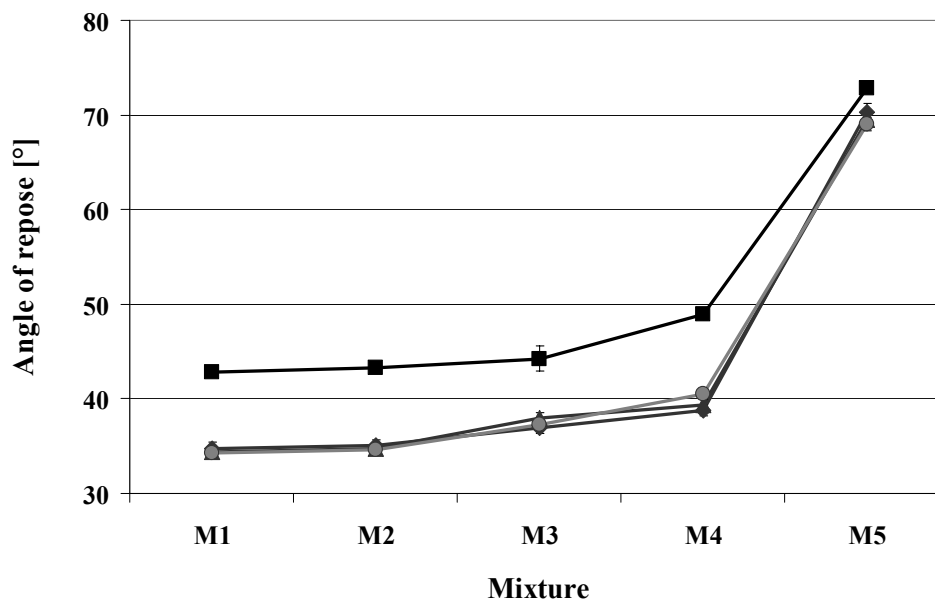

Figure 3.3   Angle of repose of Tablettose® 80 containing 0.5% AEROSIL® R 972 V (●), 0.5% AEROSIL® 200 (♦), 0.5% AEROSIL® 200 VV (▲) and without AEROSIL® (■). Error bars indicate a 95% confidence interval of six measurements.

This observation can be explained by the reduction of the particle size during the mixing process, as shown in Table 3.1. The agglomerates of Tablettose® 80 were destroyed in the plowshare-mixer (130.8 µm) and in the pin mill (23.8 µm), leading to an increase in the adhesion forces between lactose particles, which decreased the flowability and overshadowed the action of AEROSIL®. Moreover, Podczeck (1998) explained that the distribution process of one fine component on the surface of another component during mixing can be disturbed by inherent particle properties such as surface roughness. Larger clefts, which are mainly found on rough surfaces, can act as a mechanical trap for fine particles. Therefore, the agglomerate structure of Tablettose® 80, which has many irregularities and cavities, led to a general reduction of the AEROSIL® action due to the settling of AEROSIL® particles into the cavities. The ANOVA results revealed that there were no statistically significant differences between the AEROSIL® types.

3.2.2   Determination of flowability using a conveyor belt

The flow properties of each mixture were studied using the dynamic conveyor belt method. This method was chosen to simulate the filling process of a die on a rotary tablet press, where the vertical powder flow is superimposed by the horizontal movement of the moving die table. Rey (2003) used the conveyor belt method to differentiate flow properties of tableting mixtures containing pellets of different size ranges and found that this method was more selective than Pfrengle´s funnel.

Mixtures 2 and 4 containing Avicel® PH 101, Starch 1500® or Tablettose® 80 with various AEROSIL® types were investigated to support the angle of repose results. The powder mass accumulating on the balance was plotted versus time. The flow profiles of Avicel® PH 101 mixtures were linear within 6 minutes indicating that the sample flowed continuously out of the funnel (Figure 3.4).
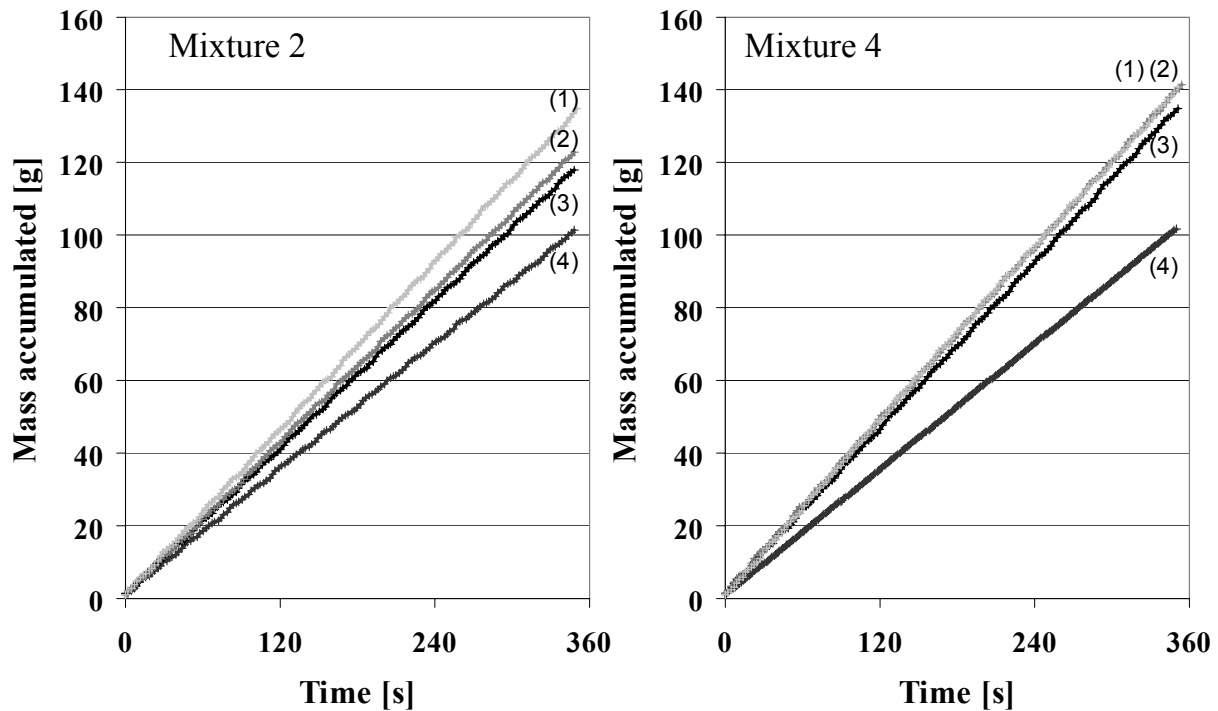
Figure 3.4   Mass accumulated vs. time for mixtures 2 and 4 of Avicel® PH 101 containing 0.5 % AEROSIL® R 972 V (1), 0.5 % AEROSIL® 200 VV (2), 0.5 % AEROSIL® 200 (3) and without AEROSIL® (4).

Starch 1500® without AEROSIL® blocked the orifice of the funnel and therefore no slope was calculated. Statistical analyses (ANOVA and Newman-Keuls test) of the slope of the curves of Avicel® PH 101 and Starch 1500® confirmed the angle of repose results with respect to both the influence of the AEROSIL® type and the mixing conditions. For mixture 2, the flowability improvement ranking for Avicel® PH 101 and Starch 1500® was: AEROSIL® R 972 V > AEROSIL® 200 VV > AEROSIL® 200 > no AEROSIL® (Table 3.2). For mixtures 4, the slopes were significantly higher compared to mixtures 2 for AEROSIL® 200 VV and AEROSIL® 200, while no further increase in flowability was observed for AEROSIL® R 972 V. This reveals that the flowability of mixtures containing AEROSIL® 200 VV and AEROSIL® 200 was strongly influenced by the mixing conditions. A longer mixing time resulted in better powder flow, whereas flowability of AEROSIL® R 972 V was almost independent of mixing time and energy. Similar to the angle of repose, no difference was found for Tablettose® 80 between the three AEROSIL® types in the conveyor belt experiments.

Table 3.2   Analysis of mass accumulation curves of Avicel® PH 101, Starch 1500® and Tablettose® 80 mixtures.

		AEROSIL® R 972 V	AEROSIL® 200 VV	AEROSIL® 200	Without AEROSIL®
Avicel® PH 101	M2 slope	0.3813	0.3500	0.3397	0.2878
	± *s.d.*	0.0017	0.0027	0.0027	0.0010
	M4 slope	0.3947	0.3971	0.3810	0.2661
	± *s.d.*	0.0068	0.0093	0.0057	0.0228
Starch 1500®	M2 slope	0.3915	0.3566	0.3377	-
	± *s.d.*	0.0038	0.0098	0.0040	-
	M4 slope	0.3872	0.3707	0.3696	-
	± *s.d.*	0.0065	0.0050	0.0032	-
Tablettose® 80	M2 slope	0.3545	0.3576	0.3707	0.3182
	± *s.d.*	0.0042	0.0107	0.0044	0.0064
	M4 slope	0.3623	0.3623	0.3737	0.3265
	± *s.d.*	0.0035	0.0035	0.0029	0.0046

3.2.3   Determination of flowability factor using a ring shear tester

The determination of flow function using a ring shear cell was first introduced by Jenike (1964). The flowability was measured with Jenike´s shear cell in an effort to put powder flow studies and hopper design on a more fundamental basis. The flowability factor (ff_c) is defined by the ratio of the consolidating stress or major principal stress at stationary flow (σ_1) and of the unconfined yield strength (σ_c):

$$ff_c = \sigma_1 / \sigma_c$$

The flowability factor is used to classify the flow behavior of bulk solids according to Jenike´s powder classification as shown below.

$ff_c < 1$ non flowing

$1 < ff_c < 2$ very cohesive

$2 < ff_c < 4$ cohesive

$4 < ff_c < 10$ easy flowing

$10 < ff_c$ free flowing.

The meaning of the parameters consolidating stress and unconfined yield stress can be explained by a thought experiment. A bulk powder is in a vertical cylinder being open at upper and lower side, as shown in Figure 3.5. The bulk powder is consolidated by the consolidation stress (σ_1) acting vertically on its top. After completion of consolidation, the cylinder is removed in a frictionless way. Another normal stress is then applied to the column powder. The stress is increased until the consolidated bulk starts to break. The stress causing the breaking is called unconfined failure strength (σ_c).
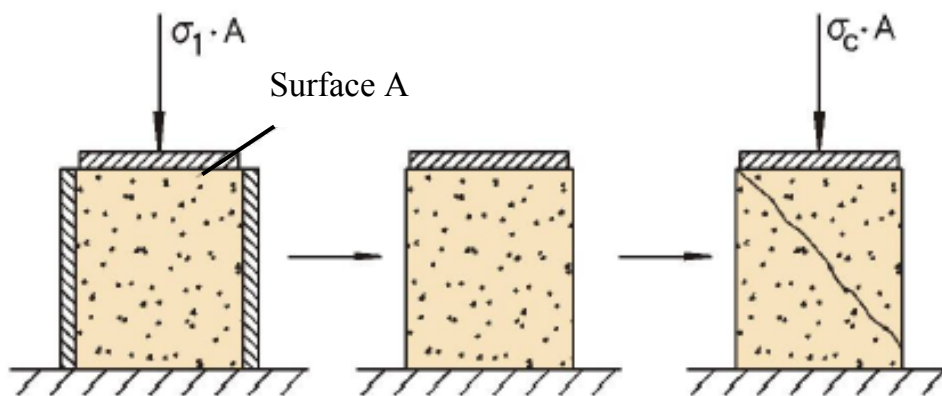
Figure 3.5   Thought experiment to explain the meaning of the parameters consolidating stress σ_1 and unconfined yield strength σ_c. Scheme taken from Schulze (1995).

The shear cell measurement method rapidly outgrew the domain of bulk solid mechanics and found applications in the pharmaceutical field. Crooks et al. (1977) determined the shear cell parameters of 12 pharmaceutical diluents. Nyqvist and Nicklasson (1985) used an annular shear cell to study the flow properties of compressible lactose containing small quantities of drug substances, while Tan and Newton (1990) found a significant correlation between the coefficient of variation of filling weight and the flowability factor for hard gelatine capsules filled with powder. Schwedes (1996) described the flow properties of bulk solids using a flow function. Recently, Ramachandruni and Hoag (2001) designed and validated an annular shear cell for pharmaceutical powder testing.

Mixtures 2 and 4 containing Avicel® PH 101, Starch 1500® or Tablettose® 80 with various AEROSIL® types were investigated using an automatic ring shear tester designed by Schulze (2005).

The flow function as the dependence of the unconfined failure strength on the major consolidation stress at steady state flow is depicted in Figure 3.6 for Avicel® PH 101. Avicel® PH 101 as bulk material exhibited the flow function with the lowest flowability factor (ff_c = 5.6), classified as easy flowing according to Jenike. Upon addition of 0.5% AEROSIL®, Avicel® PH 101 became an easy flowing material with higher flowability factor values [AEROSIL® 200 M2 (ff_c = 7.9) and AEROSIL® 200 VV M2 (ff_c = 7.1)] or even a free flowing material [AEROSIL® 200 M4 (ff_c = 26.6), AEROSIL® 200 VV M4 (ff_c = 24.5), AEROSIL® R 972 V M2 (ff_c = 23.4) and M4 (ff_c = 26.9)]. These results corroborate the previous flowability results with respect to both the influence of the AEROSIL® type and the mixing conditions.
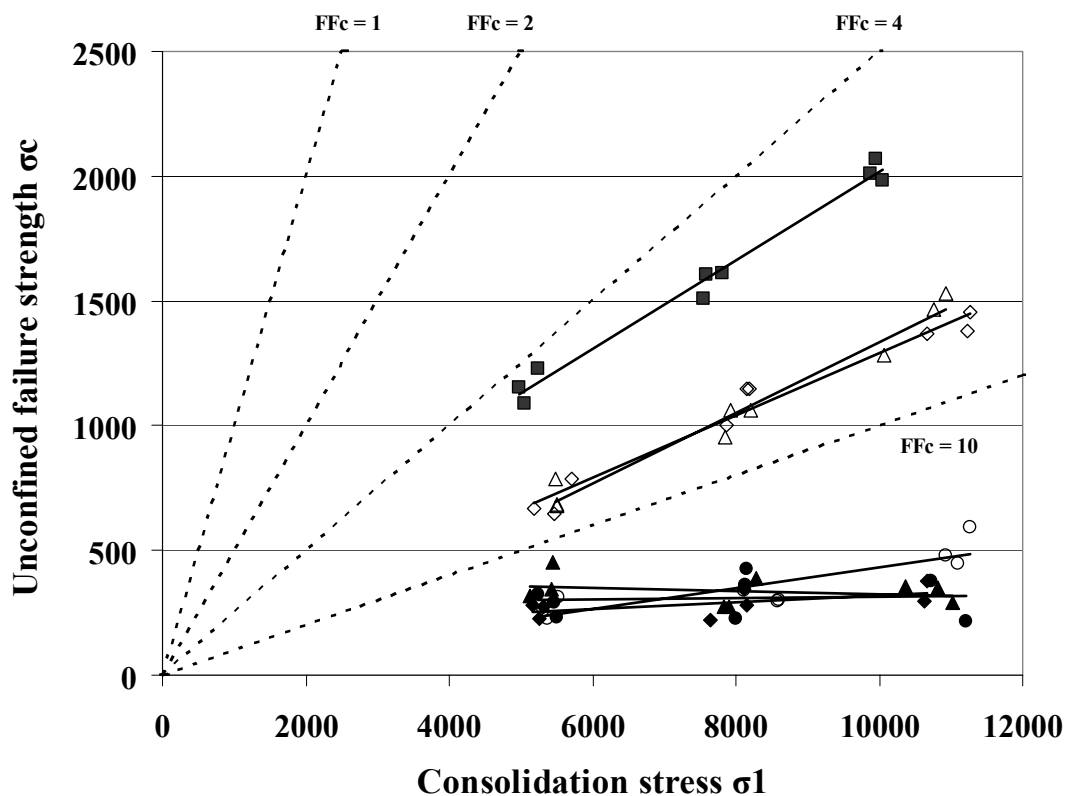
Figure 3.6   Flow function of Avicel® PH 101 containing 0.5% AEROSIL® R 972 V [M2: (○); M4: (●)], 0.5% AEROSIL® 200 [M2: (◊); M4: (♦)], 0.5% AEROSIL® 200 VV [M2: (Δ); M4: (▲)] and Avicel PH® 101 as bulk (■).
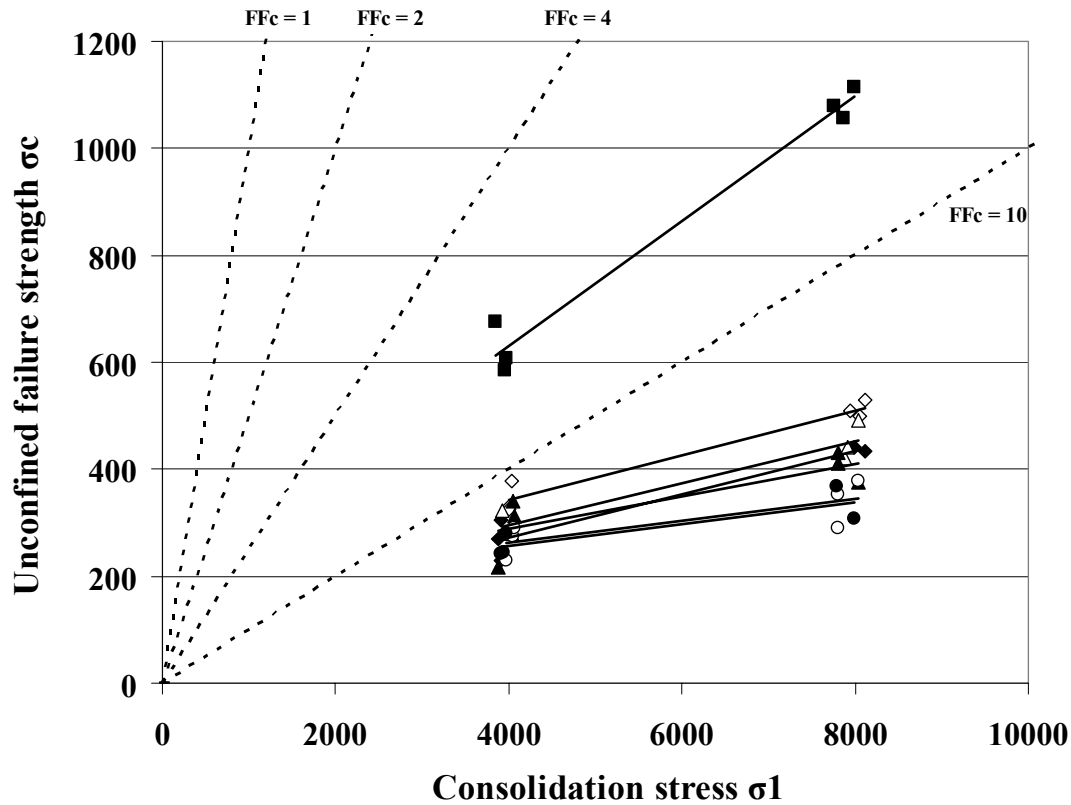
Figure 3.7   Flow function of Starch 1500® containing 0.5% AEROSIL® R 972 V [M2: (o); M4: (●)], 0.5% AEROSIL® 200 [M2: (◊); M4: (♦)], 0.5% AEROSIL® 200 VV [M2: (Δ); M4: (▲)] and Starch 1500® as bulk (■).

Starch 1500® as bulk material showed properties of an easy flowing powder with a flowability factor of 6.8 (Figure 3.7). Upon addition of 0.5% AEROSIL®, Starch 1500® became free flowing. From mixture 2 to mixture 4, the flowability factor of AEROSIL® 200, AEROSIL® 200 VV and AEROSIL® R 972 V mixtures varied from 13.7 to 17.7, from 15.6 to 16.9 and from 19.4 to 18.8, respectively. As for the angle of repose and the conveyor belt results, the ANOVA results showed that the highest flowability factor was obtained with AEROSIL® R 972 V and the mixing conditions had an influence on hydrophilic AEROSIL® types. Nevertheless, the detected differences were smaller compared to the angle of repose and conveyor belt results, probably because the flow functions of all Starch 1500®/AEROSIL® mixtures were in the free flowing region.
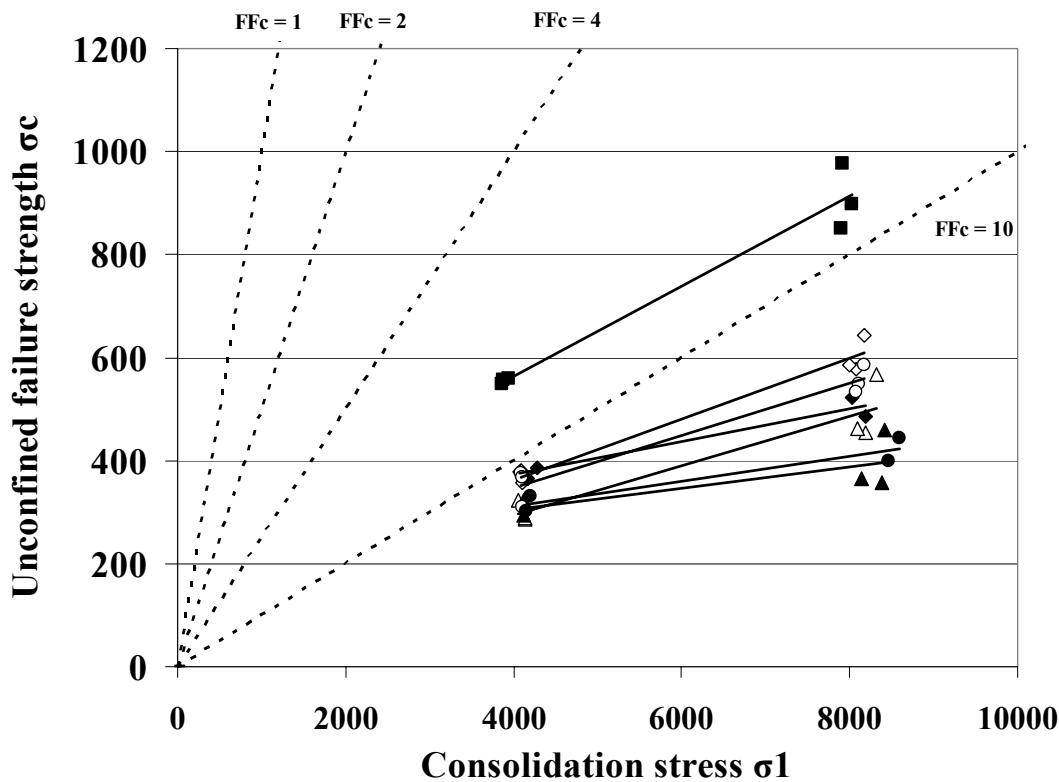
Figure 3.8   *Flow function of Tablettose® 80 containing 0.5% AEROSIL® R 972 V*
[M2: (○); M4: (●)], 0.5% AEROSIL® 200 [M2: (◇); M4: (♦)], 0.5%
AEROSIL® 200 VV [M2: (△); M4: (▲)] and Tablettose® 80 as bulk (■).

Tablettose® 80 as bulk material can be described as easy flowing with a flowability
factor of 7.9 (Figure 3.8). By the addition of 0.5% AEROSIL®, Tablettose® 80 became
a free flowing material but no differences between the three AEROSIL® types were
found.

3.3   *Influence of the chemical nature of colloidal silicon dioxide on*
         flowability

The results of the angle of repose, conveyor belt and ring shear cell investigations
revealed the influence of the mixing conditions and the type of colloidal silicon
dioxide on the flowability of Avicel® PH 101, Starch 1500® and Tablettose® 80.
Among the colloidal silicon dioxide types investigated, AEROSIL® R 972 V was the
most efficient glidant.

Two parameters could be responsible for the better flowability results of AEROSIL[®] R 972 V: first its primary particle size and its BET surface area and second its hydrophobic nature. To investigate the influence of the particle size, surface area and chemical nature, additionally two other AEROSIL[®] products, namely AEROSIL[®] R 974 V and AEROSIL[®] 130 V were selected. AEROSIL[®] 130 and AEROSIL[®] 200 are the starting materials for the synthesis of hydrophobic AEROSIL[®] R 972 and AEROSIL[®] R 974, respectively. Therefore, AEROSIL[®] R 972 and AEROSIL[®] R 974 possess the same physical properties as AEROSIL[®] 130 and AEROSIL[®] 200, respectively but the opposite behaviour towards water (Table 3.3).

Table 3.3   *Physicochemical properties of hydrophilic and hydrophobic colloidal silicon dioxide types.*

	AEROSIL[®] 200	AEROSIL[®] 200 VV	AEROSIL[®] 130 V	AEROSIL[®] R 972 V	AEROSIL[®] R 974 V
Average primary particle size (nm) [a]	12	12	16	16	12
BET surface area (m^2/g) [b]	206	201	138	111	176
Silanol group density (nm^{-2}) [a]	approx. 2	approx. 2	approx. 2	approx. 0.75	approx. 0.75
Behavior towards water	hydrophilic	hydrophilic	hydrophilic	hydrophobic	hydrophobic

[a] Typical values

[b] Batch record, ex-plant

The angle of repose of Avicel[®] PH 101 containing AEROSIL[®] 130 V or AEROSIL[®] R 974 V were measured at mixing conditions 2 and 4. To complete the powder flow characterization, poured and tapped densities of Avicel[®] PH 101 mixtures containing AEROSIL[®] 200, AEROSIL[®] 200 VV, AEROSIL[®] 130 V, AEROSIL[®] R 972 V or AEROSIL[®] R 974 V were evaluated.

3.3.1 Angle of repose

Hydrophobic colloidal silicon dioxide - AEROSIL® R 974 V

The angle of repose of Avicel® PH 101/AEROSIL® R 974 V mixtures was the same as Avicel® PH 101/AEROSIL® R 972 V mixtures. Although AEROSIL® R 974 V possesses identical physical properties to AEROSIL® 200 VV, they showed different flow properties, indicating the influence of the chemical nature of AEROSIL® on the flow-enhancement (Figure 3.9). Avicel® PH 101 mixtures containing hydrophobic AEROSIL® types exhibited lower angles of repose compared to mixtures containing hydrophilic AEROSIL® types, resulting in better flow properties. Mixtures 2 and 4 containing hydrophobic colloidal silicon dioxide showed no statistically significant differences in the angle of repose results and therefore seemed to be independent from the mixing steps.
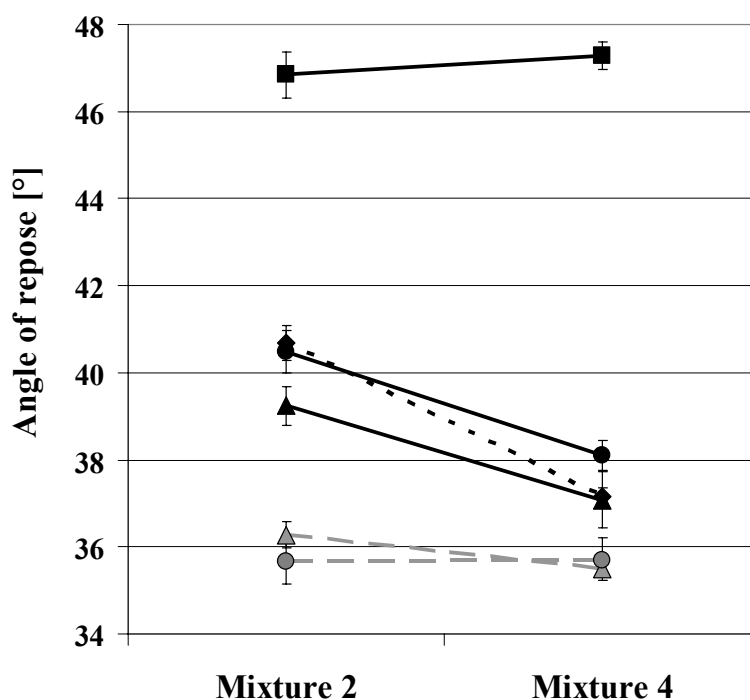
Figure 3.9   Angles of repose of Avicel® PH 101 containing 0.5% AEROSIL® R 974 V (▲), 0.5% AEROSIL® R 972 V (●), 0.5% AEROSIL® 130 V (●), 0.5% AEROSIL® 200 (♦), 0.5% AEROSIL® 200 VV (▲) and without AEROSIL® (■). Error bars indicate a 95% confidence interval of six measurements.

Hydrophilic colloidal silicon dioxide - AEROSIL® 130 V

The angle of repose of Avicel® PH 101/AEROSIL® 130 V mixtures was in the same range as for Avicel® PH 101 containing AEROSIL® 200 VV or AEROSIL® 200. Even though AEROSIL® 130 V has the same primary particle size and approximately the same BET surface area compared to AEROSIL® R 972 V, they showed different flow properties, confirming the decisive role of the chemical nature of AEROSIL® in the flow-enhancement. Mixtures containing hydrophilic AEROSIL® were influenced by the mixing conditions. From mixture 2 (gentle mixing condition in the free-fall mixer) to mixture 4 (forced mixing condition in the plowshare mixer), the angle of repose decreased by 5.5% to 8.7% of the initial values, indicating better flowabilty.

3.3.2 Poured and tapped densities

The results of poured and tapped densities (Figure 3.10) are in good agreement with the results of the angle of repose. Addition of colloidal silicon dioxide increased the tapped density of Avicel® PH 101. The AEROSIL® particles adhering to the Avicel® PH 101 surface reduced the interparticle forces between the Avicel® PH 101 particles and increased the roller friction compared to the sliding friction. During tapping, the Avicel® PH 101 particles moved closer to each other reducing the space between them. The same influence of the chemical nature of AEROSIL® and the mixing conditions was previously observed with the angle of repose. Figure 3.10 is the mirror image of Figure 3.9. The addition of hydrophobic AEROSIL® showed higher tapped densities compared to the addition of hydrophilic AEROSIL® and was not influenced by the mixing conditions.
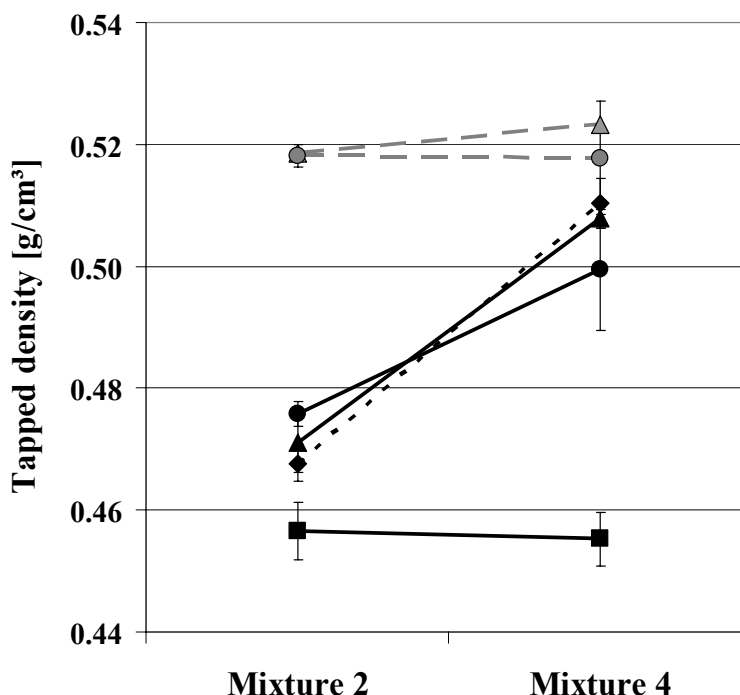
*Figure 3.10   Tapped densities of Avicel® PH 101 containing 0.5% AEROSIL® R 974 V
(▲), 0.5% AEROSIL® R 972 V (●), 0.5% AEROSIL® 130 V (●), 0.5%
AEROSIL® 200 (♦), 0.5% AEROSIL® 200 VV (▲) and without
AEROSIL® (■). Error bars indicate a 95% confidence interval of six
measurements.*

3.3.3   Comparison of hydrophilic and hydrophobic colloidal silicon dioxides

Hydrophobic AEROSIL® types improve the flow properties of Avicel® PH 101 to a
higher extent compared to hydrophilic ones. The introduction of dimethyl-silyl groups
reduces interparticular forces. The primary particle size of the colloidal silicon dioxide
type can not be held responsible for these differences because AEROSIL® 200 VV and
AEROSIL® 130 V have the same primary particle sizes as AEROSIL® R 974 V and
AEROSIL® R 972 V respectively (Table 3.3). Additionally, the flow properties of the
mixtures are not dependent on the surface area and tapped density of the AEROSIL®
types. The results indicate that other factors such as surface chemistry influence the
glidant properties of different colloidal silicon dioxide types.

3.4   Influence of the relative humidity

3.4.1   Water Uptake

One of the advantages of hydrophobic colloidal silicon dioxide, such as AEROSIL® R 972 V, is its non hygroscopic character resulting in a low and relatively constant water content under storage at all humidity levels, while the hydrophilic types adsorb water at higher relative humidities. Because of the low AEROSIL® concentration (0.5%) used in the study presented here, these differences could not be demonstrated in this investigation (Figure 3.11). The water uptake was characteristic for each excipient and ranged from -0.5% to 9.5% for Starch 1500®, from -0.5% to 7.3% for Avicel® PH 101 and from -0.2% to 0.2% for Tablettose® 80, independent on the addition of AEROSIL® or the AEROSIL® type used.
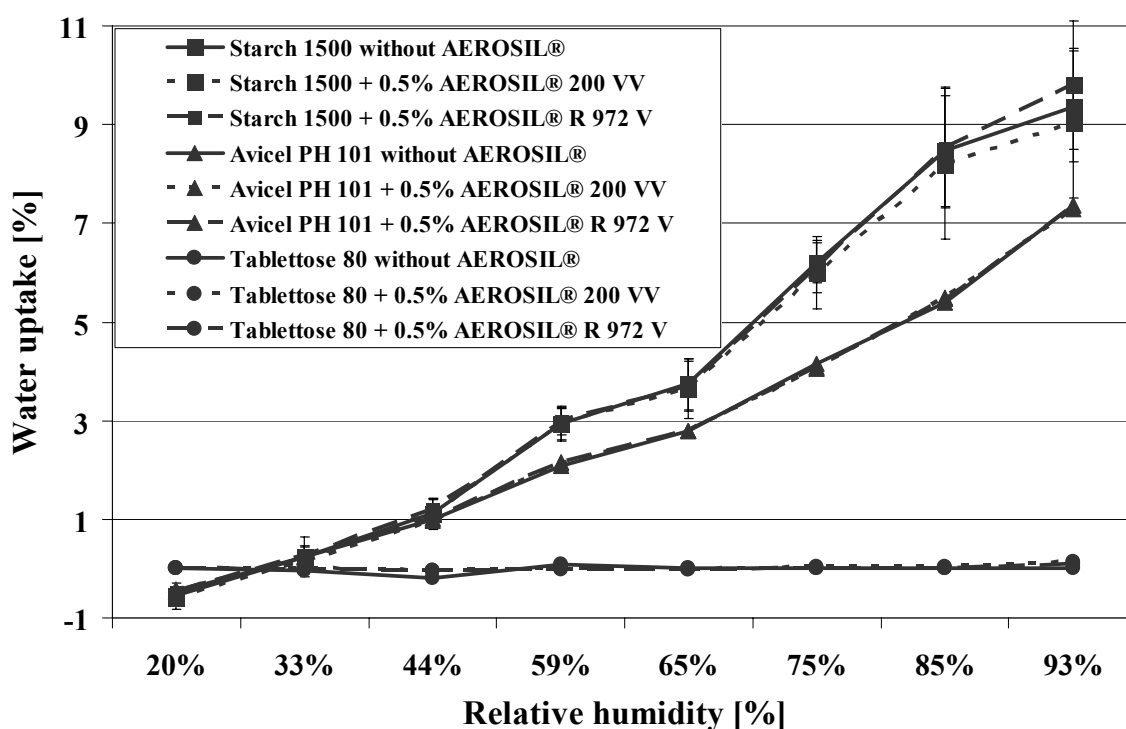
Figure 3.11   Water uptake of mixtures 4 of Starch 1500®, Avicel® PH 101 and Tablettose® 80, without AEROSIL® or containing 0.5 wt% of AEROSIL® 200 VV or AEROSIL® R 972 V, after 18 days storage at different (constant) levels of relative humidity and room temperature. Error bars indicate a 95% confidence interval of three measurements.

3.4.2 Flowability

The angle of repose revealed an interesting positive effect for all AEROSIL[®] types with respect to humidity (Figure 3.12). For each excipient, mixtures without AEROSIL[®] showed a higher angle of repose after 18 days storage in the humidity chamber, i.e. the flowability decreased. Moreover, the higher the relative humidity, the larger the increase in the angle of repose. This can be correlated to the variation of interparticulate forces with humidity. Adhesion forces increase as humidity increases resulting in a larger angle of repose (Schubert 1974, Stephenson and Thiel 1980).

On the other hand, the angle of repose values of mixtures containing 0.5% AEROSIL[®] were hardly influenced by increasing the relative humidity, even though their water uptake was the same as that of mixtures without AEROSIL[®]. In fact, AEROSIL[®] reduced or avoided, depending on the type of excipient, the increase in interparticulate forces. For Avicel[®] PH 101 and Starch 1500[®], there was no difference before and after 18 days in the humidity chambers, even at high relative humidities (Figures 3.12a and 3.12b). For Tablettose[®] 80, angles of repose of mixtures containing 0.5% AEROSIL[®] were generally larger after 18 days, but this increase was small when compared to the mixtures without AEROSIL[®] (Figure 3.12c). These results confirmed that AEROSIL[®] protects the three excipients from a flowability decrease under humid conditions. As described by Chang (1999), AEROSIL[®] acted as a moisture scavenger.

Except for the best flow enhancement, the hydrophobic colloidal silicon dioxide did not show further advantages over the hydrophilic types under the experimental conditions. Smaller angles of repose were observed for Starch 1500[®] and Tablettose[®] 80 mixtures containing the hydrophobic AEROSIL[®] R 972 V at some relative humidity levels, but the differences were not statistically significant.

The decrease in flowability of the pure excipients at increased relative humidities can be explained by the formation of a water film or an increase in capillary condensation between the excipient particles. The addition of colloidal silicon dioxide increases the surface roughness of the excipient particles and to a certain extent the average distance between them. Therefore capillary condensation would not play an important role even

at high relative humidity levels. Hence the mixtures containing colloidal silicon dioxide would retain good flow properties independent on atmospheric moisture.
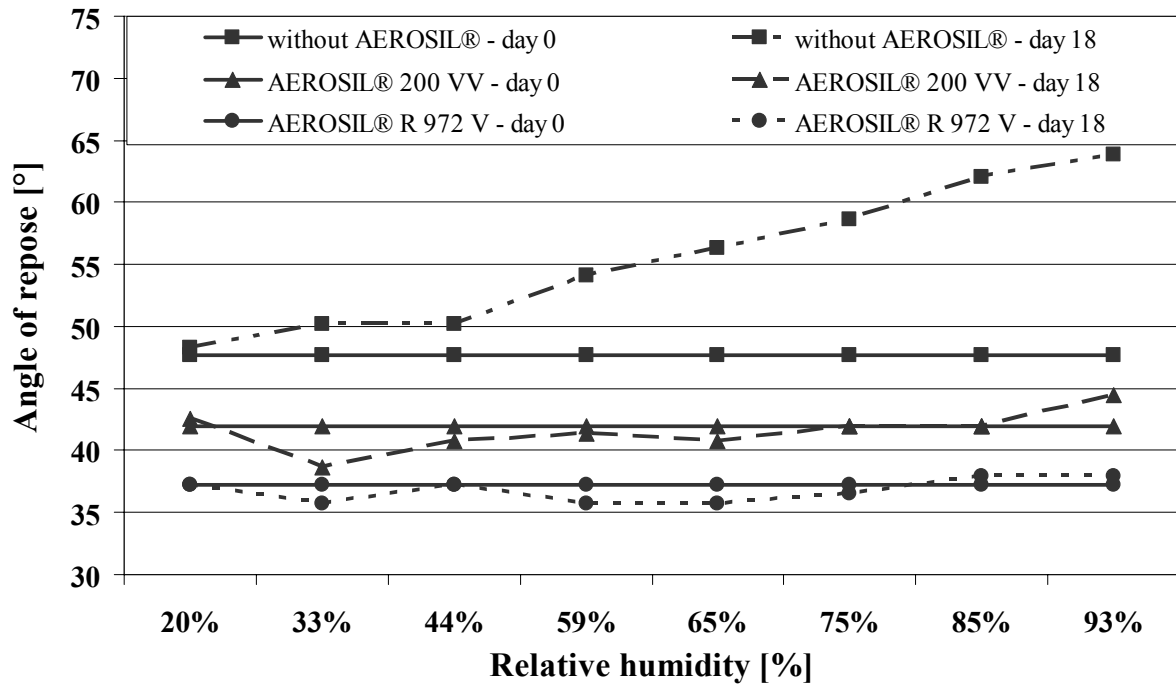
(a)
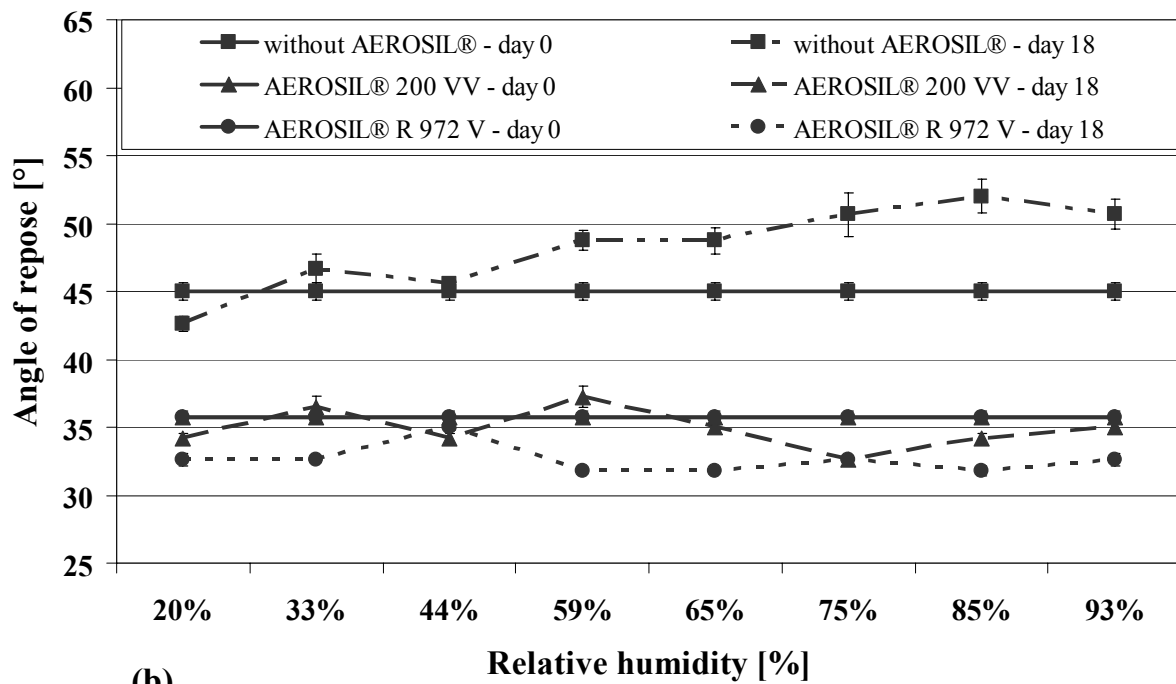
(b)
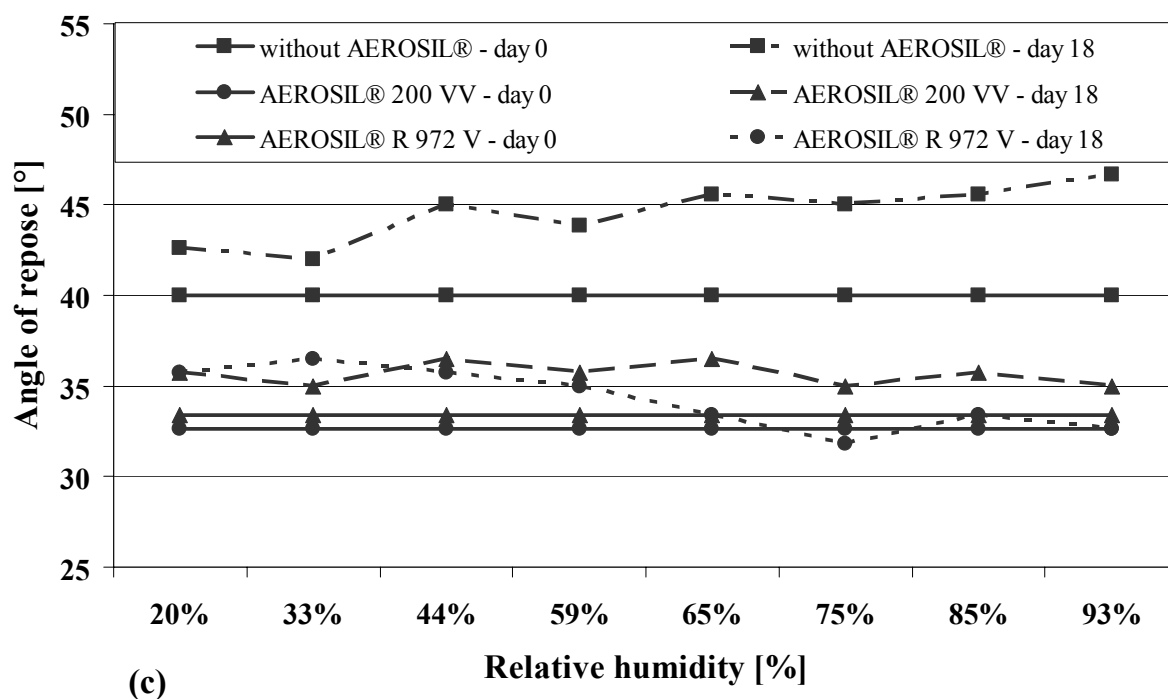
Figure 3.12   Effect of relative humidity on the angle of repose of Avicel® PH 101 (a), Starch 1500® (b) and Tablettose® 80 (c), without AEROSIL® or containing 0.5 % AEROSIL® 200 VV or AEROSIL® R 972 V after 18 days at different levels of humidity. Error bars for Starch 1500® indicate a 95% confidence interval of three measurements.

3.5   Discussion of the results

In this section, the influence of different colloidal silicon dioxide types on the flowability of binary powder mixtures was investigated using microcrystalline cellulose, pregelatinzed starch and α-lactose-monohydrate as model excipients.

The novel types AEROSIL® R 972 V and AEROSIL® 200 VV are efficient glidants. Apart from their handling advantages, compacted colloidal silicon dioxides are even superior to the non-compacted AEROSIL® 200 with respect to their powder flow enhancing properties.

Among the colloidal silicon dioxide types investigated, AEROSIL® R 972 V is the most efficient glidant. Gentle mixing conditions are sufficient to achieve high flowability enhancement with hydrophobic AEROSIL® R 972 V. The increase in

flowability obtained with hydrophilic AEROSIL® 200 VV and AEROSIL® 200 depends on the mixing conditions. Generally, the flowability of Avicel® PH 101 and Starch 1500® mixtures containing hydrophilic colloidal silicon dioxide increases with higher mixing time and energy. Furthermore, the angles of repose correlate well with the mass accumulation curves obtained by the conveyor belt method and the flowability factor obtained by the ring shear tester.

Complementary flowability measurements with AEROSIL® R 974 V and AEROSIL® 130 V were performed to investigate the importance of the chemical nature of AEROSIL®. Compared to the hydrophilic AEROSIL® their hydrophobic analogues are able to improve the flowability of Avicel® PH 101 faster and more intensively. The primary particle size, surface area and tapped density of the colloidal silicon dioxide type are not responsible for these differences. The results indicate that surface chemistry influences the glidant properties of different colloidal silicon dioxide types.

At low glidant concentrations the moisture uptake of the excipients is not influenced by any of the colloidal silicon dioxide types. The water adsorption is characteristic for the pure excipients. However, after equilibrating at high relative humidity levels, all excipient mixtures containing AEROSIL® maintain a good flowability. On the contrary, the flowability of the pure excipients turns strongly cohesive. This proves that the compacted colloidal silicon dioxide types are at least as efficient anti-caking agents as their non-compacted counterparts.

CHAPTER 4

SURFACE ANALYSIS OF BINARY POWDER MIXTURES

BY SCANNING ELECTRON MICROSCOPY AND

X-RAY PHOTOELECTRON SPECTROSCOPY

4.1 Introduction

In the previous chapter, it has been observed that colloidal silicon dioxide improved the flow characteristics in general, but hydrophobic colloidal silicon dioxides were more effective compared to the hydrophilic types under gentle mixing conditions. In order to analyze and elucidate the differences between the colloidal silicon dioxide types on powder flowability, scanning electron microscopy (SEM) images were taken to visualize the degree of colloidal silicon dioxide particle coverage and distribution on the substrate surface.

To support the qualitative SEM images, quantitative X-ray photoelectron spectroscopy (XPS) measurements were performed. XPS was developed in the mid 1960s by Siegbahn and his research group. Siegbahn was awarded the Nobel Prize for Physics in 1981 for his work in XPS (Siegbahn 1986). XPS, also known as electron spectroscopy for chemical analysis, is a surface analysis technique used to obtain chemical information about the surfaces of solid materials. The phenomenon is based on the photoelectric effect outlined by Einstein in 1905, where the concept of photon was used to describe the ejection of electrons from a surface when photons impinge upon it. The XPS technique is highly surface specific due to the short range of photoelectrons that are excited from the solid. The energy of photoelectrons leaving the sample is determined using a concentric hemispherical analyser and this gives a spectrum with a series of photoelectron peaks. The binding energy of the peaks is characteristic of each element. The peak areas can be used (with appropriate sensitivity

factors) to determine the composition of the material´s surface. The shape of each peak and the binding energy can be slightly altered by the chemical state of the emitting atom. Hence, XPS can provide chemical bonding information as well. XPS is not sensitive to hydrogen and helium atoms, but can detect all other elements.

The applications of XPS in the field of material science and engineering are numerous. Analysis of thin contamination of films, measurement of elemental composition of insulating materials and identification of the chemical state are examples. However, only few investigations were reported in the pharmaceutical field to date (Wang et al. 1999, Feng and Huang 2001).

The effect of different colloidal silicon dioxide types on a microscopic level was investigated using Avicel[®] PH 101 mixtures. In addition, Starch 1500[®] mixtures containing different concentration of AEROSIL[®] 200 VV were investigated in order to evaluate the effect of the AEROSIL[®] concentration on flowability and surface coverage. Finally, XPS measurements of Starch 1500[®] were compared to Avicel[®] PH 101 in order to investigate the influence of the excipient´s structure on the distribution of colloidal silicon dioxide agglomerates.

4.2   Surface coverage of Avicel[®] PH 101 by colloidal silicon dioxide agglomerates

4.2.1   Scanning electron microscopy images

Avicel[®] PH 101/AEROSIL[®] mixtures prepared under mixing conditions 2 and 4 were investigated using a scanning electron microscope. This study included AEROSIL[®] 200, AEROSIL[®] 200 VV and AEROSIL[®] R 972 V. Figure 4.1 depicts the corresponding SEM images. Samples were carefully checked to make sure that the differences observed are representative for each particular mixture.
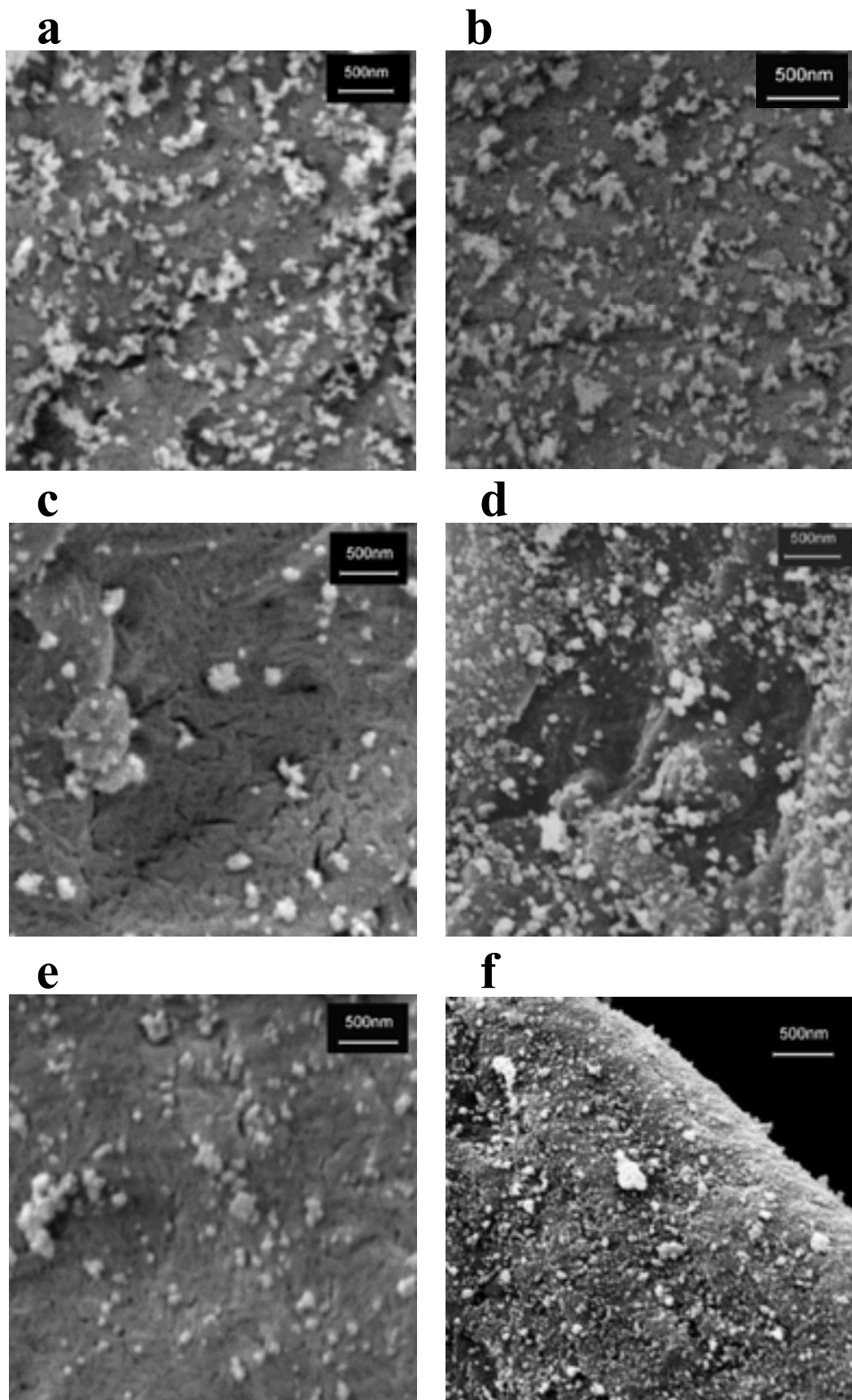
Figure 4.1   SEM images of Avicel® PH 101 containing 0.5% AEROSIL® R 972 V [M2: (a); M4 (b)], 0.5% AEROSIL® 200 [M2: (c); M4: (d)] and 0.5% AEROSIL® 200 VV [M2: (e); M4: (f)]. The bar represents 500 nm.

Comparison of Figures 4.1a, 4.1c and 4.1e shows that the surface of Avicel® PH 101 was covered with small particles of colloidal silicon dioxide (aggregates and agglomerates), however, to varying degrees. The distribution of AEROSIL® R 972 V on the surface of Avicel® PH 101 (Figure 4.1a) was regular, uniform and homogeneous without enrichment of AEROSIL® particles at edges or in cavities. Additional mixing in the plowshare mixer (Figure 4.1b) did not influence the degree and uniformity of coverage of hydrophobic colloidal silicon dioxide.

Although the proportion of colloidal silicon dioxide in the mixture was the same for every sample, the coverage of Avicel® PH 101 was less extensive and the distribution was less homogeneous for mixtures containing hydrophilic colloidal silicon dioxide (Figures 4.1c and 4.1e) compared to hydrophobic type (Figures 4.1a) under mixing condition 2. Furthermore, large AEROSIL® particles of up to 500 nm in size could be detected on the Avicel® PH 101 surfaces or in cavities (Figure 4.2), indicating that the colloidal silicon dioxide agglomerates were not sufficiently broken up.
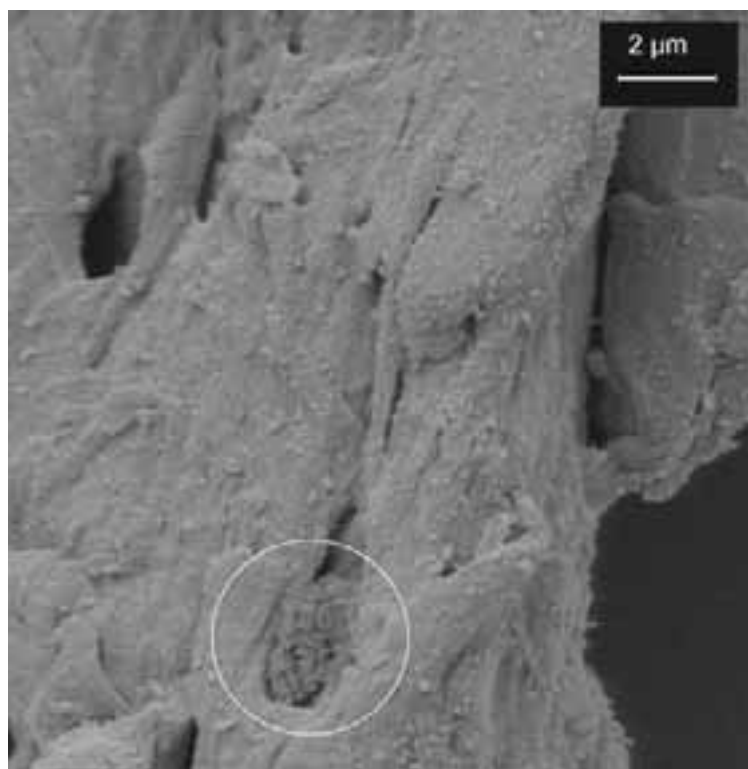
Figure 4.2   SEM images of Avicel® PH 101 containing 0.5% AEROSIL® 200 VV after mixing condition 2. The bar represents 2 µm.

Figures 4.1d and 4.1f show higher degree of dispersion indicating that higher energy mixing conditions were necessary to achieve a homogeneous distribution of hydrophilic colloidal silicon dioxide particles.

The differences in the distribution of colloidal silicon dioxide agglomerates on a substrate surface were also observed by Meyer and Zimmerman (2004). The effect of 0.2% of different glidants, including two hydrophilic AEROSIL® (AEROSIL® 200 and AEROSIL® 300) and two hydrophobic AEROSIL® (AEROSIL® R 805 and AEROSIL® R 812) in binary powder mixtures was investigated using cornstarch as model excipient. SEM images revealed that at three mixing times studied the surface coverage by the hydrophilic AEROSIL® was lower than that one achieved by the hydrophobic type.

4.2.2   X-ray photoelectron spectroscopy analysis

The same sample mixtures as for SEM were investigated in order to measure the degree of dispersion of AEROSIL® on Avicel® PH 101 surface. The evaluation of Si 2p photoelectron signals allowed a quantitative comparison on the shielding of the substrate by AEROSIL® particles (Albers 1998). Table 4.1 shows the results of the quantitative evaluations of the XPS spectra. Amounts of oxygen and carbon additionally to silicium contributed to the total coverage of 100%.

Table 4.1   XPS-Spectra of Avicel® PH 101 alone and of mixtures containing 0.5 % of AEROSIL® R 972 V, AEROSIL® 200 VV and AEROSIL® 200.

Avicel® PH 101 containing	AEROSIL® R 972 V		AEROSIL® 200 VV		AEROSIL® 200		No AEROSIL®
	M2	M4	M2	M4	M2	M4	Bulk
C 1s	29.8	39.5	37.7	27.2	37.0	25.8	43.4
O 1s	63.0	50.2	59.6	64.6	59.8	64.9	56.6
Si 2p	**7.22**	**10.3**	**2.76**	**8.25**	**3.25**	**9.21**	**0.0**

In spite of the given bulk concentration of SiO_2 (0.5%), the values of Si 2p for 0.5 cm^2 of powder surface ranged between 2.76 and 10.3 atomic percent. Due to the high surface selectivity of XPS, samples showing the best dispersion of the colloidal silicon dioxide particles to the substrate could be identified. All samples prepared under mixing condition 4 and samples containing hydrophobic AEROSIL® R 972V showed much higher concentrations of silicon than samples prepared under mixing condition 2. The qualitative impressions and trends suggested by SEM (Figure 4.1) were confirmed by quantitative XPS measurements (Table 4.1).

The actual degree of surface coverage was even higher than shown by the Si 2p signals in Table 4.1. It is necessary to take into consideration the corresponding inorganic oxygen of the SiO_2 particles covering the oxygen- and carbon-containing structures of the organic substrate. This means that in Table 4.1 the inorganic oxygen signal contribution of the SiO_2 particles and the organically bound oxygen of the Avicel® PH 101 added up to the complete O 1s signal. The same holds for the carbonaceous species. Since XPS was not only able to identify and to quantify the presence of different elements but also to identify the different types of chemical bonds, additional information was obtained. Figure 4.3 compares the C 1s signals of the pure cellulose substrate and of a sample covered with AEROSIL® R 972 V (Si 2p value: 10.3%, Table 4.1). Table 4.2 shows the corresponding binding energy values.

Table 4.2   *Results of Gaussian/Lorentzian line shape analyses of the C 1s signal of Avicel® PH 101 containing 0.5% of AEROSIL® R 972 V and without AEROSIL®.*

Avicel® PH 101 containing	No AEROSIL®		AEROSIL® R 972 V	
	eV	%	eV	%
C 1s peak 1	285.3	7	284.5	46
C 1s peak 2	286.8	83	285.9	41
C 1s peak 3	288.8	10	288.0	13
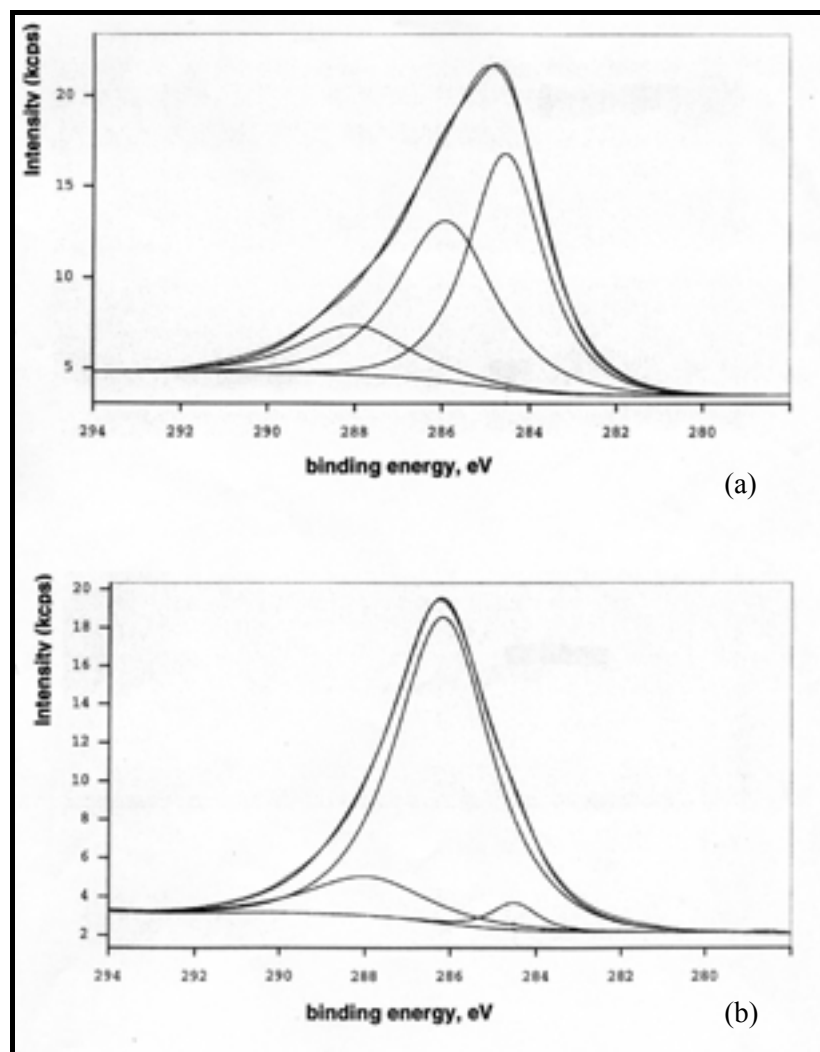
*Figure 4.3   Binding energy values of the carbon atoms of Avicel® PH 101 containing
                0.5% of AEROSIL® R 972 V (a) and no AEROSIL® (b).*

The C 1s signal of pure Avicel® PH 101 was dominated by the peak around 286.8 eV.
With respect to high resolution XPS data reported by Beamson and Briggs (1992), it
follows that the signal at about 285/286 eV was due to CH_X-type functions in side
chains, such as $-CH_2$-CH_3 as known from ethylcellulose or the O-CH_2-CH_2-CH_2-OH
in hydroxypropylcellulose, the signal at about 286/287 eV corresponded to the C
atoms in the ring which are directly connected to the OH-groups and -CH_2-OH and the
signal at about 288/289 eV showed the C atoms bridging oxygen atoms in and between
the rings. This indicates that the binding energy values for the aliphatic carbon species
in cellulose were enhanced due to the numerous adjacent electronegative oxygen
entities.

On the other hand, in case of the AEROSIL® R 972 V-covered material, the aliphatic components, which were enriched in the topmost atomic layers of the silica particles that shield the Avicel® PH 101 substrate, were selectively detected by means of XPS. The binding energy values of these carbon atoms were detected at lower binding energy (Figure 4.3). The Gaussian/Lorentzian line shape analyses, as summarized in Table 4.2, show that 46% of the detected surface-carbon on the Avicel® PH 101/ AEROSIL® R 972 V sample was purely aliphatic (-CH$_3$).

XPS could differentiate between aliphatic carbon entities of the cellulose substrate and the aliphatic chains in the topmost atomic layers of the finely dispersed particles of silanized silica such as AEROSIL® R 972 V. It can be measured how much of the aliphatic carbon at the surfaces of the modified Avicel® PH 101 samples may contribute to hydrophobic conditions (CH$_2$-chains without adjacent oxygen atoms, at 285 eV binding energy and less) and to hydrophilic conditions (CH$_2$-entities of the cellulose rings). The difference between the C 1s peak 2 of Avicel® PH 101 and Avicel® PH 101 containing 0.5 % AEROSIL® R 972 V gave the exact surface coverage of AEROSIL® R 972 V on Avicel® PH 101, i.e. 42 %, corresponding to a 10.3 % surface coverage given by Si 2p (Table 4.1) and to the qualitative impression of Figure 4.1b.

4.2.3   Influence of the chemical nature of colloidal silicon dioxide on surface coverage

SEM and XPS analyses indicated that the degree and uniformity of coverage of the AEROSIL® R 972 V on the Avicel® PH 101 surface was higher and independent from the mixing conditions when compared to AEROSIL® 200 and AEROSIL® 200 VV. This observation can be explained by the nature of AEROSIL®. The primary particles of colloidal silicon dioxide are not isolated but are fused together in relatively stable chain-like aggregates, which in turn form larger agglomerates. The prevailing forces within the agglomerates are hydrogen bonds. The silanol groups react with organosilicon compounds to create hydrophobic AEROSIL® as shown in Figure 4.4. In this, the density of silanol groups per nm^2 decreases from 2 to 0.75 (Chapter 2,

Table 2.1). Consequently the hydrogen bonds within the agglomerates of hydrophobic AEROSIL® are fewer, leading to softer agglomerates compared to the hydrophilic types. Agglomerates of hydrophobic AEROSIL® are therefore easily broken up and reach their final size and optimum distribution already under gentle mixing conditions (mixture 2), while higher energies of mixing (mixture 4) are required to break up agglomerates of hydrophilic AEROSIL® in order to achieve uniform coverage.
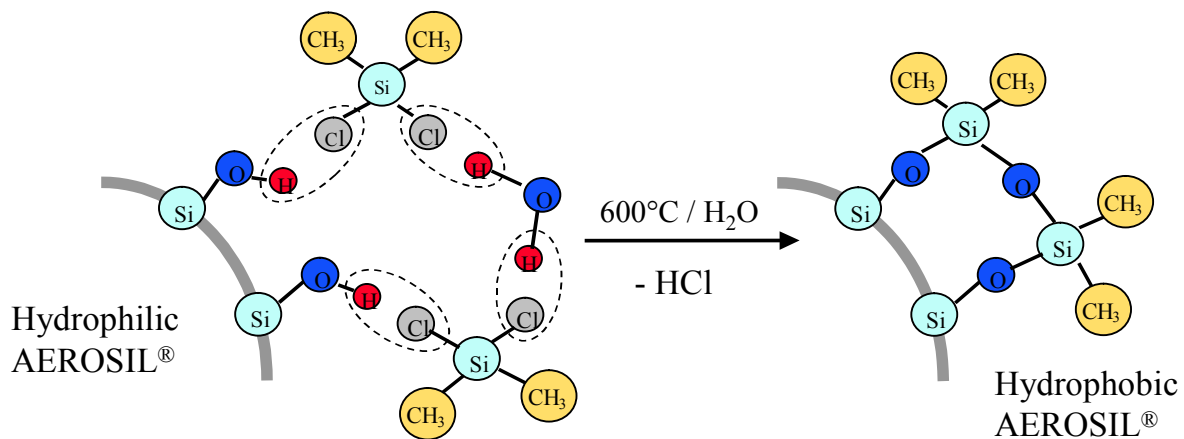
Figure 4.4   Hydrophobic treatment of AEROSIL®.

A study of Fuji et al (1999) confirmed this hypothesis in comparing the adhesion force of non porous amorphous silica particles (Adma fine SO-C5) before and after hydrophobic treatment by different concentrations of hexamethyldisilazane. The silanol and trimethylsilyl group densities of the silica particles were evaluated and the adhesion force between two silica particles were measured using an atomic force microscope. Measurements performed between 40–60% r.H. showed that the adhesion force between two silica particles decreased as the silanol group density decreased. This result is in accordance with a study of Barthel (1995), who found that a silica surface exhibited higher surface energy than silylated hydrophobic silica due to the reduced silanol groups.

4.2.4 Correlation between surface coverage and angle of repose

The degree of coverage observed qualitatively by SEM images correlated to the flow-enhancement. XPS investigations confirmed this trend. Although, there was no linear correlation between the angle of repose and the Si 2p values, two clusters were formed when correlating the two parameters as shown in Figure 4.5. One cluster contained the mixtures 2 with AEROSIL® 200 and AEROSIL® 200 VV at high angles of repose and low Si 2p values, while the other represented all mixtures 4 and the mixture 2 of AEROSIL® R 972 V at low angles of repose and increased AEROSIL® coverage (higher Si 2p values).
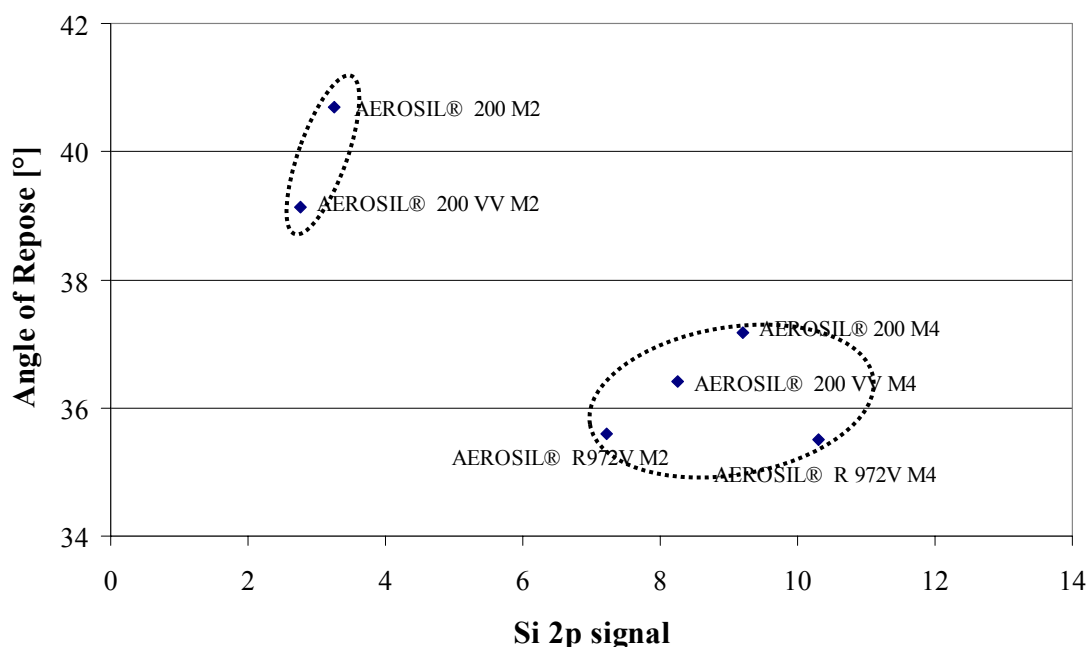
Figure 4.5   *Correlation of angle of repose and XPS Si 2p signal intensity of Avicel®*
              PH 101/ AEROSIL® mixtures.

SEM and XPS studies provide an explanation for the flow-enhancement and the sensitivity of the various AEROSIL® types to the mixing steps. AEROSIL® R 972 V provided the best flow-enhancement of Avicel® PH 101 compared to AEROSIL® 200 VV and AEROSIL® 200 due to its high degree of coverage. A higher degree of coverage allowed a better action of the glidant particles. Avicel® PH 101 containing 0.5% AEROSIL® R 972 V showed equal angle of repose values for mixture 2 and mixture 4, as the degree of coverage of AEROSIL® R 972 V in both mixtures was the

same. Under mixing condition 2, the agglomerates of AEROSIL[®] R 972 V have reached their final size and optimum distribution. Hence the high speed mixer (mixture 4) showed no increase in the degree of coverage. The hydrophobic agglomerates were rapidly broken down and a stable distribution of AEROSIL[®] R 972 V resulted. For hydrophilic AEROSIL[®], the angle of repose of Avicel[®] PH 101 containing AEROSIL[®] 200 VV and AEROSIL[®] 200 decreased because the degree of coverage of AEROSIL[®] increased through the additional mixing.

Ohta et al. (2004) investigated different types of silica particles and suggested that the optimum mixing ratio, leading to the best Carr´s index, was closely related to the surface coverage of filler by glidant. Meyer and Zimmerman (2004) and Zimmermann et al. (2004) reported that the effectiveness of a nanomaterial to act as a glidant correlated to its degree of coverage on the excipient particle. An increase in surface coverage with increased mixing time resulted in decreasing tensile strength.

4.3   Surface coverage of Starch 1500[®] by AEROSIL[®] 200 VV

Figure 4.6 depicts the influence of the AEROSIL[®] 200 VV concentrations on the angle of repose of Starch 1500[®] under two different mixing conditions. As expected, addition of colloidal silicon dioxide improved the flowability of Starch 1500[®]. Under mixing condition 2, with increasing AEROSIL[®] 200 VV concentration, the angle of repose continuously decreased, reaching its minimum value of 33.8° at 0.25% AEROSIL[®] 200 VV, and then increased to 38.8° with 1% AEROSIL[®] 200 VV. Under mixing condition 4, the course of the angle of repose as a function of the colloidal silicon dioxide concentration was almost parallel to mixing condition 2, resulting in a optimum between 0.125 and 0.25%. Nevertheless, the angle of repose values were lower, indicating better flowability due to additional mixing.
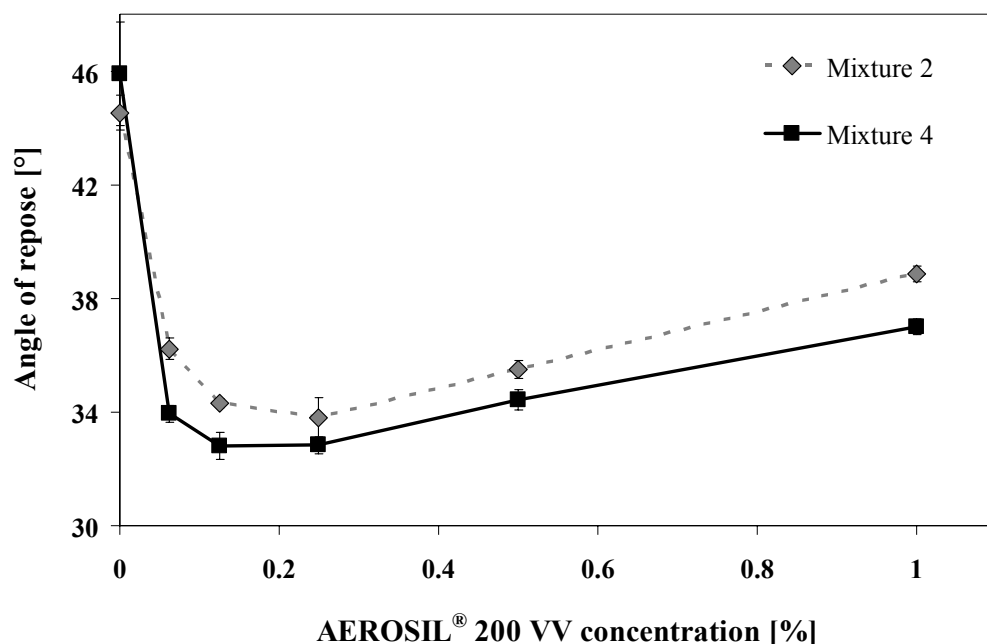
Figure 4.6   Effect of AEROSIL® 200 VV concentration and mixing conditions on the angle of repose of Starch 1500® mixtures. Error bars indicate the 95 % confidence interval of six measurements.

In order to elucidate the differences in the influence of the AEROSIL® 200 VV concentration, XPS measurements were performed to determine the degree of AEROSIL® particle coverage and distribution on Starch 1500® surface (Figure 4.7).
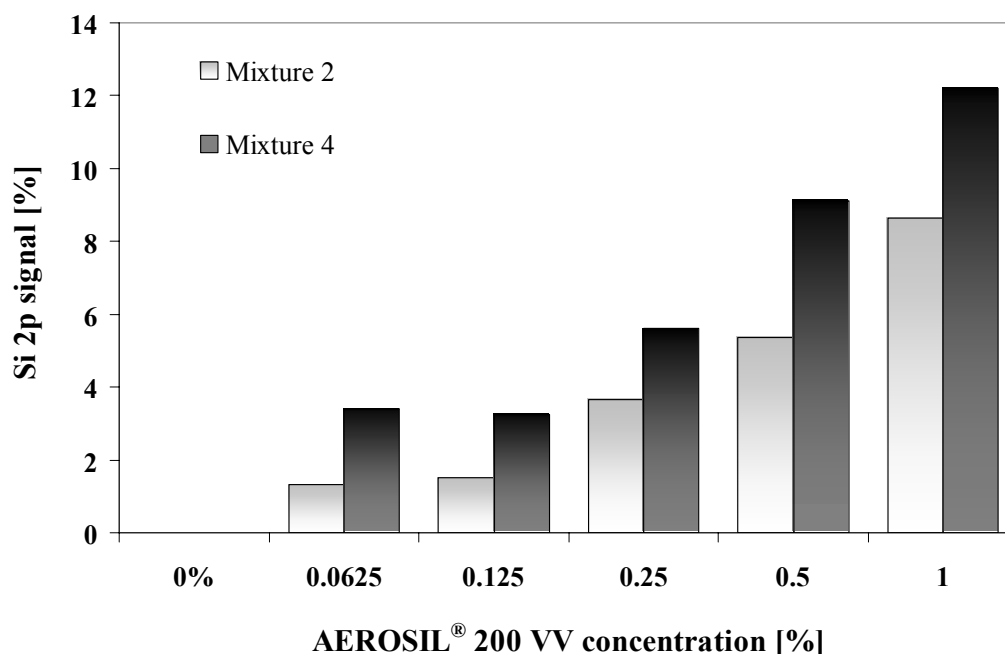
Figure 4.7   Si 2p signals of Starch 1500® mixtures in dependence of the AEROSIL® concentration and mixing process.

With increasing AEROSIL® 200 VV concentration, the Si 2p signal increased, i.e. the degree of coverage of Starch 1500® surface by AEROSIL® particles increased. Furthermore, for a given AEROSIL® concentration, samples prepared under mixing condition 4 showed higher concentration of silicium compared to mixing condition 2. As described before, agglomerates and aggregates of AEROSIL® 200 VV were further destroyed through additional mixing. Consequently, a greater number of smaller agglomerates and aggregates of AEROSIL® 200 VV were available to cover the surface of Starch 1500®. This better coverage reduced the interparticle adhesion force between the Starch 1500® particles, leading to a reduction of the angle of repose.
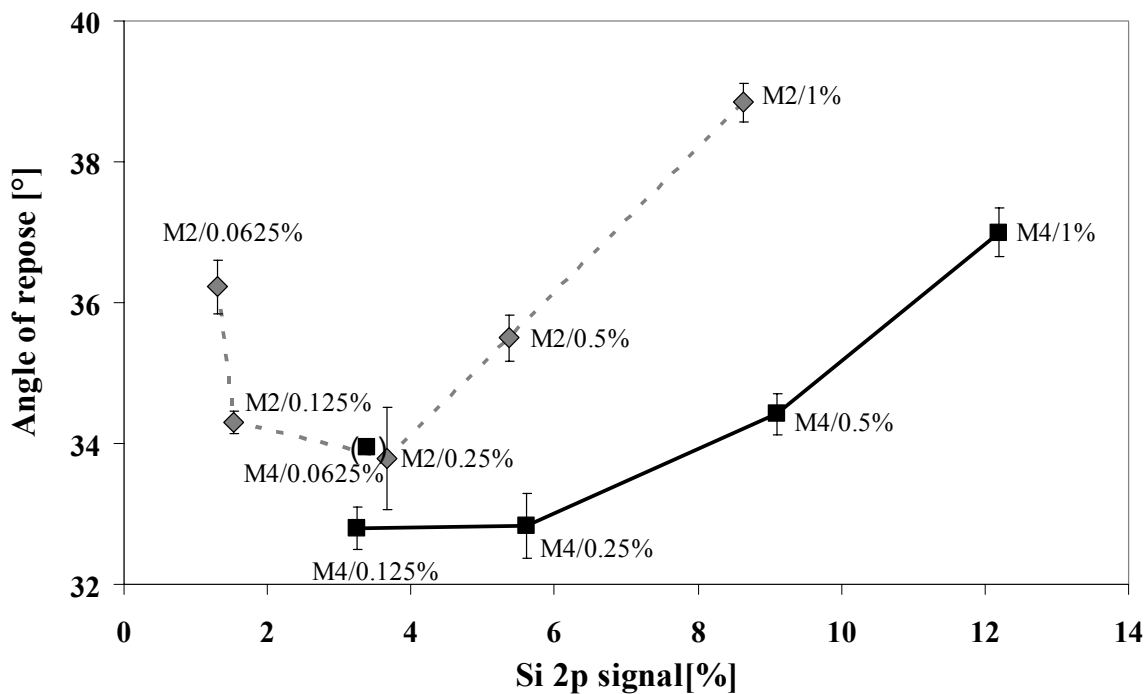
*Figure 4.8   Angle of repose as a function of the Si 2p signal of Starch 1500®
mixtures. Error bars indicate the 95 % confidence interval of six
measurements.*

Figure 4.8 shows the angle of repose as a function of the surface coverage (Si 2p signals). The Si 2p signals revealed that higher AEROSIL® concentration resulting in higher AEROSIL® particle coverage did not automatically lead to a lower angle of repose. Mixture 2 containing 1% AEROSIL® and mixture 4 containing 0.5% AEROSIL® showed approximately the same Si 2p values (8.63% for M2/1% and 9.1%

for M4/0.5%) but a huge difference in the angle of repose (38.8° for M2/1% and 34.4° for M4/0.5%). The mixture containing the lowest AEROSIL® concentration showed best flowability, indicating that the size of the agglomerates plays a key role in the flow-enhancement. The AEROSIL® agglomerates of the mixture containing 0.5% AEROSIL® were smaller (through additional breaking up in the plowshare mixer) in order to reach the same degree of coverage as the mixture containing 1% AEROSIL®. As described by Rumpf (1974), the smaller the particles adsorbed on the surface, the stronger the reduction of the van der Waals forces and the better the flow-enhancement. These findings are supported by comparing mixture 2 containing 0.5% AEROSIL® and mixture 4 containing 0.25% AEROSIL®.

4.4   Influence of the excipient´s structure on the distribution of colloidal silicon dioxide agglomerates

Assuming that surface coverage of an excipient by a glidant is the dominating factor in flow enhancement of powders, there should be a correlation between the surface of the excipient and the required amount of colloidal silicon dioxide to achieve a certain degree of flowability under defined mixing conditions. Avicel® PH 101/AEROSIL®- and Starch 1500®/AEROSIL® mixtures containing the same amount of colloidal silicon dioxide based on the surface area of the excipient were compared. The BET surface area of Avicel® PH 101 was 4 times higher compared to Starch 1500® (Table 4.3). Therefore, mixtures 2 and 4 of Starch 1500® and Avicel® PH 101 containing 0.125 and 0.5 wt% AEROSIL® 200 VV, respectively, were investigated.

Table 4.3   BET surface area of Avicel® PH 101 and Starch 1500®

	Avicel® PH 101	Starch 1500®
BET surface area [m²/g]	1.238	0.307

XPS measurements did not provide the expected identical AEROSIL® coverage (Table 4.4). The Si 2p signal of Avicel® PH 101/AEROSIL® mixtures was higher compared

to Starch 1500®/AEROSIL®, indicating a better degree of coverage and dispersion of AEROSIL® 200 VV on the Avicel® PH 101 surface. This difference could be explained on one hand by the surface area measurements and on the other by the affinity of AEROSIL® to the excipient surface.

Table 4.4   *Si 2p values of Avicel® PH 101 containing 0.5% AEROSIL® 200 VV and Starch 1500® containing 0.125% AEROSIL® 200 VV.*

	Avicel® PH 101	*Starch 1500®*
Si 2p signal mixture 2	2.76	1.52
Si 2p signal mixture 4	8.25	3.24

Scanning electron micrographs have shown that Avicel® PH 101 has a matchstick-like or rod-like structure composed of fibrils with radius of 10-15 nm (Bolhuis and Chowan 1996). Due to this structure, surfaces of cavities were not attainable by AEROSIL® agglomerates but were included into the BET surface measurement. Therefore, the 1.238 m²/g of Avicel® PH 101 was an overestimated surface reachable by AEROSIL® agglomerates. Furthermore, XPS as a short range method is able to detect the signal of SiO_2 on planes and edges, the cavities and pores free from AEROSIL® agglomerates were not detected during the measurement, leading to higher Si 2p signals than expected. In contrast, Starch 1500® consists of individual nearly round particles and aggregates thereof bonded by hydrolyzed starch showing a smooth surface. Therefore the 0.307 m²/g is a realistic attainable surface area for the AEROSIL® agglomerates and detectable by XPS measurement.

With respect to high resolution XPS data reported by Beamson and Briggs (1992), it follows that the signal at about 285/286 eV was due to CH_X-type functions in side chains, the signal at about 286/287 eV corresponded to the C atoms in the ring which are directly connected to the OH-groups and the signal at about 288/289 eV showed the C atoms bridging O atoms in and between the rings.

Table 4.5 shows the binding energy values for Starch 1500® and Avicel® PH 101. Although the two substrates are based on glucose monomers, XPS measurements

revealed that for Avicel® PH 101, the Gaussian/Lorentzian line shape analyses of the C 1s signal was dominated by the peak at about 286/287 eV (83%), while for Starch 1500® this signal was only 44%. The Starch 1500® signal at 285/286 eV was with 39% in the same order of magnitude, while the corresponding Avicel® PH 101 signal was only 7%. The differences were due to the stereochemical configuration of the monomer units. In Avicel® PH 101, the glucose units are linked by β-1,4-glucosidic bonds, forming a long straight-chain molecular structure. Starch 1500® comprises amylose, consisting of glucose linked by α-1,4-glucosidic bonds (forming a helix of 6 glucose units), and amylopectin, consisting of glucose units linked by α-1,4-glucosidic bonds in the linear part and branched by α-1,6-glucosidic bonds (Tänzer 2000). The outer envelope of Starch 1500® consists mainly of amylopectin (Ammon 2004), leading to a branched-chain molecular structure detectable by XPS and attainable for the adhesion of AEROSIL® agglomerates.

Table 4.5   *Results of Gaussian/Lorentzian line shape analyses of the C1s signal of pure Avicel® PH 101, Starch 1500® and two native starches.*

	Avicel® PH 101		Starch 1500®		Native starch (commercial sample)		Extra white maize starch	
	eV	%	eV	%	eV	%	eV	%
C 1s peak 1	285.3	7	285.6	39	285.1	45	285.5	47
C 1s peak 2	286.8	83	287.2	44	286.8	38	287.1	37
C 1s peak 3	288.8	10	289.9	17	288.4	17	288.7	16

The C1s signal of Avicel® PH 101, was dominated by the peak around 286/287 eV corresponding to the C atoms in the ring which are directly connected to the OH-groups. Through the straight-chain structure, a large number of OH-groups is present on the surface of Avicel® PH 101 attracting AEROSIL® agglomerates by hydrogen bonds. For Starch 1500®, the C1s signal around 286/287 eV was lower. Due to the branched-chain molecular structure of Starch 1500®, the OH-groups, being present at its surface and attainable for AEROSIL® agglomerates, were lower. Therefore, the difference in the outer molecular structure resulted in higher anchor possibilities on the

Avicel® PH 101 surface compared to Starch 1500®, leading to a better degree of coverage of AEROSIL® 200 VV on the Avicel® PH 101 surface. The results of Gaussian/Lorentzian line shape analyses of the C 1s signal of Starch 1500® were confirmed by the analysis of two other starches (Table 4.5).

4.5   Discussion of the results

SEM and XPS analyses of mixtures containing microcrystalline cellulose and AEROSIL® show a correlation between the degree and uniformity of coverage of the colloidal silicon dioxide particles on the excipient's surface and the flow enhancement exerted by the glidant. The higher the extent of coverage, the better the flow enhancement.

Surface analyses show that agglomerates of AEROSIL® R 972 V reach their final size and optimum distribution already under gentle mixing conditions, while higher mixing energies are required to break up the agglomerates of both AEROSIL® 200 and AEROSIL® 200 VV in order to achieve a uniform coverage. The hydrophobic agglomerates are softer compared to the hydrophilic ones, due to the lower silanol group density on its surface. Therefore, they are easier to break up and faster distributed on Avicel® PH 101 surface. In consequence, the higher number of adsorbable hydrophobic agglomerates leads to lower angle of repose results, i.e to better flow enhancement.

Furthermore, the angle of repose and XPS investigation of Starch 1500® mixtures containing different concentration of AEROSIL® 200 VV reveal that the size of the agglomerates plays a key role in the flow-enhancement. When the extent of coverage is identical, smaller agglomerates are more effective in enhancing flowability.

A comparison between Starch 1500® and Avicel® PH 101 based on XPS and specific surface area results shows that the excipient's surface influences the action of the glidant.

CHAPTER 5

ADHESION FORCE MEASUREMENTS

BY ATOMIC FORCE MICROSCOPY

5.1   Introduction

After having visualized the colloidal silicon dioxide particle (aggregates and agglomerates) coverage and distribution on the excipient´s surface, the interparticulate forces within the powder mixture were determined to complete the characterization of the glidant action. Techniques used for the determination of interparticulate forces include the vibration method, the centrifuge technique, and the impact separation method (Podczeck 1998, Podczeck and Newton 1995, Lam and Newton 1991). These methods determine the adhesion force by measuring the proportion of drug particles that detach from a surface at a given force. They are not applicable to AEROSIL$^{®}$ due to the small diameter of the agglomerates and the resulting high adhesion forces.

Atomic force microscopy (AFM) presents an alternative technique. The adhesion force is determined using single particle detachment. AFM was developed by Binning et al. (1986) to overcome the limitations of scanning tunnelling microscopy in achieving atomic resolution of metals and semiconductors. It enables high-resolution topographical imaging of surfaces and records fundamental properties of sample surfaces. By mounting a particle to a cantilever, AFM permits the measurement of forces between this specific particle and a substrate surface. For this purpose, the probe particle is glued to the end of a microfabricated cantilever and the substrate is attached to the flat surface on the AFM piezoelectric transducer, which is used to change the relative position between the particle and the substrate. The cantilever deflection is recorded as it interacts with the moving substrate and is converted into an interaction force. Interaction forces can be studied over a wide range of environmental conditions such as temperature, humidity, and gas atmosphere.

AFM has paved the way for new experiments. The applications are numerous and concern various fields including physics, biophysics, biochemistry, microelectronics and metallurgical engineering (Finot et al. 1999, Mueller et al. 1999, Gillies et al. 2002, Agache et al. 2002). Recently, AFM has found application in the pharmaceutical field by determining the interaction forces between a single particle of crystalline lactose and a lactose tablet (Sindel and Zimmerman 2001). Additional studies have been reported on lactose, especially for inhalation therapy. Heng et al. (2000) evaluated the surface roughness of four lactose carriers. Ibrahim et al. (2000) measured the adhesion force of individual lactose particles to the surface of gelatine capsules. Begat et al. (2003 and 2004) examined the influence of milling on the surface stability of salbutamol sulphate. Louey et al. (2001) investigated the adhesional properties of nine lactose carriers, while Eve et al. (2002) ranked the interaction forces between micronized salbutamol particles and glass, lactose and a fluoropolymer. Furthermore, AFM has been used under controlled atmosphere to characterize the effect of humidity on drug-drug interactions and on adhesion forces between lactose monohydrate and micronized zanamivir (Young et al. 2003, Bérard et al. 2002) In addition, Wang et al. (2003) has used AFM to model adhesion phenomena in tablet compression. To date, AFM investigations on the effect of glidants have been reported by Otsuka (1998), Fuji et al. (1999), Weth et al. (2001) and Ohta et al. (2003).

The purpose of this chapter is to measure and compare the interparticulate forces within Avicel® PH 101 mixtures in determining adhesion forces between an Avicel® PH 101 functionalized cantilever (Avicel® PH 101 probe) and Avicel® PH 101/AEROSIL® mixtures or Avicel® PH 101 as bulk.

5.2   Determination of interparticulate forces within Avicel® PH 101/ AEROSIL® mixtures using an atomic force microscope colloid probe

5.2.1 Determination of the cantilever spring constant

As described in chapter 7 (7.7.10), the cantilever spring constant was determined using a dynamic method (Cleveland et al. 1993). The diameter of a glass sphere of known density (ρ = 2500 kg/m^{-3}) was determined using a stage microscope and was found to be 30 µm. The change in resonance frequency of the cantilever with and without the added glass sphere was then measured using an atomic force microscope. The loaded and unloaded resonance frequencies were 47.24 kHz and 12.47 kHz, respectively. As the spring constant is proportional to the cube of the unloaded resonant frequency, it can be calculated using the following equation:

$$ k = \frac{\frac{2}{3}\pi^3 \rho \left(-d_0^3\right)}{\frac{1}{f_0^2} - \frac{1}{f_1^2}} \qquad\qquad k = \frac{\frac{2}{3}\pi^3 2500 \left(-0.00003^3\right)}{\frac{1}{47240^2} - \frac{1}{12470^2}} $$

$$ k = 0.2332 \ \ N/m $$

where,   k: the spring constant (N/m)
             ρ: density of the glass sphere (kg/m³)
             f_0: loaded resonance frequency (Hz)
             f_1: unloaded resonance frequency (Hz)
             d_0: diameter of the glass sphere (m)

The calculated spring constant was in the same range as reported in previous AFM colloid probe studies performed in the pharmaceutical field: Tsukada et al. (2004), Bérard et al. (2002), Weth et al. (2001), Sindel and Zimmerman (2001), Louey et al. (2001), Wang et al. (2002), Young et al. (2002) and Ibrahim et al. (2000) used a cantilever with a spring constant ranging from 0.12 to 0.58 N/m.

5.2.2 Control of the Avicel[®] PH 101 functionalized cantilever

To be sure that the Avicel[®] PH 101 functionalized cantilever remained uncontaminated and intact during the course of the experiments, the particle integrity was examined under an optical microscope after each measurement cycle and the 300-500 values from each single run were evaluated in order to ascertain whether a systematic increase or decrease due to a change in the surface of the Avicel[®] PH 101 probe had occurred. In all experiments, no systematic time dependent variation between single values within a run was detected, and the optical observation indicated no change of the Avicel[®] PH 101 probe surface.

5.2.3 Analysis of the adhesion force measurements

The adhesion force measurements including AEROSIL[®] 200, AEROSIL[®] 200 VV and AEROSIL[®] R 972 V were performed between an Avicel[®] PH 101 functionalized cantilever and Avicel[®] PH 101/AEROSIL[®] mixtures or Avicel[®] PH 101 as bulk. Other alternative configurations used to investigate glidants with an atomic force microscope colloid probe are reported in the literature. Fuji et al. (1999) and Weth et al. (2001) glued a silica particle ($\varnothing = 1.7$ μm and $\varnothing = 110$ μm, respectively) onto the cantilever and another on a flat silicon plate, while Ohta et al. (2003) measured the adhesion force between a silica particle ($\varnothing = 0.9$-1.0 μm) affixed to a cantilever and a flat tablet surface of a filler.

The diameter of the glidant particle investigated in this study was in the nanometer range. Therefore, the affixing of AEROSIL[®] on the cantilever was not realizable. Consequently, the filler was glued to the cantilever and the adhesion measurement was performed between the colloid probe and a powder mixture. When compared to Ohta's configuration using a filler tablet, this system better simulates the phenomena within a powder mixture for a correlation between flowability and adhesion force. Furthermore, this configuration allows an investigation of the influence of the mixing on the glidant properties of the AEROSIL[®].

Individual adhesion measurement

A typical plot of an individual measurement cycle is presented in Figure 5.1.
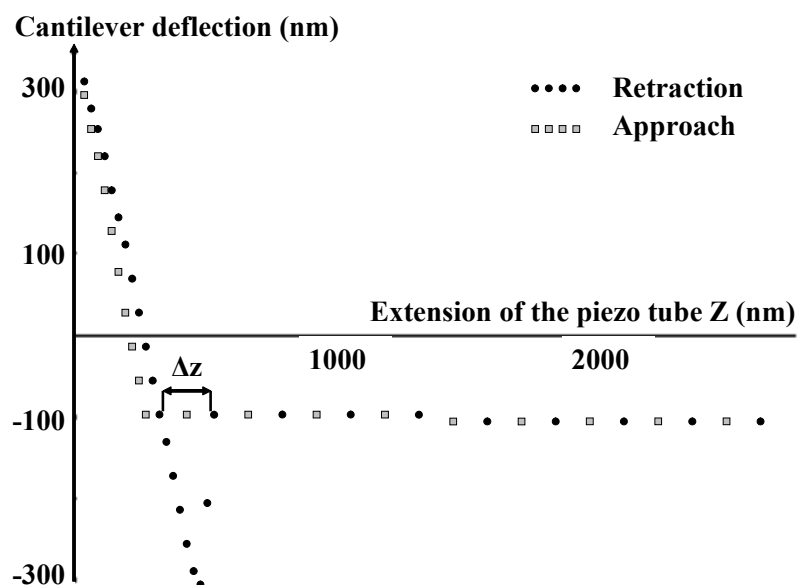
Figure 5.1   Illustration of the measurement of deflection of the cantilever versus the extension of the piezo tube of an individual adhesion measurement between an Avicel® PH 101 functionalized cantilever and Avicel® PH 101 containing 0.5% AEROSIL® 200.

Adhesion measurements were performed at least at 50 individual sites for Avicel® PH 101/AEROSIL® mixtures and 30 sites for Avicel® PH 101 as bulk. Ten force plots were recorded at each site. Table 5.1 shows the number of adhesion force measurements analyzed for each mixture.

Table 5.1   Number of individual adhesion measurements analyzed for the different mixtures investigated.

Mixtures	Number of adhesion measurements
Avicel® PH 101 as bulk	254
Avicel® PH 101/ AEROSIL® 200 M2	536
Avicel® PH 101/ AEROSIL® 200 M4	543
Avicel® PH 101/ AEROSIL® 200 VV M2	600
Avicel® PH 101/ AEROSIL® 200 VV M4	573
Avicel® PH 101/ AEROSIL® R 972 V M2	485
Avicel® PH 101/ AEROSIL® R 972 V M4	597

Histogram of adhesion forces

Each adhesion measurement series was classified according to 2 nN intervals. Figure 5.2 depicts a histogram of experimental measurements, as an example.
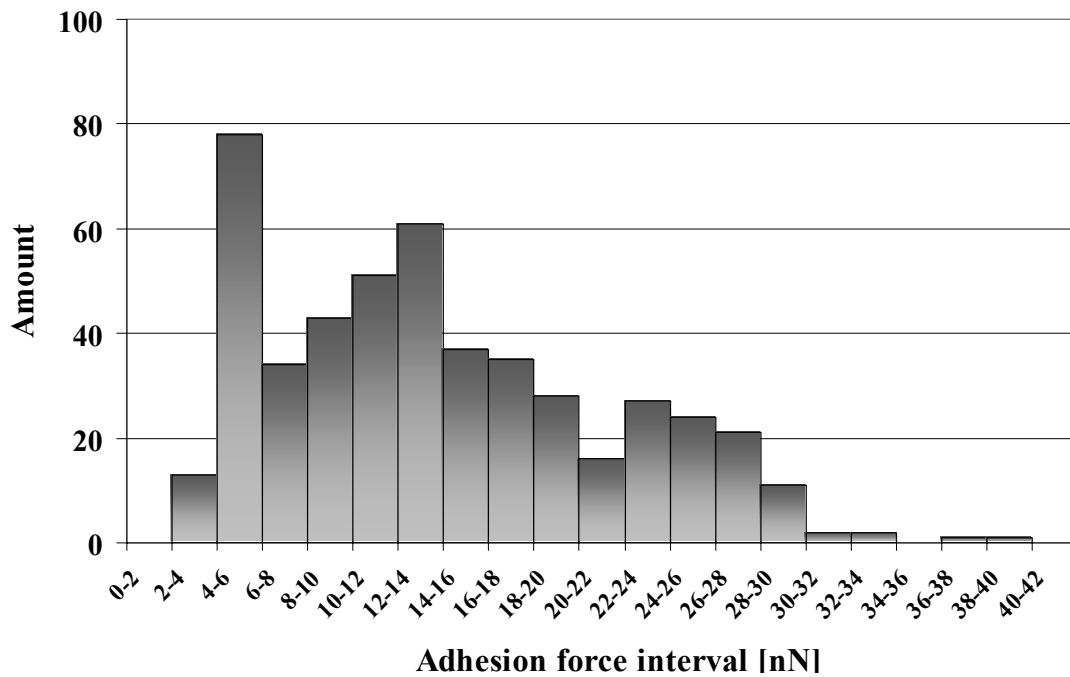
Figure 5.2   Histogram of adhesion measurements for mixture 2 of Avicel[®] PH 101 containing AEROSIL[®] R 972 V.

Cumulative distribution of adhesion force measurements

The cumulative distributions (Q_0) of the adhesion forces were calculated for each sample and are shown in Figure 5.3a and 5.3b. The curves represent the cumulative experimental measurements standardized to 1.

A non-normal distribution is described in each graph. To characterize the samples, the mean, the standard deviation and the standard error of the mean were calculated (Table 5.2). Furthermore, the different samples were compared using a nonparametric Kruskal-Wallis or H-test followed by a Dunn´s comparison test.
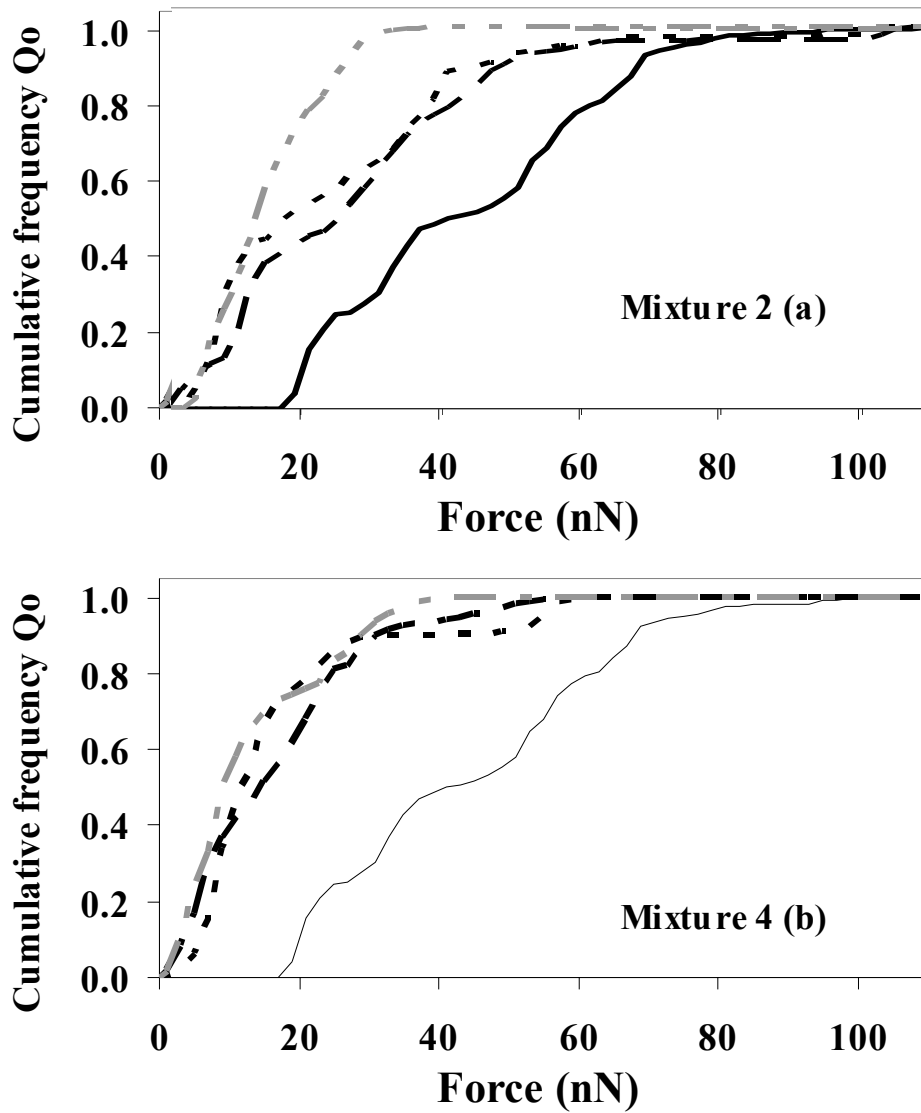
Figure 5.3 *Cumulative adhesion forces between an Avicel® PH 101 particle attached to the cantilever and Avicel® PH 101 as bulk (━━━) or Avicel® PH 101 containing 0.5% AEROSIL® 200 (▪▪▪▪▪), 0.5% AEROSIL® 200 VV (━ ━), 0.5% AEROSIL® R 972 V (━ ▪ ━) for mixtures 2 (a) and mixtures 4 (b).*

Table 5.2 *Mean, standard deviation (s. d.) and standard error (s. e.) of measurements of the adhesion force distributions.*

	Mixture 2				Mixture 4		
	Avicel® PH 101	AEROSIL® 200	AEROSIL® 200 VV	AEROSIL® R 972 V	AEROSIL® 200	AEROSIL® 200 VV	AEROSIL® R 972 V
mean (nN)	44.8	25.2	28.4	13.9	17.5	17.4	13.8
s. d. (nN)	19.3	19.8	20.9	7.4	14.1	8.7	9.9
s. e. (nN)	1.2	0.9	0.9	0.3	0.6	0.4	0.4

5.2.4 Influence of colloidal silicone dioxide on adhesion forces of Avicel® PH 101

The cumulative frequencies, means and nonparametric statistical test results confirmed that colloidal silicon dioxide reduced the adhesion force between the Avicel® PH 101 functionalized cantilever and the Avicel® PH 101 sample. The results corroborate with the sphere-sphere contact model (Figure 2.3) that describes the position of a small particle between two larger spheres – in this case colloidal silicon dioxide between two Avicel® PH 101 particles. The glidant particles increase the distance between the two larger excipient particles and reduced the van der Waals forces between them.

Measurements performed with mixtures 2

Adhesion forces obtained with Avicel® PH 101 without AEROSIL® or with AEROSIL® 200, AEROSIL® 200 VV and AEROSIL® R 972 V ranged from 18 to 110 nN, from 2 to 106 nN, from 2 to 110 nN and from 2 to 40 nN, respectively. Differences in adhesion between individual sites were expected for Avicel® PH 101 and could be explained by the matchstick-like or rod-like structure of Avicel® PH 101 (Bolhuis and Chowan 1996). As a result of this structure, the number of contact points between the Avicel® PH 101 particle mounted to the cantilever and the sample varied from one site to the other, leading to a large adhesion force range. This situation is depicted in Figure 5.4a. Mixtures 2 of Avicel® PH 101 containing either compacted or non-compacted hydrophilic colloidal silicon dioxide showed no statistically significant differences in their adhesion force means. The means were smaller compared to pure Avicel® PH 101, as expected, but the range of adhesion was still high. This observation can be attributed to the degree of coverage of AEROSIL® on Avicel® PH 101. SEM analysis reported in Chapter 4 (4.2.1) revealed that the surface of Avicel® PH 101 was not completely covered by hydrophilic colloidal silicon dioxide under mixing conditions 2. Consequently, during the measurement, it is possible for the cantilever to contact an Avicel® PH 101 surface with no, few or many AEROSIL® particles, as depicted schematically in Figure 5.4b. These various contact point possibilities resulted in a wide range of adhesion forces.
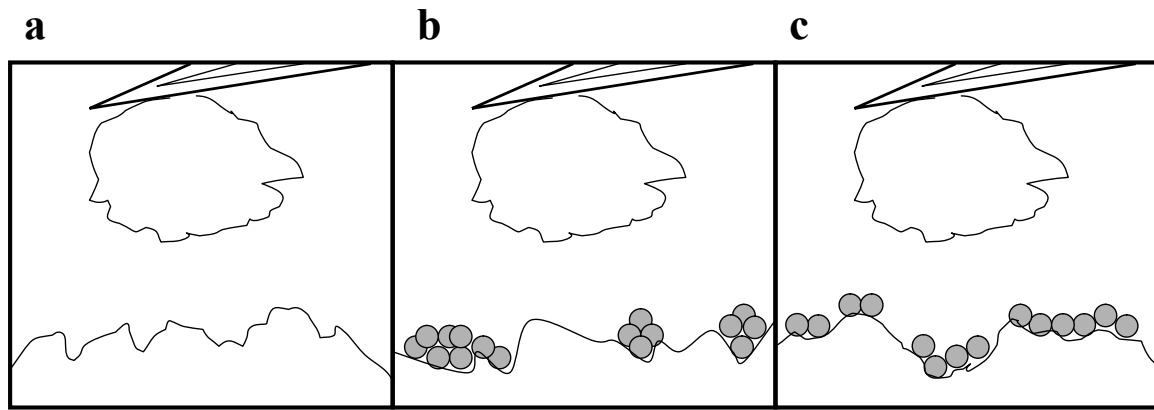
Figure 5.4. *Schematic representation of three contact possibilities between the Avicel® PH 101 functionalized tip and the Avicel® PH 101 sample during the adhesion force measurements, focusing on the coverage of Avicel® PH 101 sample by colloidal silicon dioxide:*

(a) Avicel® PH 101-Avicel® PH 101 contact;

(b) Avicel® PH 101-Avicel® PH 101 or/and Avicel® PH 101-colloidal silicon dioxide-Avicel® PH 101 contact;

(c) Avicel® PH 101-colloidal silicon dioxide-Avicel® PH 101 contact.

By contrast, addition of 0.5% hydrophobic AEROSIL® R 972 V led to a small range and statistically significant lower mean of the adhesion force. As shown by SEM images, the distribution of hydrophobic AEROSIL® on Avicel® PH 101 was homogeneous after gentle mixing in the free-fall mixer. This homogeneous coverage allowed a higher Avicel® PH 101-colloidal silicon dioxide-Avicel® PH 101 contact (Figure 5.4c). Consequently, more AEROSIL® agglomerates were available to increase the distance between two Avicel® PH 101 particles and to reduce the van der Waals forces between them. In this, a smaller adhesion force mean and a smaller range of the adhesion force were observed compared to the mixtures 2 of Avicel® PH 101 containing hydrophilic AEROSIL® 200 and AEROSIL® 200 VV.

Measurements performed with mixtures 4

Through additional mixing in the high speed mixer (mixture 4), the mean, standard deviation and range of the adhesion force decreased for mixtures containing hydrophilic AEROSIL®. The smaller range of the adhesion force distribution, from 1 to 74 nN and from 1 to 60 nN for AEROSIL® 200 and AEROSIL® 200 VV

respectively, was attributed to a better distribution of the colloidal silicon dioxide, as observed by SEM images (Figures 4.1). Schematically, the measurements under mixing conditions 4 could be described by Figure 5.4c. In this case, primarily Avicel$^{®}$ PH 101-colloidal silicon dioxide-Avicel$^{®}$ PH 101 contact occurred. Consequently, the means for both mixtures 4 were statistically significantly smaller compared to mixture 2 and approached the mean of mixture 4 of Avicel$^{®}$ PH 101 containing hydrophobic colloidal silicon dioxide. Mixtures 2 and 4 containing AEROSIL$^{®}$ R 972 V presented no statistically significant differences in adhesion force means and showed nearly the same curve shape and range of adhesion force distribution, as they already presented the same degree and uniformity of coverage. This observation indicated that adhesion force was dependent on the degree and uniformity of coverage of the colloidal silicon dioxide on the Avicel$^{®}$ PH 101 surface.

5.3   Correlation between angle of repose and adhesion force

As shown in Figure 5.5, the correlation between the angle of repose and the mean adhesion force was linear.
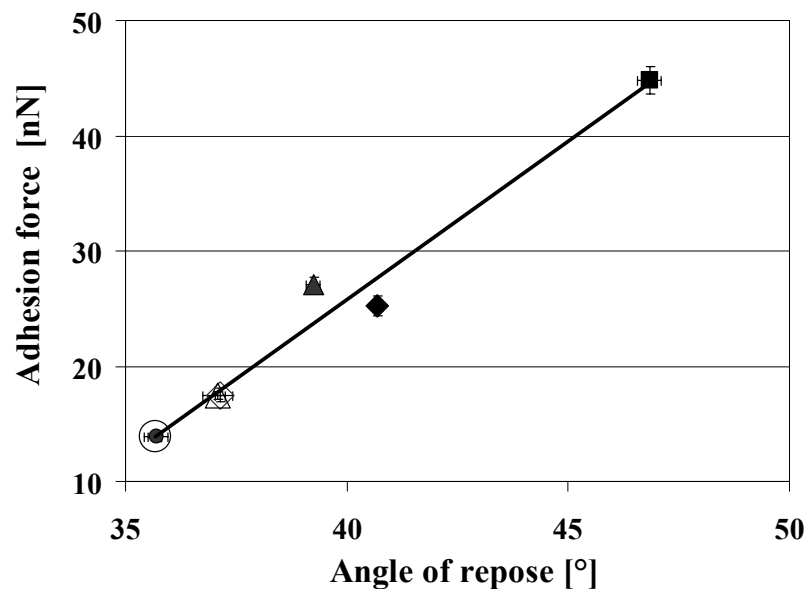
Figure 5.5   Correlation between the angle of repose and the adhesion force mean of Avicel$^{®}$ PH 101 containing 0.5% AEROSIL$^{®}$ R 972 V [M2: (●); M4: (O)], 0.5% AEROSIL$^{®}$ 200 [M2: (♦); M4: (◊)], 0.5% AEROSIL$^{®}$ 200 VV [M2: (▲); M4: (Δ)] and Avicel$^{®}$ PH 101 as bulk (■). Error bars indicate the standard error of the mean.

The smaller the angle of repose, the smaller the adhesion between the Avicel® PH 101 particle affixed to the cantilever and the sample surface. As described and measured by Ohta et al. (2003), adhesion forces between a glidant and a pharmaceutical filler control flowability. In a previous study, Otsuka (1998) compared the tensile strength of a powder bed to adhesive force between glidant and substrate and found that the flowability was improved with the reduction of adhesion force.

5.4   Discussion of the results

The measurement of interparticulate forces within Avicel® PH 101 mixtures shows that colloidal silicon dioxide reduces the adhesion force between the Avicel® PH 101 particles. The experimental findings are in good agreement with the theory described by the sphere-sphere model. The reduction is influenced by the AEROSIL® type and mixing time and could be explained by SEM and XPS analyses. A rapid reduction of the agglomerates and aggregates of AEROSIL® during mixing allows a high degree of coverage of the Avicel® PH 101 surface. Due to fewer silanol groups on the surface, agglomerates of hydrophobic AEROSIL® are softer and therefore easier to break up compared to the hydrophilic types. The better and faster extent of coverage of hydrophobic AEROSIL® leads to a higher reduction of the cohesion between Avicel® PH 101 particles.

Moreover, the adhesion measurements correlate with the angle of repose and confirm that adhesion forces between a glidant and a pharmaceutical filler dominate flowability. In addition, atomic force microscopy is a powerful tool to measure the adhesion force between pharmaceutical excipients.

This investigation underlines the technological importance of an optimum mixing process, highlighting that colloidal silicon dioxide has to be well distributed to optimally fulfil its glidant properties.

CHAPTER 6

INVESTIGATION OF THE EFFECT OF COMPACTED

HYDROPHOBIC AND HYDROPHILIC COLLOIDAL SILICON DIOXIDES

ON TABLETING PROPERTIES OF PHARMACEUTICAL EXCIPIENTS

6.1   Introduction

In the previous chapters, the glidant properties of compacted hydrophilic and hydrophobic colloidal silicon dioxides were compared to a non-compacted type. The flowability studies including angle of repose, dynamic conveyor belt, ring shear cell method and poured and tapped densities have shown differences between the colloidal silicon dioxide types when mixed with Avicel® PH 101 or Starch 1500®. Besides their handling advantages, the compacted colloidal silicon dioxides were superior to the non-compacted with respect to their powder flow enhancing properties. Furthermore, the hydrophobic colloidal silicon dioxide types were more effective compared to the hydrophilic ones under gentle mixing conditions. The better flow characteristic was due to a higher degree and uniformity of coverage of the hydrophobic colloidal silicon dioxide on the excipient's surface, which led to a higher adhesion force reduction between the particles as determined by atomic force microscopy. For Tablettose® 80, there was only a limited improvement in flowability, but there was no difference between the various colloidal silicon dioxide types. This was due to the agglomerated structure of Tablettose® 80, where the colloidal silicon dioxide particles settle to a higher extent in the cavities of the agglomerates.

On the basis of these results, the aim of this chapter is to investigate the influence of different hydrophobic and hydrophilic colloidal silicon dioxide types on the tableting properties of Avicel® PH 101, Starch 1500® and Tablettose® 80. The study is based on binary mixtures produced under mixing condition 2 (gentle mixing) to show the

influence of colloidal silicon dioxide on compression parameters and tablet properties. Moreover, ternary mixtures containing magnesium stearate as a third component were evaluated in order to study the effect of colloidal silicon dioxide on the film formation of magnesium stearate.

6.2   Compression parameters

6.2.1   Heckel plots

Paronen and Ilkka (1996) described the process of volume reduction of a powder mass under pressure and enumerated different stages: die filling, rearrangement of particles, deformation by elastic changes, permanent deformation by plastic flow or particle failure by brittle fracturing. Numerous mathematical expressions dealing with the characterization of tablet dimensions and changes involved in the densification process have been suggested. These equations have been critically reviewed and compiled in the literature (Leuenberger 1986). Three of them have been widely applied to pharmaceutical purposes, namely Heckel, Kawatika and Cooper Eaton, in order to give basic indications of the tabletability and to predict the properties of the formulation (Paronen and Ilkka 1996).

The porosity function according to Heckel describes the volume reduction or change in relative density of a powder mass under pressure. Heckel plots can be accomplished by two ways: the volume of a powder column, and its corresponding porosity, can be measured either during compression or after ejection of the compact from a die. Instrumentation of tablet press enables continuous monitoring of the powder column height during the volume reduction process (Dressler 2002). This method is referred as "in die" or "at pressure" and was used in study. In the "ejected tablet" or "at zero pressure" method, the dimensions of a compact are measured after ejection.
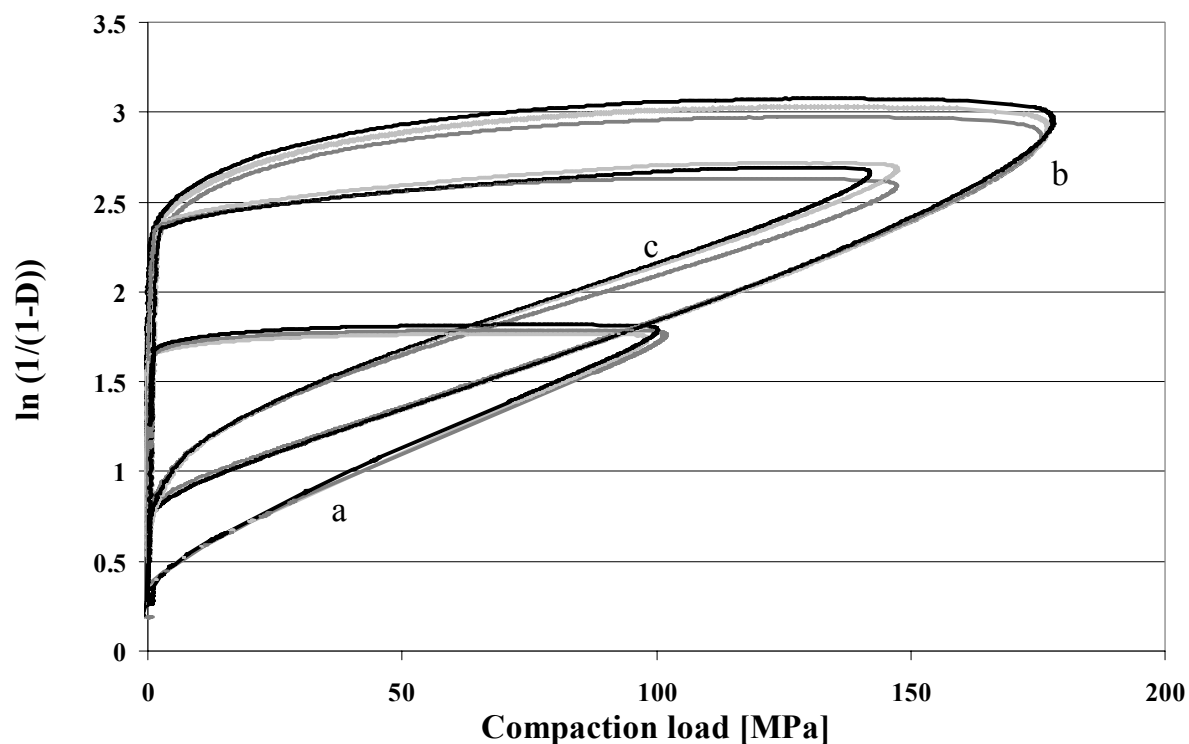
*Figure 6.1   Heckel plot of Avicel® PH 101 (a), Starch 1500® (b) and Tablettose® 80
(c) containing 0.5% AEROSIL® R 972 V (▬▬), 0.5% AEROSIL® 200 VV
(▬▬) and without AEROSIL® (▬▬).*

The Heckel plots of Avicel® PH 101, Starch 1500® and Tablettose® 80 containing
0.5% AEROSIL® R 972 V, 0.5% AEROSIL® 200 VV and no additives are depicted in
Figure 6.1 and the respective yield pressures are displayed in Table 6.1. The yield
pressure (reciprocal of the slope) is indicative for the plastic behaviour of the material.
A lower value for the yield pressure is related to a greater amount of plasticity in the
material. The plasticity decreased in the following order: Avicel® PH 101 > Starch
1500® > Tablettose® 80. These results are consistent with previous studies performed
by Zhang et al. (2003) and Dressler (2002).

The shape of the Heckel plots was also characteristic for each excipient. Duberg and
Nyström (1986) have used the initial part curvature of the Heckel plot as an indication
of particle fragmentation. The correlation coefficient describing the linearity of the
Heckel plots have been used for the same purpose. During the early stages of
compression the densification of Tablettose® 80 was more extensive than that of
Avicel® PH 101 and Starch 1500®. Ilkka and Paronen (1993) explained that the
fragmentation of large aggregates and fracturing of surface asperities of Tablettose® 80

facilitate the further rearrangement and densification at low pressure levels. Thus, the nonlinear plot of Tablettose® 80 indicated fragmentation (Figure 6.1c) and the linear plot of Avicel® PH 101 showed deformation by plastic flow (Figure 6.1a). The initial curvature of Starch 1500® revealed poor packing of powder and small particle size (Figure 6.1b). Nyström et al. (1993) have shown that the decompression phase gave information about elastic component of the particles. Elastic properties result in an increase of porosity, i.e. a decrease of the plot in the decompression phase. The decompression curve of Avicel® PH 101 was approximately horizontal, indicating no elastic deformation. Starch 1500® showed high elastic expansion, while Tablettose® 80 had a limited elastic component. The Heckel plot shapes and the yield pressures of the excipients were not influenced by the presence of either AEROSIL® or the type of AEROSIL® used, indicating that addition of 0.5% AEROSIL® did not influence the tabletability of the excipients.

Table 6.1   Mean and standard deviation (n = 10) of yield pressure of Avicel® PH 101, Starch 1500® and Tablettose® 80 containing 0.5% AEROSIL® R 972 V, 0.5% AEROSIL® 200 VV and without AEROSIL®.

	without AEROSIL®	*AEROSIL® 200 VV*	*AEROSIL® R 972 V*
Avicel® PH 101	79.1 ± 0.9	80.0 ± 0.7	78.9 ± 0.6
Starch 1500®	99.7 ± 2.8	100.8 ± 2.5	100.7 ± 2.4
Tablettose® 80	106.6 ± 2.9	106.4 ± 3.6	104.4 ± 3.0

6.2.2 Residual and ejection forces

The residual and ejection force values are depicted in Figures 6.2, 6.3 and 6.4 for Avicel® PH 101, Starch 1500® and Tablettose® 80 tablets, respectively. For Avicel® PH 101 tablets, the addition of AEROSIL® increased the residual and ejection forces but only for compaction loads above 100 MPa. Hydrophobic AEROSIL® led to a larger increase in residual forces. For Starch 1500®, the residual and ejection force was increased by the addition of AEROSIL® but there was no difference between the various AEROSIL® types.

*Figure 6.2   Residual and ejection forces of tablets compressed from Avicel® PH 101,
               containing 0.5% AEROSIL® 200 VV (Δ), 0.5% AEROSIL® 200 (◊), 0.5%
               AEROSIL® 130 V (○), 0.5% AEROSIL® R 972 V (●), 0.5% AEROSIL® R
               974 V (▲) and without AEROSIL® (■). Error bars represent the 95%
               confidence interval of ten measurements.*
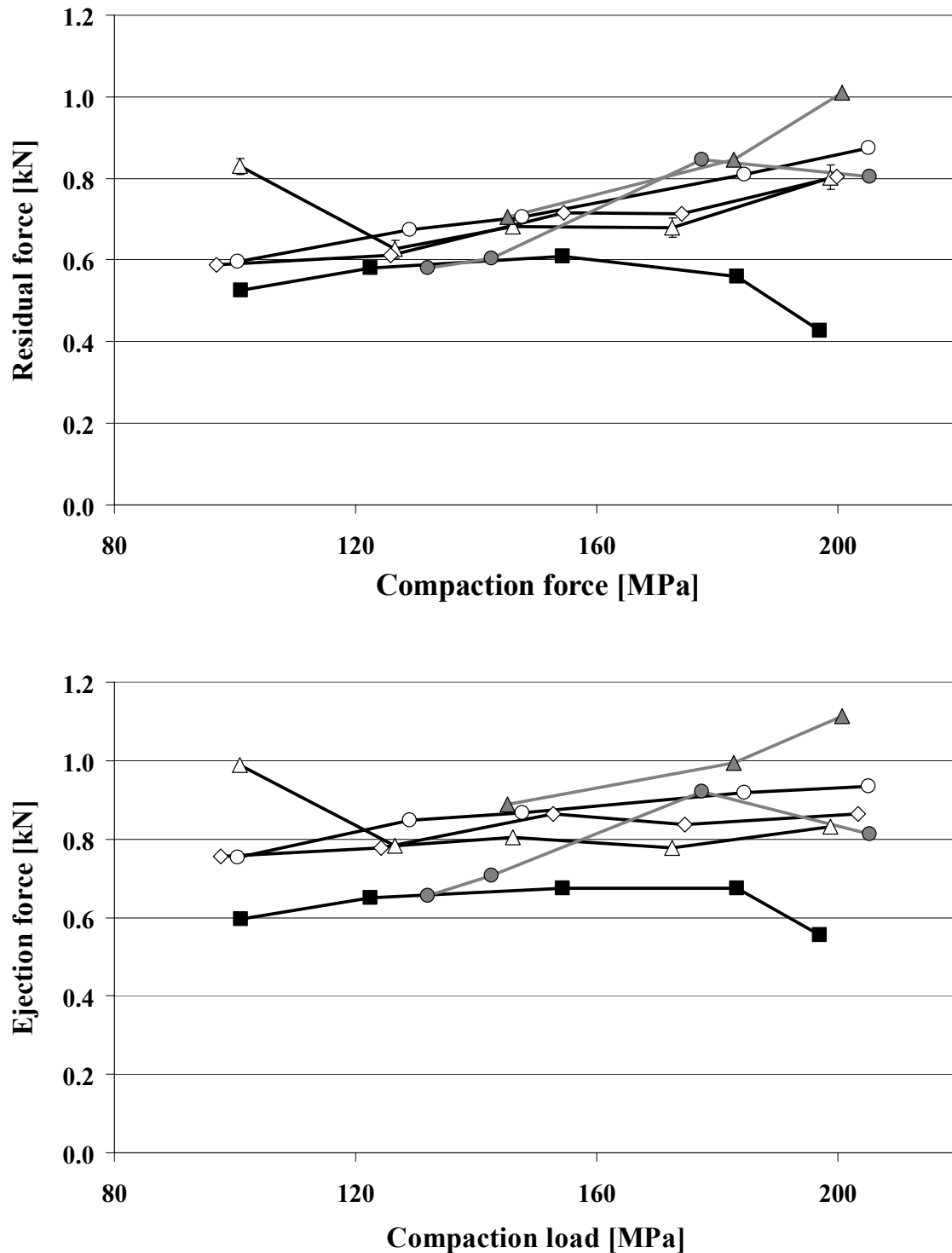
Figure 6.3   Residual and ejection forces of tablets compressed from Starch 1500®, containing 0.5% AEROSIL® 200 VV (Δ), 0.5% AEROSIL® 200 (◊), 0.5% AEROSIL® 130 V (○), 0.5% AEROSIL® R 972 V (●), 0.5% AEROSIL® R 974 V (▲) and without AEROSIL® (■). Error bars represent the 95% confidence interval of ten measurements.
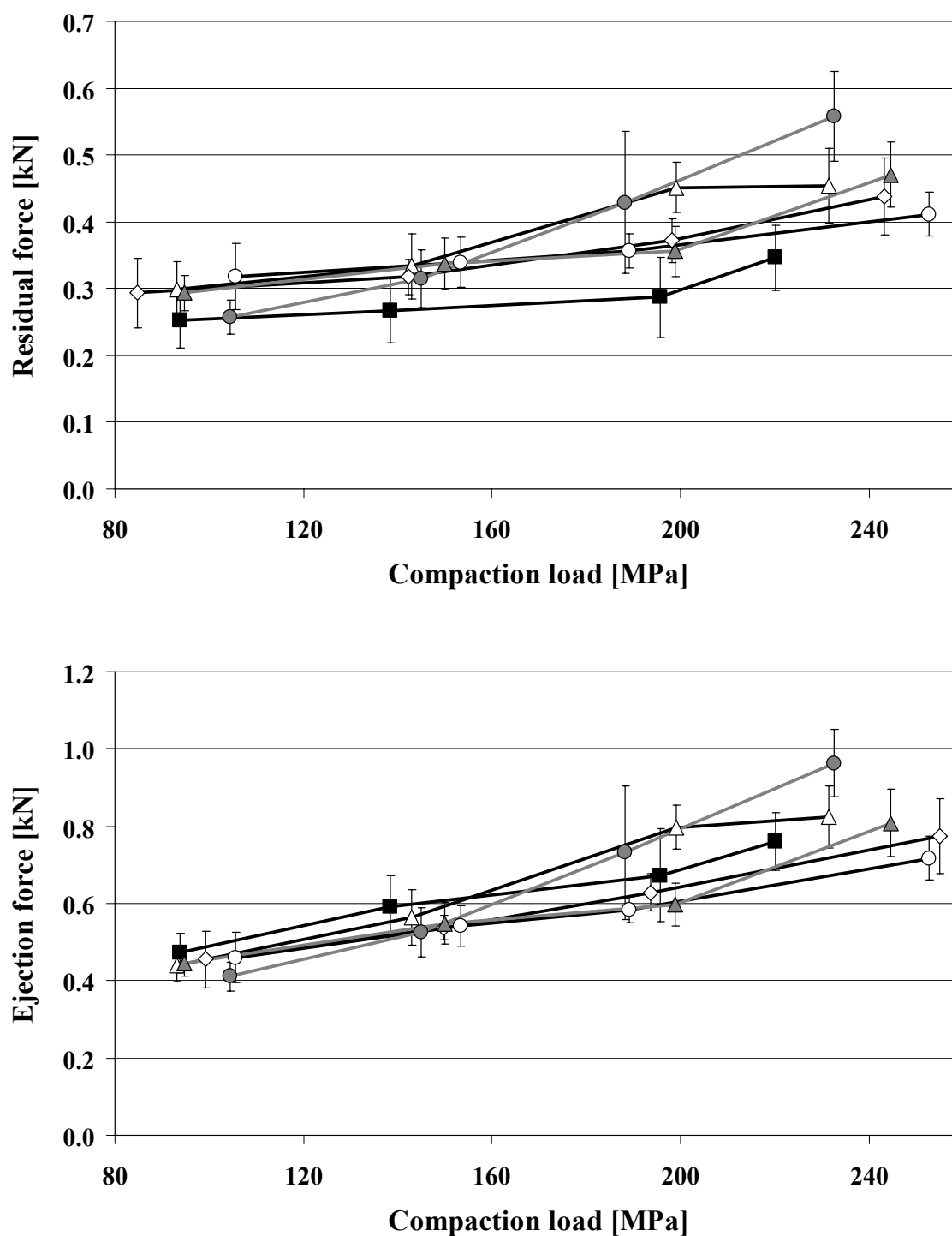
Figure 6.4   Residual and ejection forces of tablets compressed from Tablettose® 80, containing 0.5% AEROSIL® 200 VV (∆), 0.5% AEROSIL® 200 (◊), 0.5% AEROSIL® 130 V (○), 0.5% AEROSIL® R 972 V (●), 0.5% AEROSIL® R 974 V (▲) and without AEROSIL® (■). Error bars represent the 95% confidence interval of ten measurements.

For tableting of Tablettose 80®, it was necessary to prelubricate the die with oleic acid. This prelubrication, however, leads to a reduction of the residual and ejection forces compared to Starch 1500® and Avicel® PH 101. Moreover due to the discontinuous tableting process, the measurements showed a higher variation, which is depicted with the higher 95% confidence interval.

The residual and ejection forces were not affected by the addition of AEROSIL®.

6.3 Tablet parameters

6.3.1 Tablet strength and bonding capacity

Avicel® PH 101

Figure 6.5 depicts the relationship between radial tensile strength and compaction pressure of tablets compressed from pure Avicel® PH 101 and AEROSIL®/Avicel® PH 101 mixtures. Tablets compressed without AEROSIL® produced higher values of radial tensile strength. The strong binding properties were due to the plastic deformation and the rough surface texture of microcrystalline cellulose (Bolhuis and Chowhan 1996). The interparticulate bonding forces in cellulose are hydrogen and van der Waals forces (Gustafsson et al. 2003). The hydrogen bonds on the extremely large surface area were brought into close contact during the plastic deformation resulting in an extremely good compactibility. Furthermore, because of the irregular particle morphology Nyström et al. 1993 suggested that the presence of mechanical interlocking may contribute to the tensile strength of microcrystalline cellulose tablets.

Blending with colloidal silicon dioxide turned the powder into a binary system where three attraction force possibilities can occur: cohesion between Avicel® PH 101 particles, cohesion between colloidal silicon dioxide particles and adhesion between Avicel® PH 101 and colloidal silicon dioxide. Addition of 0.5% colloidal silicon dioxide reduced the radial tensile strength of the tablets (Figure 6.5). The small colloidal silicon dioxide particles act as spacers between the Avicel® PH 101 particles reducing the interparticle attraction forces between the Avicel® PH 101 surfaces.
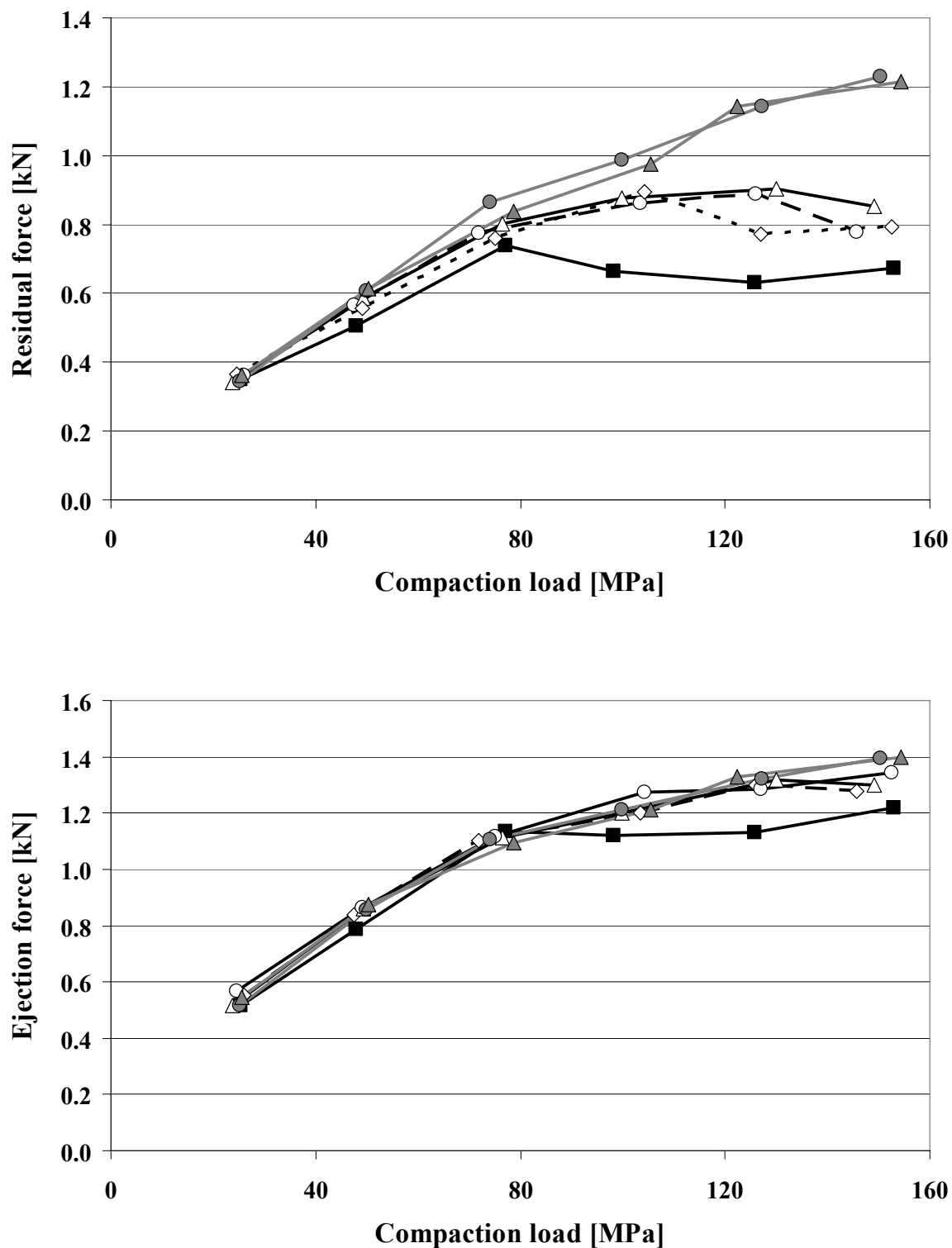
Figure 6.5   *Radial tensile strength of tablets compressed from Avicel® PH 101, containing 0.5% AEROSIL® 200 VV (Δ), 0.5% AEROSIL® 200 (◊), 0.5% AEROSIL® 130 V (○), 0.5% AEROSIL® R 972 V (●), 0.5% AEROSIL® R 974 V (▲) and without AEROSIL® (■). Error bars represent the 95% confidence interval of ten measurements.*

These results are in agreement with the adhesion force measurements performed with atomic force microscopy (Chapter 5, Table 5.2), where the adhesion force increased in the following order: hydrophobic AEROSIL®/Avicel® PH 101 < hydrophilic AEROSIL®/Avicel® PH 101 < Avicel® PH 101/Avicel® PH 101. The adhesive interaction between Avicel® PH 101 and colloidal silicon dioxide was lower compared to the cohesive attraction forces between Avicel® PH 101 particles. Therefore, tablets prepared with Avicel® PH 101/colloidal silicon dioxide mixtures will be slightly weakened by the presence of AEROSIL®. The hydrophobic AEROSIL® led to a stronger decrease in tablet strength, due to the lower density of silanol groups (Chapter 2, Table 2.1). The better distribution of the hydrophobic AEROSIL® on the Avicel® PH 101 surface (Chapter 4, Figure 4.1), decreasing the contact area between two Avicel® PH 101 particles, was also responsible for the reduction of tablet strength.
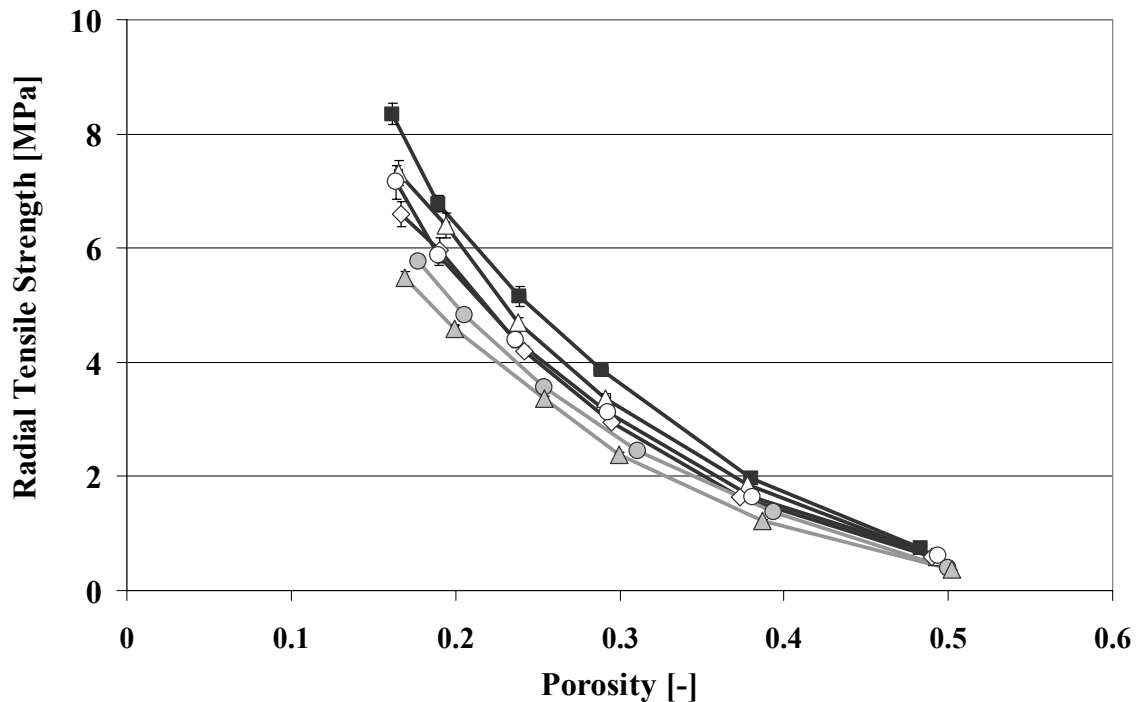
Figure 6.6   Radial tensile strength as a function of tablet porosity for tablets compressed from Avicel® PH 101, containing 0.5% AEROSIL® 200 VV (Δ), 0.5% AEROSIL® 200 (◊), 0.5% AEROSIL® 130 V (○), 0.5% AEROSIL® R 972 V (●), 0.5% AEROSIL® R 974 V (▲) and without AEROSIL® (■). Error bars represent the 95% confidence interval of ten measurements.

Previous studies performed by van der Voort Maarschalk et al. (1996), Zuurman et al. (1999) and van Veen et al. (2000, 2005) have demonstrated that the interaction between particles in a tablet can be derived from the relationship between radial tensile strength and porosity. Figure 6.6 shows the radial tensile strength/porosity profiles for Avicel® PH 101/colloidal silicon dioxide mixtures and indicates that the addition of colloidal silicon dioxide modified the radial tensile strength/porosity profiles. At the same porosity, tablets compressed with Avicel® PH 101 and colloidal silicon dioxide showed lower radial tensile strength values compared to Avicel® PH 101 tablets, indicating a decrease in the bonding capacity of the material. The calculated radial tensile strength values at 20% porosity shown in Table 6.2 confirmed that hydrophobic AEROSIL® (4.54-5.01 MPa) led to a higher reduction of the interparticle bonding compared to hydrophilic AEROSIL® (5.43-5.97 MPa). The radial tensile strength calculated at 20% for AEROSIL® 200 and Avicel® PH 101 tablets agreed with the results of a study performed by van Veen et al. (2005).

Table 6.2   *Radial tensile strength calculated from the Ryshkewitch-Duckworth relation at 20% porosity for Avicel® PH 101 and Starch 1500®, and at 10% porosity for Tablettose® 80.*

	Radial tensile strength [MPa]		
	Avicel® PH 101	Starch 1500®	Tablettose® 80
without AEROSIL®	6.48	0.88	2.24
AEROSIL® 200	5.43	1.42	1.50
AEROSIL® 200 VV	5.97	1.38	1.52
AEROSIL® 130 V	5.57	1.30	1.47
AEROSIL® R 972 V	5.01	/	1.46
AEROSIL® R 974 V	4.54	/	1.34

However, tablets compressed at a pressure exceeding 50 and 75 MPa for hydrophilic and for hydrophobic AEROSIL®, respectively, displayed acceptable radial tensile strength values and the friability of the tablets was lower than 1%. An increase of the compaction load, when tableting Avicel® PH 101 with colloidal silicon dioxide, led to tablets displaying the same properties as pure Avicel® PH 101 tablets. Therefore, considering the flowability enhancement induced by AEROSIL®, improving the powder flow into the hopper and the die of the tablet press, the use of hydrophilic and hydrophobic colloidal silicon dioxide facilitates the tableting of Avicel® PH 101.

Starch 1500®

The radial tensile strength of Starch 1500® tablets (Figure 6.7) was low compared to Avicel® PH 101, because the plastic deformation was too slow to produce strong interparticle bonding during compression (Mattsson and Nyström 2001). Furthermore a large proportion of the total deformation of Starch 1500® was elastic during compaction at high strain rates (Bolhuis and Chowhan 1996, Rees and Rue 1978)
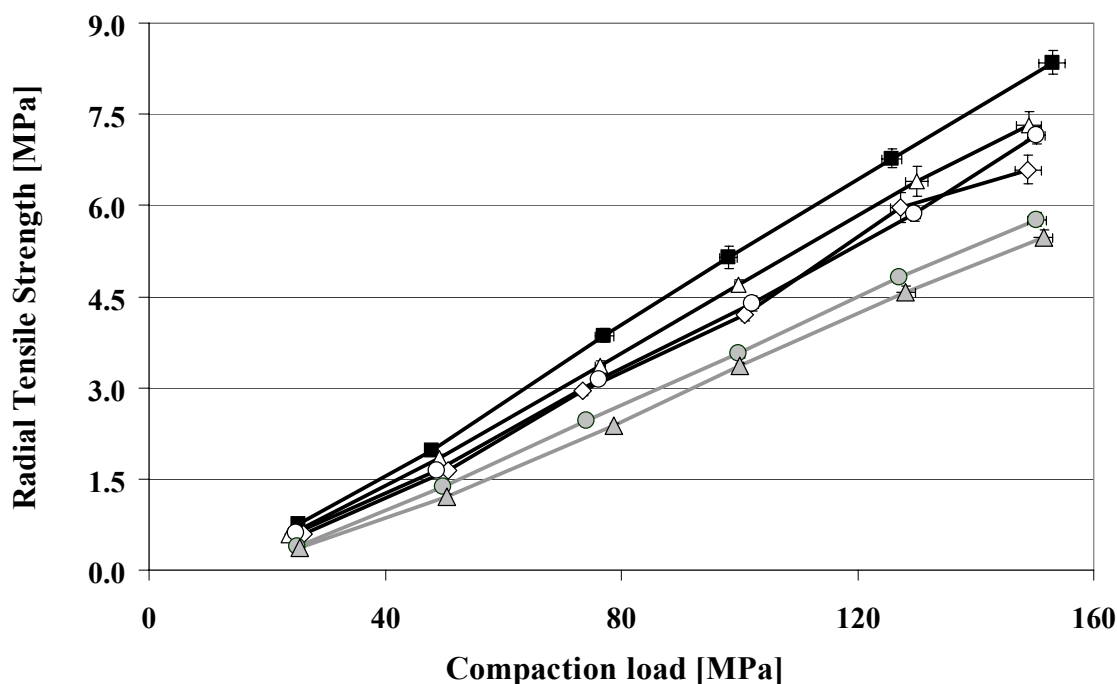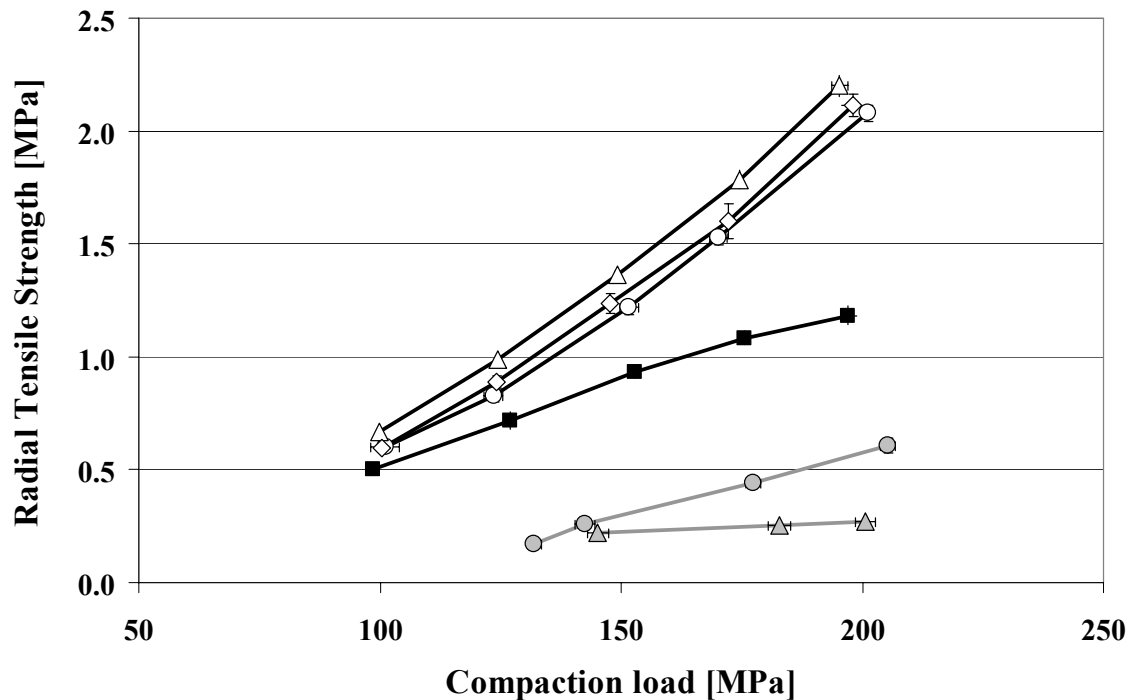
Figure 6.7   Radial tensile strength of tablets compressed from Starch 1500®, containing 0.5% AEROSIL® 200 VV (Δ), 0.5% AEROSIL® 200 (◊), 0.5% AEROSIL® 130 V (○), 0.5% AEROSIL® R 972 V (●), 0.5% AEROSIL® R 974 V (▲) and without AEROSIL® (■). Error bars represent the 95% confidence interval of ten measurements.

The radial tensile strength of Starch 1500® increased when mixed with 0.5% hydrophilic colloidal silicon dioxide and decreased when mixed with 0.5% hydrophobic colloidal silicon dioxide.

Meyer and Zimmermann (2004) showed that for the same mixing conditions, the surface coverage of the hydrophobic AEROSIL® on Starch 1500® was more extensive than that achieved with the hydrophilic counterpart. Additionally, the following interparticle force ranking was determined using a tensile strength tester: hydrophobic AEROSIL®/Starch 1500® < hydrophilic AEROSIL®/ Starch 1500® < Starch 1500®/ Starch 1500®. The presence of hydrophobic AEROSIL® interfered with the bonding of Starch 1500® and as the adhesive interaction between Starch 1500® and colloidal silicon dioxide was much less than the cohesive attraction between Starch 1500® particles, the radial tensile strength was dramatically weakened. Furthermore, the more extensive surface coverage of hydrophobic AEROSIL® on Starch 1500® reduced the

surface contact between two Starch 1500® particles, even considering that the packing density in the die was increased when compared to Starch 1500® without AEROSIL® (Table 6.3).

Table 6.3   Packing densities of Starch 1500® mixtures in the die (standard deviations in parentheses, n = 50)

	Packing density in the die [g/cm³] Starch 1500®
without AEROSIL®	0.631 (0.003)
AEROSIL® 200	0.673 (0.001)
AEROSIL® 200 VV	0.697 (0.001)
AEROSIL® 130 V	0.689 (0.003)
AEROSIL® R 972 V	0.717 (0.007)
AEROSIL® R 974 V	0.714 (0.002)

The effect of hydrophobic AEROSIL® on the radial tensile strength of the tablets was greater for Starch 1500® compared to Avicel® PH 101, due to the low starting radial tensile strength values of Starch 1500® tablets. Therefore, tablets could only be compressed at a compaction pressure greater than 125 MPa and 150 MPa for AEROSIL ® R 972 V and AEROSIL® R 974 V, respectively. The radial tensile strength/porosity profile of hydrophobic AEROSIL® did not fit the Ryskewitch-Duckworth relation, probably because of the very low radial tensile strength values (Figure 6.8). Nevertheless it can be seen that the relationship between the radial tensile strength and the porosity changed dramatically, especially for AEROSIL® R 974 V and that the bonding capacity of Starch 1500® was decreased. This deleterious effect was reported by Ohta et al. (2003) who studied the mechanism of enhancing flowability and tablet hardness by glidants in pharmaceutical powder mixture and found that hydrophobic glidants weakened tablet hardness.

Figure 6.8   Radial tensile strength as a function of tablet porosity for tablets compressed from Starch 1500®, containing 0.5% AEROSIL® 200 VV (Δ), 0.5% AEROSIL® 200 (◊), 0.5% AEROSIL® 130 V (○), 0.5% AEROSIL® R 972 V (●), 0.5% AEROSIL® R 974 V (▲) and without AEROSIL® (■). Error bars represent the 95% confidence interval of ten measurements.

Tablets compressed with hydrophilic AEROSIL® and Starch 1500® showed an increase in the radial tensile strength. This result could be explained by the consolidation behavior of Starch 1500®. Admixing 0.5% AEROSIL® to Starch 1500® increased the packing density of the mixture in the die (Table 6.3). Starch 1500® particles were brought into closer contact, allowing a better binding between the particles (Nyström et al. 1993). There seems to be a balance between the weakening of interparticle bonding through the hydrophilic AEROSIL®, the increase of the packing density in the die and the surface coverage of AEROSIL® on Starch 1500®, which led to an increase in radial tensile strength at the same porosity (Figure 6.8), indicating an increase in the bonding capacity of Starch 1500®.

This interpretation was confirmed by testing a mixture of 1% AEROSIL® 200 VV and Starch 1500® under mixing condition 2 and a mixture of 0.5% AEROSIL® 200 VV and Starch 1500® under mixing condition 4. Increasing the colloidal silicon dioxide concentration or increasing the mixing time increased the surface coverage of

AEROSIL$^®$ 200 VV particles on Starch 1500$^®$. The radial tensile strength values of tablets pressed from those mixtures at the same compression pressure interval (100-200 MPa) were lower than those of the 0.5% AEROSIL$^®$ 200 VV/Starch 1500$^®$ tablets under mixing condition 2, as a result of decreased Starch 1500$^®$/Starch 1500$^®$ surface contact (Figure 6.9). Furthermore the two mixtures additionally tested presented the same surface coverage of AEROSIL$^®$ 200 VV particles on Starch 1500$^®$ but different packing density in the die (0.664 and 0.710 for 1% AEROSIL$^®$ 200 VV/Starch 1500$^®$ M2 and 0.5% AEROSIL$^®$ 200 VV/Starch 1500$^®$ M4, respectively). Tablets compressed with 0.5% AEROSIL$^®$ produced higher values of radial tensile strength compared to 1% AEROSIL$^®$, because of closer contact between Starch 1500$^®$ particles in the die.
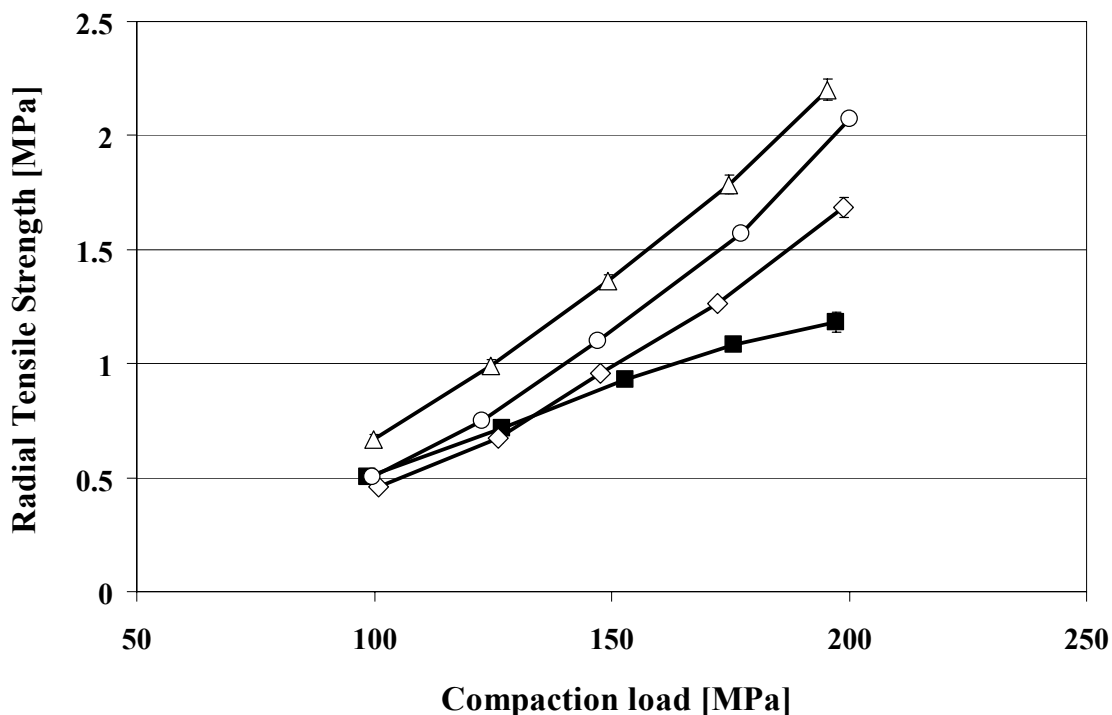
Figure 6.9   Radial tensile strength of tablets compressed from Starch 1500$^®$, containing 0.5% AEROSIL$^®$ 200 VV M2 (Δ), 0.5% AEROSIL$^®$ 200 VV M4 (○), 1% AEROSIL$^®$ 200 VV M2 (◊) and without AEROSIL$^®$ (■). Error bars represent the 95% confidence interval of ten measurements.

Tablettose® *80*

Figure 6.10 depicts the radial tensile strength of tablets compressed with Tablettose® 80 as a function of the compaction load.
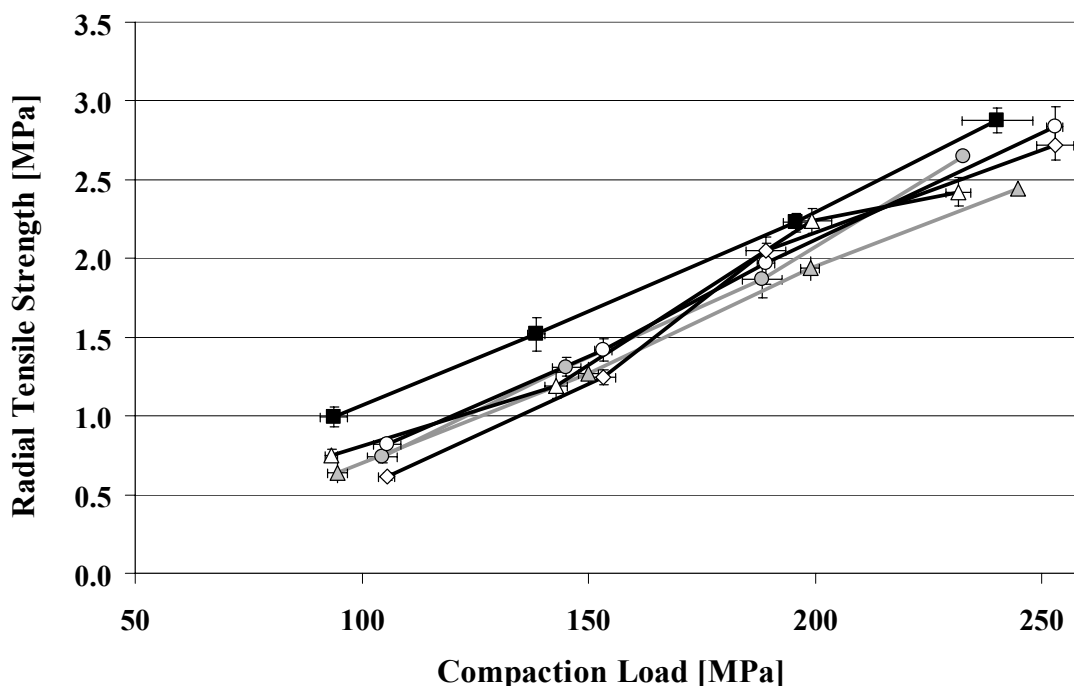
Figure 6.10   Radial tensile strength of tablets compressed from Tablettose® 80, containing 0.5% AEROSIL® 200 VV (Δ), 0.5% AEROSIL® 200 (◊), 0.5% AEROSIL® 130 V (○), 0.5% AEROSIL® R 972 V (●), 0.5% AEROSIL® R 974 V (▲) and without AEROSIL® (■). Error bars represent the 95% confidence interval of ten measurements.

Tablets compressed with Tablettose® 80 showed only a slight decrease in radial tensile strength (Figure 6.10). This can be explained first by the porous structure of the material and second by the brittle nature of α-lactose-monohydrate, which fragmented during compression and produced new surfaces, free of AEROSIL® and available for bonding. Consequently, attraction forces between Tablettose® 80 and colloidal silicon dioxide and between colloidal silicon dioxide particles were much lower compared to those between Tablettose® 80 particles, leading to a small decrease in the radial tensile strength and no difference between hydrophobic and hydrophilic materials. Figure 6.11 shows that the addition of colloidal silicon dioxide modified the radial tensile strength/porosity profiles. The decrease in radial tensile strength at same porosity

confirmed the reduced bonding capacity of the material. Furthermore, the same radial tensile strength values were calculated for colloidal silicon dioxide/Tablettose® 80 tablets at 10% porosity (Table 6.2), indicating no difference between hydrophobic and hydrophilic colloidal silicon dioxide.
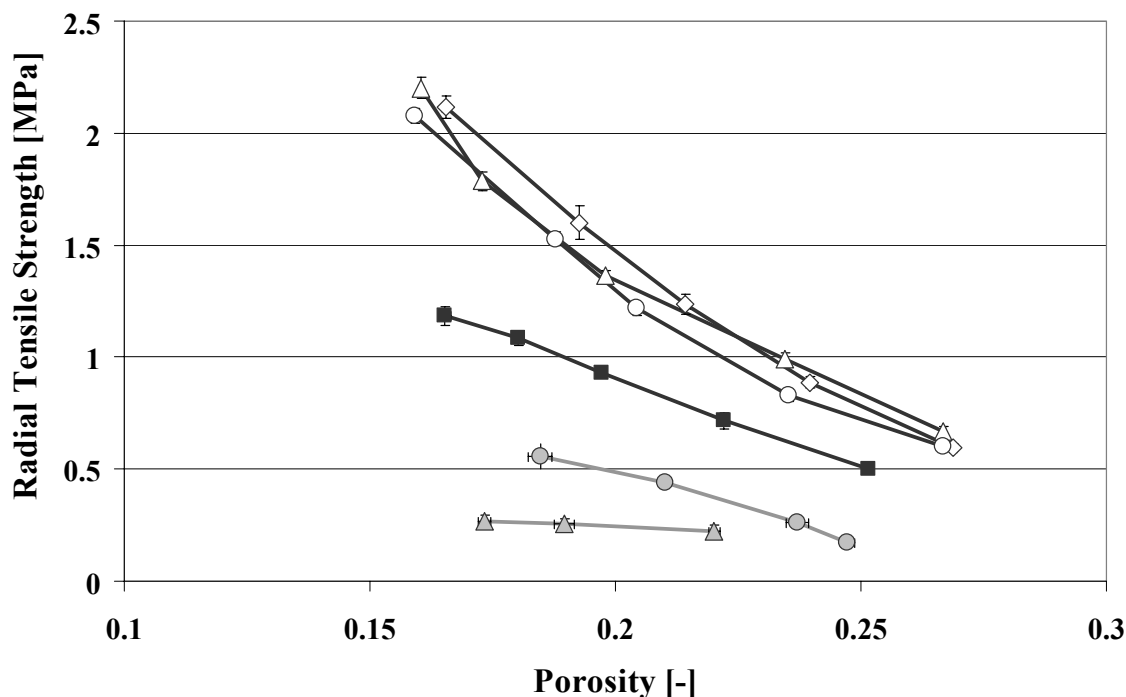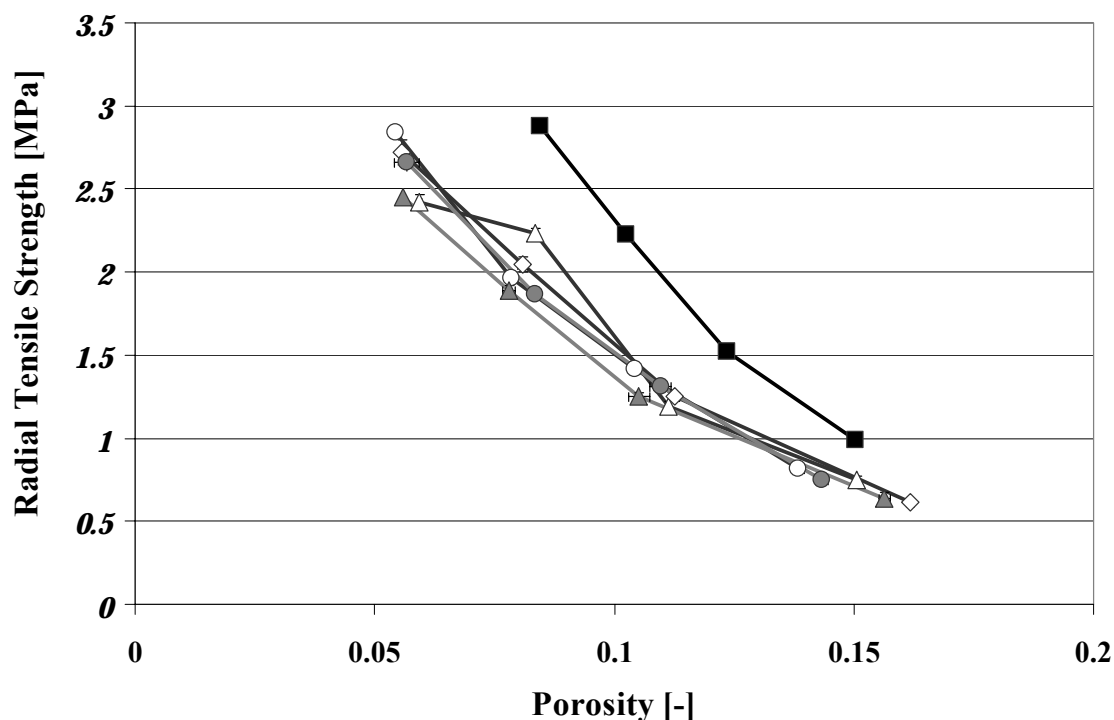

Figure 6.11 Radial tensile strength as a function of the tablet porosity of tablets compressed from Tablettose® 80, containing 0.5% AEROSIL® 200 VV (Δ), 0.5% AEROSIL® 200 (◊), 0.5% AEROSIL® 130 V (○), 0.5% AEROSIL® R 972 V (●), 0.5% AEROSIL® R 974 V (▲) and without AEROSIL® (■). Error bars represent the 95% confidence interval of ten measurements.

6.3.2 Friability

Figure 6.12 shows the friability of the tablets compressed from Avicel® PH 101, Starch 1500® and Tablettose® 80 containing different types of colloidal silicon dioxide.

a. Avicel® PH 101
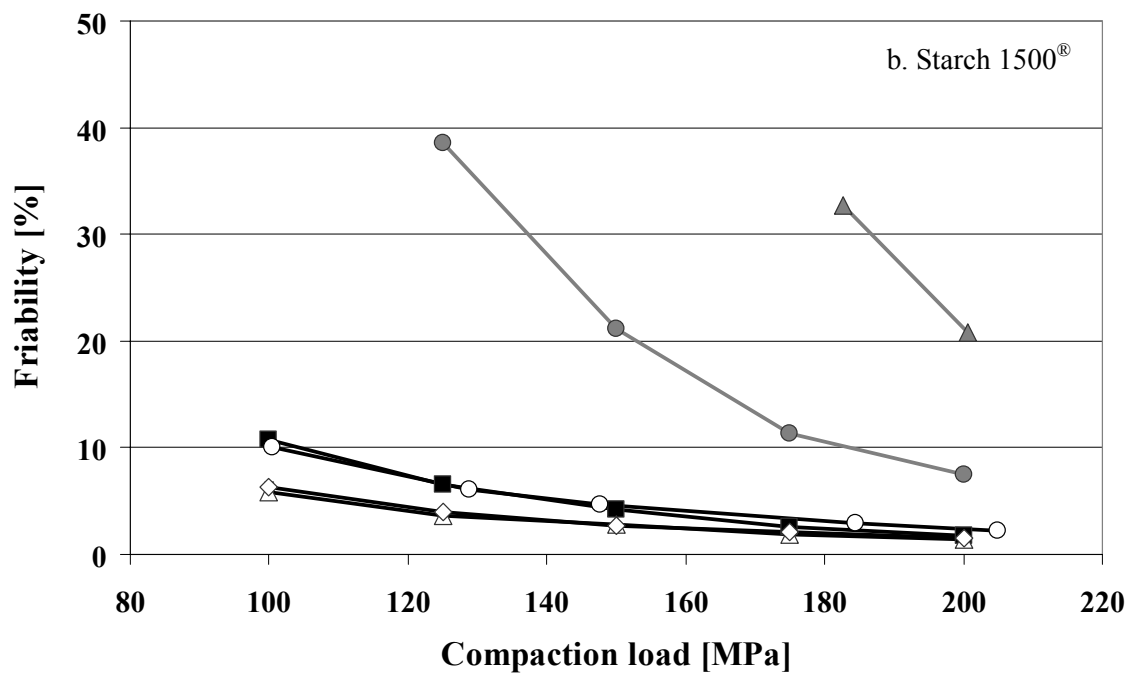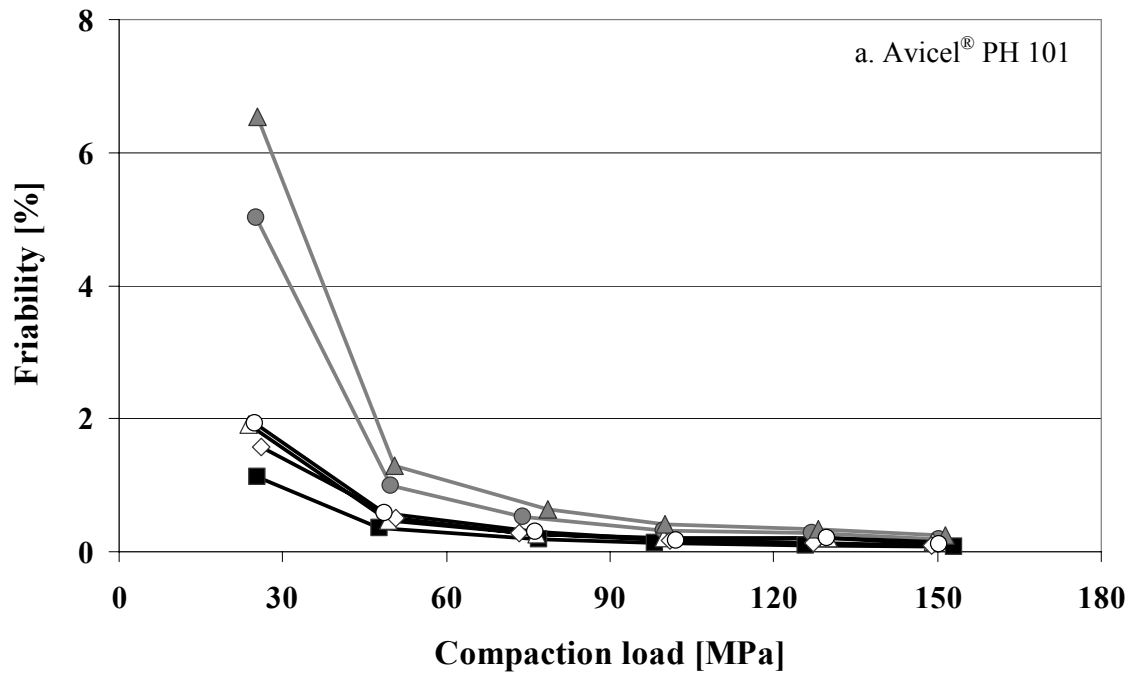
b. Starch 1500®

Figure 6.12 *Friability of the tablets compressed from Avicel® PH 101 (a), Starch 1500® (b) and Tablettose® 80 (c), containing 0.5% AEROSIL® 200 VV (△), 0.5% AEROSIL® 200 (◊), 0.5% AEROSIL® 130 V (○), 0.5% AEROSIL® R 972 V (●), 0.5% AEROSIL® R 974 V (▲) and without AEROSIL® (■).*

According to Ph. Eur. 5th Ed., a maximum loss of 1 per cent of the tablet mass is considered to be acceptable for most products. For Avicel® PH 101, addition of AEROSIL® increased the friability, whereby the hydrophobic type led to a higher increase. Nevertheless, at compression force greater than 75 MPa, the difference in the friability between the different tablets became very small and all friability results were below 1%. For Starch 1500®, the friability of the tablets was higher than 1%. Addition of hydrophilic AEROSIL® slightly decreased the friability, while addition of hydrophobic AEROSIL® dramatically increased the friability. For Tablettose® 80, the friability of the tablets was not influenced by addition of AEROSIL®.

The friability results are in good agreement with the tensile strength results. A tablet with high tensile strength exhibited low friability.

6.4   Moisture study

6.4.1 Sorption isotherm of tablets

One of the characteristics of hydrophobic colloidal silicon dioxide powder is its low and relatively constant water uptake at all humidity levels, while hydrophilic colloidal silicon dioxide powder adsorbs more water with increasing relative humidity (Technical bulletin Degussa 2003). Tablets containing 0.5% hydrophilic or hydrophobic AEROSIL® were compressed in order to evaluate the influence of the nature of AEROSIL® on the water uptake of tablets. The study includes tablets compressed from Avicel® PH 101, Starch 1500® and Tablettose® 80, containing 0.5% AEROSIL® 200 VV, 0.5% AEROSIL® R 972 V and without AEROSIL®. Figure 6.13 depicts the water uptake of tablets after seven days storage at various relative humidities.
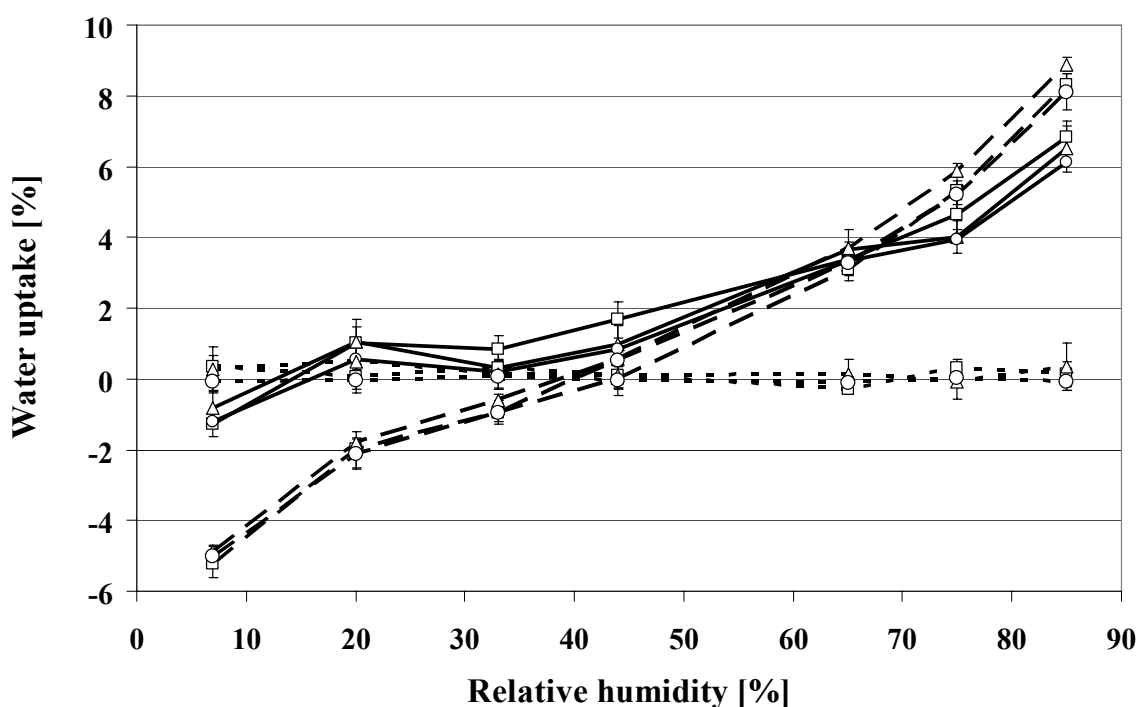
Figure 6.13   Sorption isotherms of tablets compressed from Avicel® PH 101 (———), Starch 1500® (— —) and Tablettose® 80 (- - - -), containing 0.5% AEROSIL® 200 VV (Δ), 0.5% AEROSIL® R 972 V (○) and without AEROSIL® (□), after 7 days storage at various levels of relative humidity and 20°C. Error bars represent the 95% confidence interval of ten measurements.

Even though the water uptake behavior of hydrophobic and hydrophilic colloidal silicon dioxide powders differs greatly, the water uptake of the tablets during storage was not affected by the addition of colloidal silicon dioxide. The water uptake was characteristic for each excipient and independent from the presence of different AEROSIL® types.

6.4.2 Tablet Strength

Figure 6.14 shows a decrease in tablet tensile strength for Avicel® PH 101 and Starch 1500® with increasing relative humidity. For Tablettose® 80, the radial tensile strength of the tablets remained constant at all relative humidity levels. For each excipient, the changes in the radial tensile strength were identical for hydrophobic and hydrophilic AEROSIL® types.
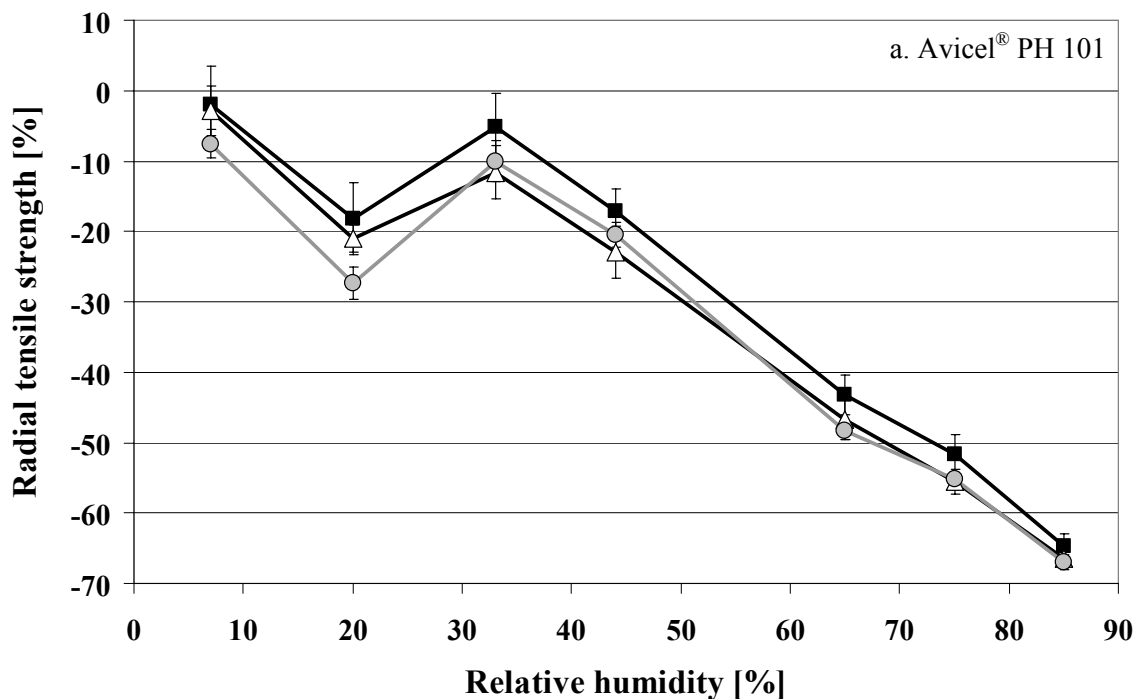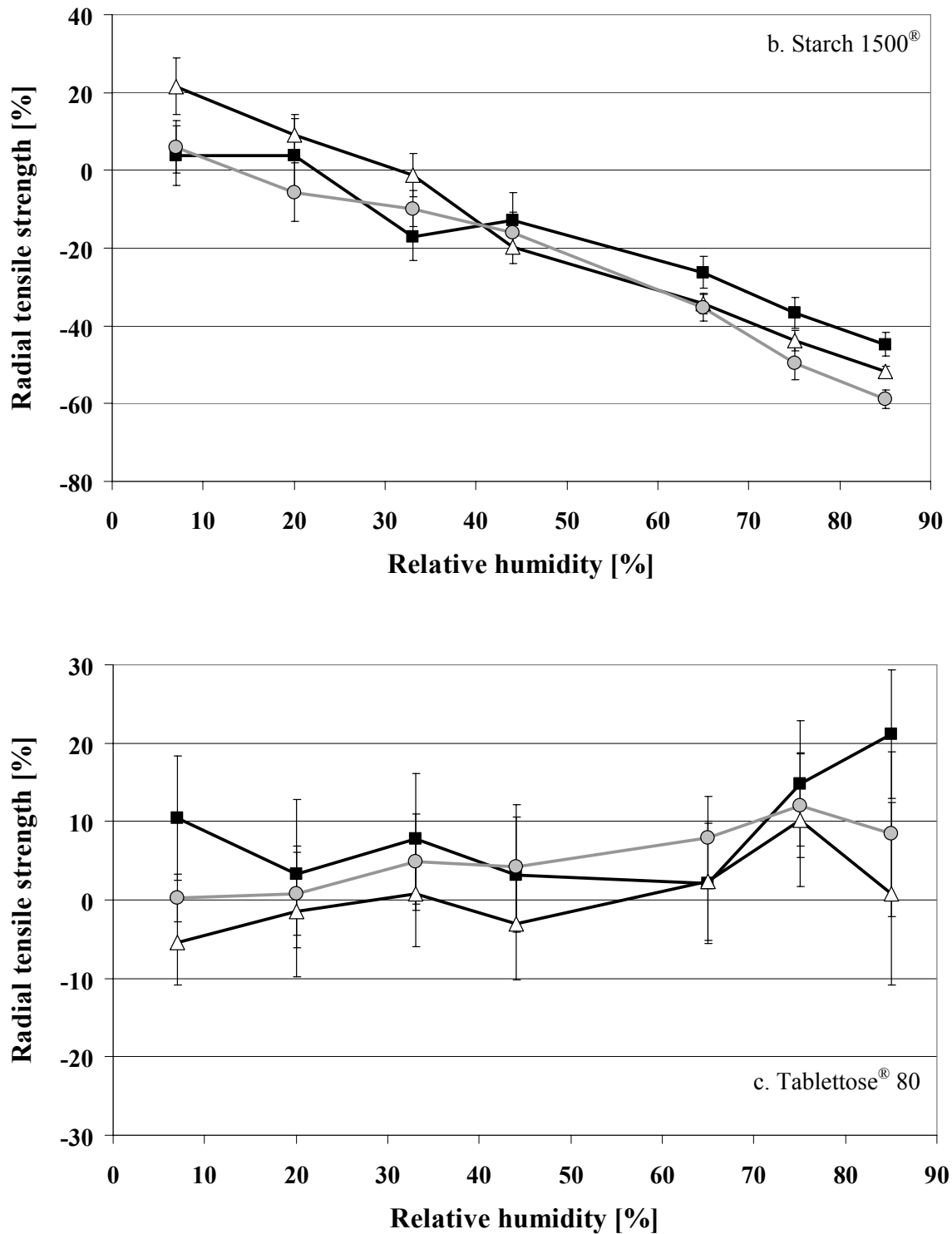
Figure 6.14   Changes (expressed in percent) in the radial tensile strength of tablets compressed from Avicel® PH 101 (a), Starch 1500® (b) and Tablettose® 80 (c), containing 0.5% AEROSIL® 200 VV (Δ), 0.5% AEROSIL® R 972 V (●) and without AEROSIL® (■). Error bars represent the 95% confidence interval of ten measurements.

6.5   Effect of colloidal silicon dioxide on the film formation of magnesium stearate

6.5.1   Influence of magnesium stearate on the radial tensile strength of tablets containing the pure excipient

Lubricants, as magnesium stearate, are commonly included in tablet formulations in order to reduce die wall friction during compaction and ejection of the tablets. Their presence, however, may cause undesirable changes in tablet properties (Bolhuis and Hölzer 1996).

Table 6.4   Residual and ejection forces of tablets compressed at 100 MPa for Avicel® PH 101 and at 200 MPa for Starch 1500® and Tablettose® 80.

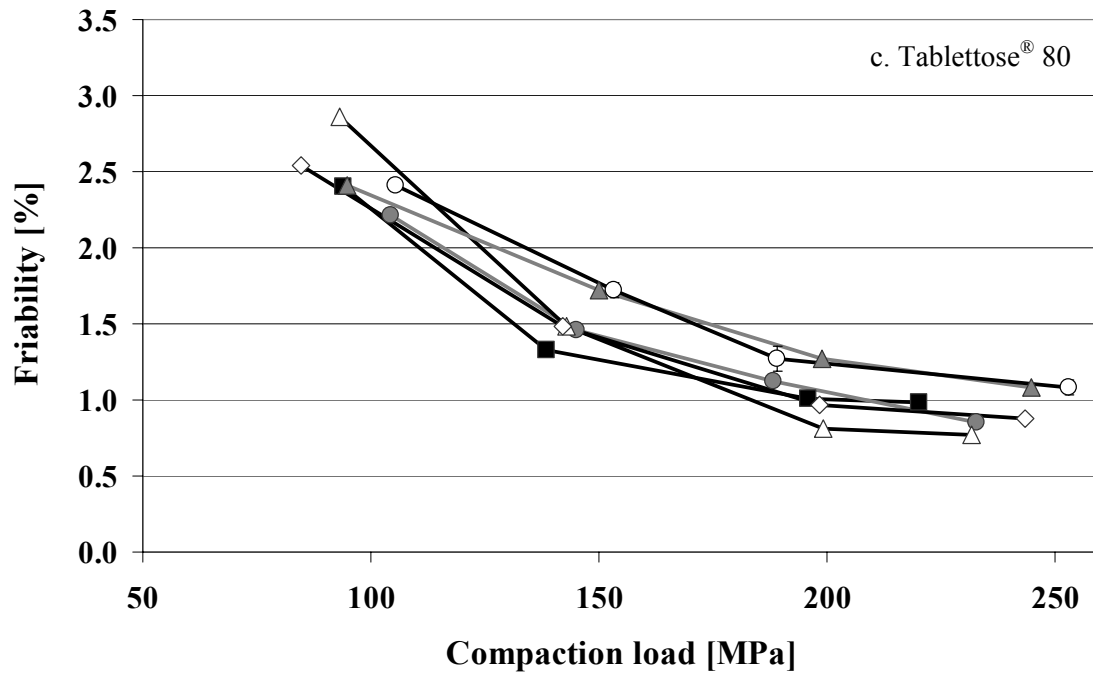|	Avicel® PH 101		Starch 1500®		Tablettose 80®	
	Residual force [kN]	Ejection force [kN]	Residual force [kN]	Ejection force [kN]	Residual force [kN]	Ejection force [kN]
no additives	0.66	1.12	0.56	0.67	0.28[a]	0.67[a]
magnesium stearate (MS)[b]	0.06	0.16	0.10	0.18	0.24	0.68
MS + AEROSIL® 200[c]	0.06	0.16	0.13	0.26	0.35	0.69
MS + AEROSIL® 200 VV[c]	0.05	0.16	0.13	0.21	0.45	0.74
MS + AEROSIL® R 972 V[c]	0.08	0.18	0.20	0.27	0.48	0.80

[a] Prelubrication with oleic acid   [b] amount: 0.5%   [c] amounts: 0.5%

As shown in Table 6.4, the addition of 0.5% magnesium stearate reduced the residual and ejection forces for Avicel® PH 101 and Starch 1500®. A comparison for Tablettose® 80 was not possible because the die was prelubricated with oleic acid in order to successfully compress pure Tablettose® 80. Nevertheless, besides its good lubricating properties, magnesium stearate reduced the radial tensile strength of tablets of pure Avicel® PH 101, Starch 1500® or Tablettose® 80 (Figure 6.15).
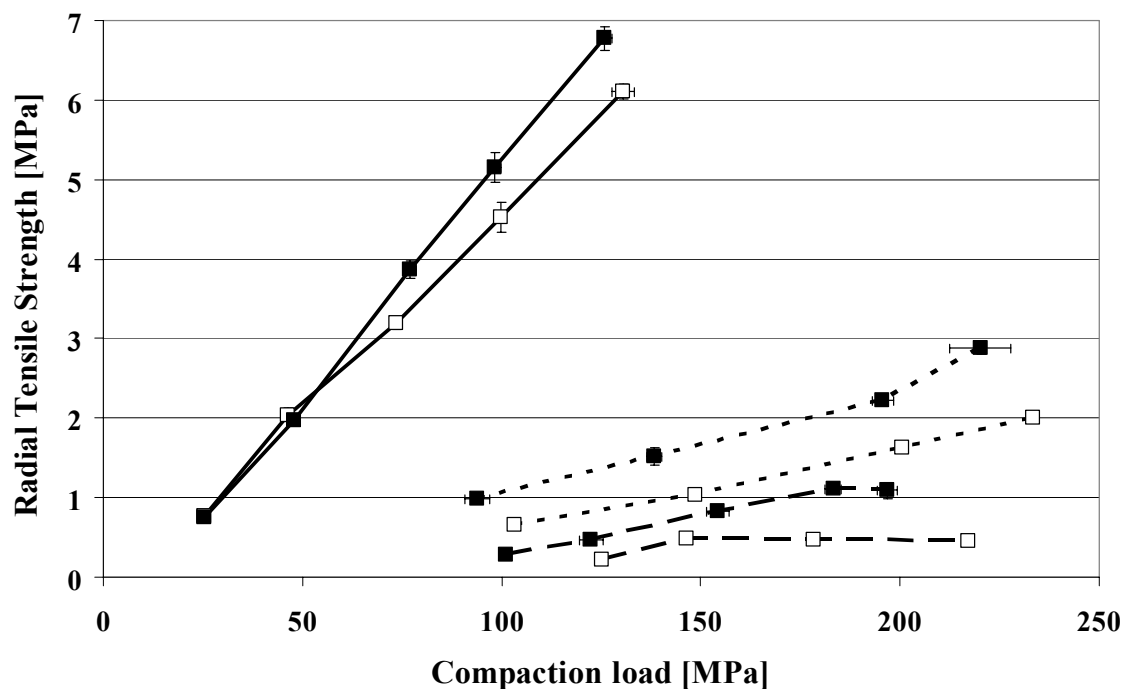
*Figure 6.15   Radial tensile strength of tablets compressed from Avicel® PH 101 (——),
Starch 1500® (— —) and Tablettose® 80 (- - - -) as pure substance (■)
and containing 0.5% magnesium stearate (□).*

The results obtained are in good agreement with previous work. As described by
Bolhuis and Hölzer (1996), magnesium stearate forms a lubricant film around the
excipient particles during the mixing process, and this film interferes with the bonding
properties of the excipient particles by acting as a physical barrier. The decrease in
radial tensile strength can be explained by the formation of weaker bonds between
lubricant/lubricant particles rather than strong excipient/excipient bonds.

6.5.2   Influence of colloidal silicon dioxide on the radial tensile strength of tablets containing magnesium stearate

The formation of a lubricant film during mixing can be influenced by numerous
factors including a third component, such as colloidal silicon dioxide. Lerk et al.
(1977) showed that AEROSIL® 200 can significantly suppress the negative effect of
the lubricant on the binding properties. A greater effect was found when the host
particles were first mixed with AEROSIL® and subsequently for a short time with

magnesium stearate. Therefore, a chronological mixing step was chosen to investigate the effect of compacted hydrophilic and hydrophobic colloidal silicon dioxide on film formation of magnesium stearate. The results obtained were then compared with the more commonly used AEROSIL® 200.

Avicel® PH 101

Figure 6.16   Radial tensile strength of tablets compressed from Avicel® PH 101 containing 0.5% magnesium stearate (□), 0.5% magnesium stearate and 0.5% AEROSIL® (AEROSIL® 200 VV (Δ), AEROSIL® 200 (◊), AEROSIL® R 972 V (●)) and no additives (■). Error bars represent the 95% confidence interval of ten measurements.

Figure 6.16 shows that tablets compressed from Avicel® PH 101, hydrophilic AEROSIL® and magnesium stearate showed the same radial tensile strength/ compaction profile as pure Avicel® PH 101 tablets and exhibited residual and ejection forces identical to Avicel® PH 101/magnesium stearate tablets (Table 6.4). These results showed that under these mixing conditions, hydrophilic AEROSIL® restored the bonding properties of Avicel® PH 101, while maintaining the good lubricating property of magnesium stearate. A theoretical understanding of the different

particle/particle interactions and the phenomena observed was provided by Rowe (1988). He calculated the adhesive and cohesive interactions between microcrystalline cellulose, magnesium stearate and colloidal silicon dioxide. On the basis of the results, he found that microcrystalline cellulose would be preferentially enrobed by colloidal silicon dioxide and that the majority of magnesium stearate will be coated by colloidal silicon dioxide. The predictions are consistent with the results reported by Staniforth and Ahmed (1986, 1987), who additionally explained that the positive influence of colloidal silicon dioxide on tablet strength of microcrystalline cellulose, without adversely increasing the ejection force, was due to the ability of colloidal silicon dioxide to enrobe magnesium stearate in a protective coat, which was broken down under the high shear forces existing close to the wall.

Tablets containing Avicel® PH 101, *hydrophobic* AEROSIL® and magnesium stearate showed lower radial tensile strength/compaction profiles compared to tablets containing Avicel® PH 101, *hydrophilic* AEROSIL® and magnesium stearate. The range of the differences in the radial tensile strength between both tablets was the same as between tablets containing hydrophilic AEROSIL®/Avicel® PH 101 and hydrophobic AEROSIL®/Avicel® PH 101 tablets (Figure 6.5), indicating that hydrophobic AEROSIL® interfered with magnesium stearate to the same extent as hydrophilic AEROSIL®. The residual and ejection forces were the same as for Avicel® PH 101 and magnesium stearate tablets, showing that the lubricating property of magnesium stearate was retained.

Starch 1500®

The addition of 0.5% magnesium stearate to Starch 1500® strongly reduced the radial tensile strength (Figure 6.17) and the residual and ejection forces of the tablets (Table 6.4). Tablets compressed from Starch 1500®, AEROSIL® and magnesium stearate displayed greater radial tensile strength values and greater residual and ejection forces compared to tablets produced from Starch 1500®/magnesium stearate. However, residual and ejection forces were much lower than for pure Starch 1500® tablets and indicated a good lubrication. The increase in the radial tensile strength was dependent

on the nature of the AEROSIL®. Hydrophilic AEROSIL® led to much higher radial tensile strength values compared to hydrophobic AEROSIL®, as already demonstrated for binary mixtures (Figure 6.7). These results showed that AEROSIL®, especially hydrophilic types, restored the bonding properties of Starch 1500®, while maintaining the good lubricating property of magnesium stearate.
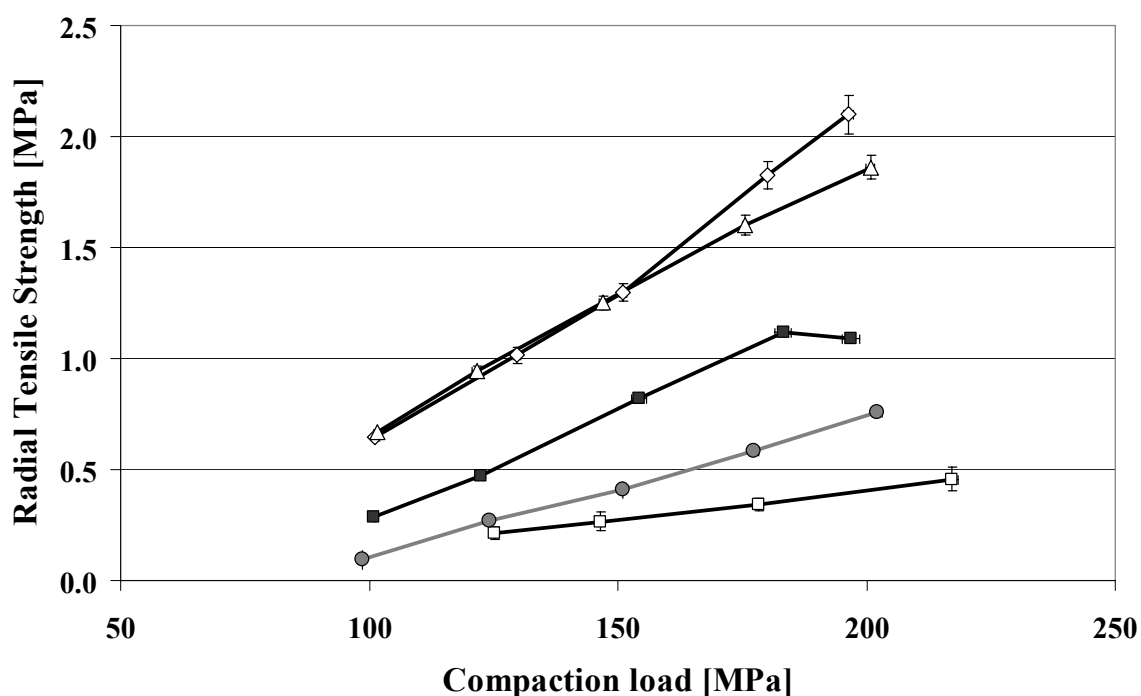
Figure 6.17 Radial tensile strength of tablets compressed from Starch 1500®
containing 0.5% magnesium stearate (□), 0.5% magnesium stearate and
0.5% AEROSIL® (AEROSIL® 200 VV (Δ), AEROSIL® 200 (◊),
AEROSIL® R 972 V (●)) and no additives (■). Error bars represent the
95% confidence interval of ten measurements.

Tablettose® 80

The addition of 0.5% magnesium stearate to Tablettose® 80 slightly reduced the radial tensile strength of the tablets (Figure 6.18). Tablets containing Tablettose® 80, AEROSIL® and magnesium stearate displayed higher residual and ejection forces (Table 6.4) and practically the same radial tensile strength values as compared to Tablettose® 80/magnesium stearate tablets. There was no difference between the AEROSIL® types. The interaction between AEROSIL® and magnesium stearate was

limited by the creation of new surfaces of Tablettose® 80, by fragmentation during tableting, being free of lubricant and glidant.
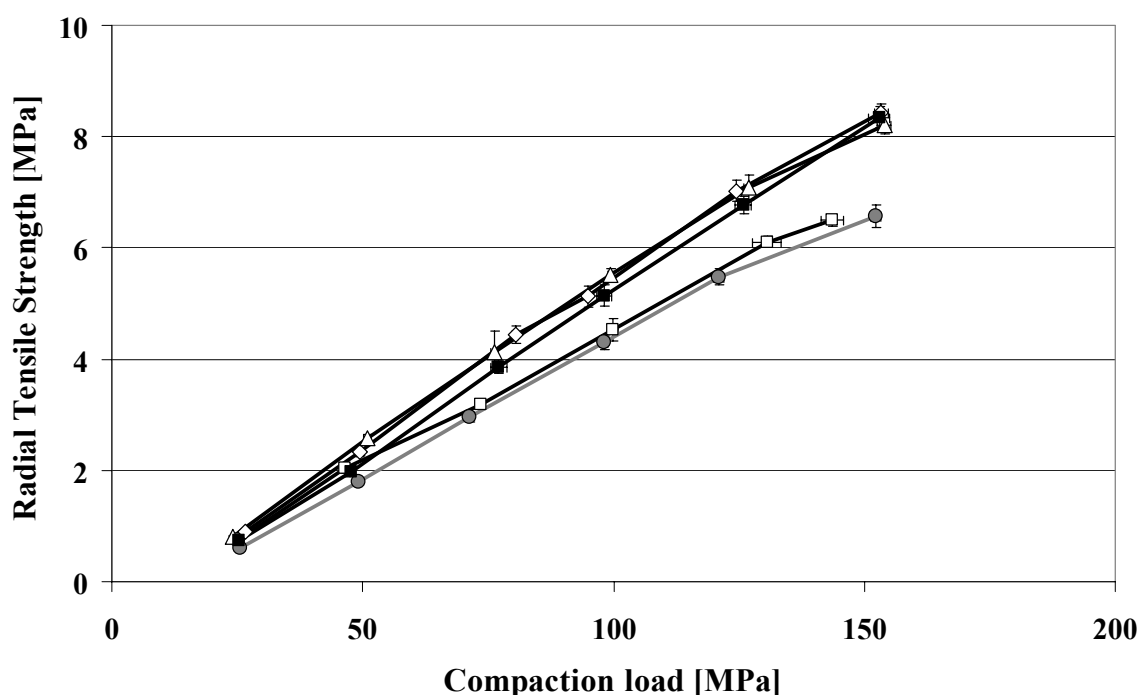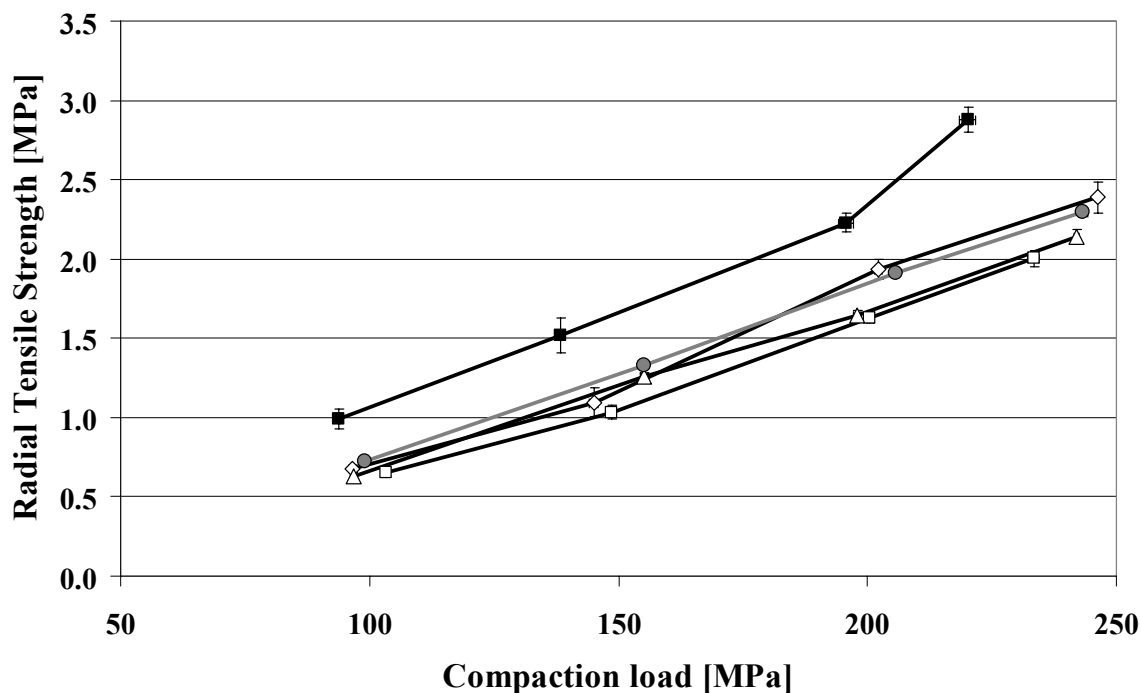

Figure 6.18   Radial tensile strength of tablets compressed from Tablettose® 80 containing 0.5% magnesium stearate (□), 0.5% magnesium stearate and 0.5% AEROSIL® (AEROSIL® 200 VV (Δ), AEROSIL® 200 (◊), AEROSIL® R 972 V (●)) and no additives (■). Error bars represent the 95% confidence interval of ten measurements.

6.6   Discussions of the results

In this chapter, the influence of hydrophobic and hydrophilic colloidal silicon dioxide on the compression and tablet parameters of Avicel® PH 101, Starch 1500® and Tablettose® 80 was investigated.

The Heckel plots, describing the densification of a powder under pressure, are characteristic for each excipient and are not altered by the addition of colloidal silicon dioxide. Addition of AEROSIL® increases the residual and ejection forces for Avicel® PH 101 and Starch 1500® and has no influence on Tablettose® 80 tablets. However, the residual and ejection forces remain in an acceptable range for tablet production purposes.

The influence of colloidal silicon dioxide on tablet strength is dependent on its hydrophobic and hydrophilic nature and on the compaction characteristics of the excipients. The differences can be explained by the Ryshkewitch-Duckworth relationship. For Avicel® PH 101, hydrophilic colloidal silicon dioxide slightly reduces the radial tensile strength of the tablets (-10%), whereas the hydrophobic type leads to a larger reduction (-30%). For Starch 1500®, hydrophilic AEROSIL® increases the tablet strength while hydrophobic AEROSIL® leads to a strong decrease. Tablets compressed from AEROSIL® and Tablettose® 80 show a slight decrease in the radial tensile strength and no differences between AEROSIL® types.

None of the colloidal silicon dioxide types used show an influence on the tablet properties of Avicel® PH 101, Starch 1500® and Tablettose® 80 after seven days storage at various relative humidities.

Under the mixing conditions chosen, the deleterious effect of magnesium stearate on the bonding properties of excipient particles can be reduced, while still retaining its lubricating properties. Hydrophobic AEROSIL® interferes with magnesium stearate to the same extent as hydrophilic types.

Tablets containing AEROSIL® 200 VV or AEROSIL® 200 show the same results as far as tablet strength, moisture uptake and magnesium stearate film formation are concerned. This indicates that the densification process of AEROSIL® has no effect on tablet properties.

CHAPTER 7

MATERIALS AND METHODS

7.1 Materials

Table 7.1   Excipients and chemicals

Name	Batch-No	Manufacturer / supplier
Excipients		
AEROSIL® 200	2351	Degussa AG
AEROSIL® 200 VV	5314111	Degussa AG
AEROSIL® 130 V	1614032	Degussa AG
AEROSIL® R 972 V	919051	Degussa AG
AEROSIL® R 974 V	2615102	Degussa AG
Avicel® PH 101	6142C / 6227C / 6250C	FMC Biopolymer
Extra white maize starch	S8193	Roquette
Magnesium stearate	0266	Baerlocher GmbH
Native starch	Commercial sample	-
Oleic acid	K91145571916	Merck KGaA
Starch 1500®	IN503673 / IN504534	Colorcon Ltd
Tablettose® 80	L0145A4003 / L0211A40003	Meggle GmbH
Gases		
Nitrogen (Typ 5.0)	0652	Messer Griesheim GmbH
Helium (Typ 4.6)	0385	Messer Griesheim GmbH
Chemicals		
Magnesium chloride	TA743633 643	Merck KGaA
Potassium acetate	K29565320 205	Merck KGaA
Potassium carbonate	A493528	Merck KGaA
Potassium chloride	TA101436	Merck KGaA
Potassium nitrate	CC520963	Merck KGaA
Sodium bromide	K30615060 220	Merck KGaA

Sodium chloride	K 31900304 314	Merck KGaA
Sodium hydroxide	C294798	Merck KGaA
Sodium nitrite	S30973034	Merck KGaA

7.2   General equipment

Table 7.2   List of general equipment

Equipment	Manufacturer / supplier
Balance Mettler AE 200	Mettler Toledo GmbH
Balance Mettler AT 261 Delta range	Mettler Toledo GmbH
Balance Mettler PC 1616	Mettler Toledo GmbH
Balance Mettler PG 4002-S	Mettler Toledo GmbH
Balance Mettler PM 6100	Mettler Toledo GmbH
Balance Sartorius Talent TE	Sartorius AG
Drying oven T5050	Haraeus Holding GmbH
High speed mixer SW 1/S	Erweka GmbH
Pin mill 160Z	Hosokawa Alpine
Turbula mixer T2C	Bachofen AG
Water distillation apparatus	Wagner & Munz GmbH

7.3   Data Processing

Computer: Pentium II-MMX 233 MHz, 260 MB RAM, 8 GB hard disk

Table 7.3   List of software

Software	Manufacturer / supplier
Catman 3.1	Hottinger-Baldwin Messgeraete GmbH
Mastersizer 2000 Version 4.0	Malvern Instruments GmbH
Microsoft Excel 2000	Microsoft GmbH
Microsoft Photo Editor 2000	Microsoft GmbH
Microsoft Power Point 2000	Microsoft GmbH
Microsoft Word 2000	Microsoft GmbH
Orion 5	E.L.I. sprl
VCH Biblio for Windows 32 Bits	VCH publishing society

7.4   Preparation of the mixtures

Mixtures containing Avicel PH® 101, Starch 1500® or Tablettose 80®, respectively and various AEROSIL® types were prepared using a standardized mixing procedure. Figure 7.1 shows a mixing process for Starch 1500® as an example. The following mixers were used: a free-fall mixer (Turbula T2C, W. A. Bachofen AG), with a 2 l vessel, a maximum filling degree of 75% and a rotational speed of 42 rpm; a high speed mixer based on the plowshare principle (SW 1/S, Erweka GmbH), with a 5 l drum, a filling degree of 70% and a rotational speed of 2400 rpm. For homogenization milling of mixture 5, a pin mill (160 Z, Hosokawa Alpine) with a rotary speed of 14000 rpm was used. The amount of AEROSIL® was set at 0.5 wt% based on the total formulation.

300 g Starch 1500®
        ←——— 3 g AEROSIL® pre-sieved (mesh size 315 μm)

        ←——— 297 g Starch 1500® and mixing by hand

sieving (mesh size 800 μm)

10 min. Turbula mixer

Mixture 1

sieving (sieve 800 μm) ——→ **Mixture 2**

10 min. high speed mixer SW 1/S ——→ **Mixture 3**

10 min. high speed mixer SW 1/S ——→ **Mixture 4**

pin mill Alpine 160 Z ——→ **Mixture 5**
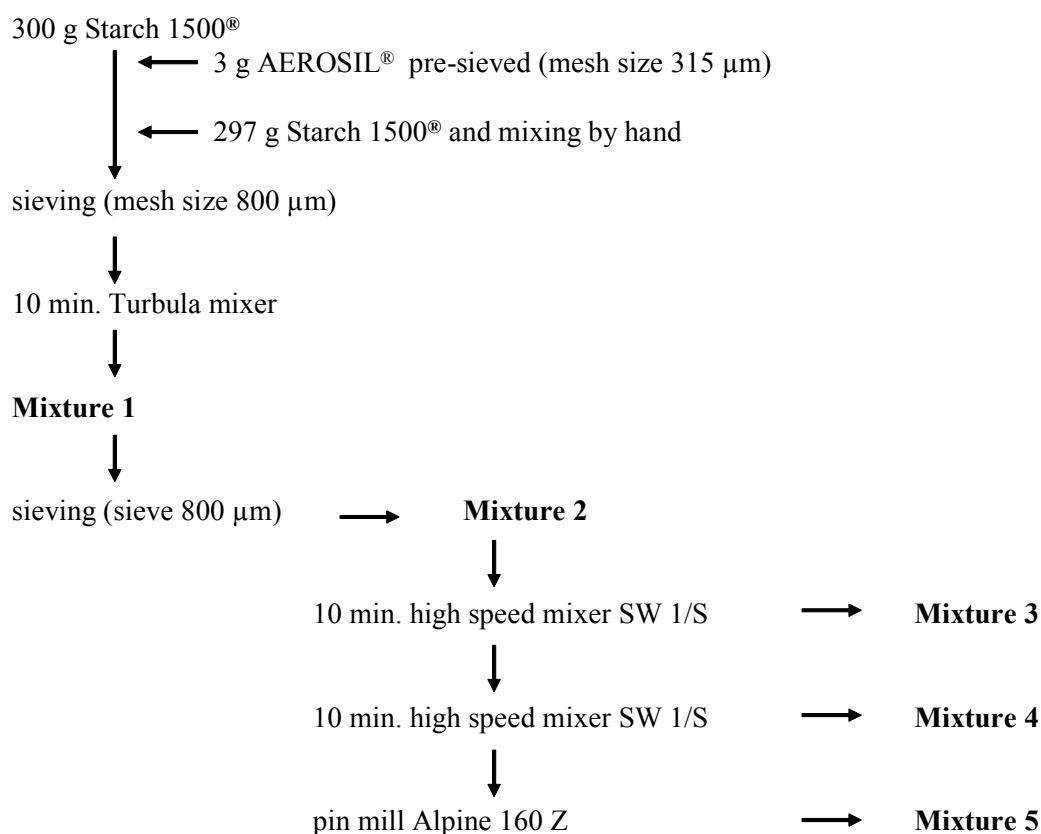
Figure 7.1   Mixing process of Starch 1500® with 0.5% AEROSIL®.

To investigate the effect of AEROSIL® on the film formation of lubricant, 0.5% magnesium stearate was sieved trough a 315 μm sieve onto the previously described mixture 2 and mixing was continued for another five minutes in the same free-fall mixer.

7.5   *Characterization of the mixtures*

7.5.1   True density

The true density was determined using a Beckman air comparison pycnometer (model 930, Beckman Instruments) at room temperature. An amount of powder representing 80% (V/V) of the sample cup was weighed exactly (model AE 200, Mettler Toledo GmbH). The zero measurement and the starting number (108.05 mL) were checked before measurements. The true density [g/mL] was calculated as the quotient of weighed substance to true volume.

The mean value of three measurements was taken.

7.5.2   Poured and tapped density

Poured (bulk) and tapped densities were measured according to the European Pharmacopeia 5th Edition. 70.0 g of Avicel$^®$ PH 101 mixtures, 100.0 g of Starch 1500$^®$ mixtures and 100.0 g of Tablettose$^®$ 80 mixtures were filled without compacting into a 250 mL graduated cylinder using a powder funnel. The cylinder containing the product was weighed to $\pm$ 0.1 g (m) (model PG 4002-S or PM 6100, Mettler Toledo GmbH), the unsettled volume (V_0) was read to $\pm$ 1 mL and the poured density (g/mL) was calculated as the quotient m/V_0. Measurements were performed in triplicate and the mean value was calculated. The values for AEROSIL$^®$ were obtained from batch records. A settling apparatus (model STAV 2003, J. Engelsmann AG) was used to measure the tapped density. The settled volume was read after 500 (V_{500}) and 1250 taps (V_{1250}). Another 1250 taps were carried out when the difference between V_{500} and V_{1250} was greater than 2 mL. The tapped density (g/mL) was expressed as the quotient of m/V_{1250} or m/V_{2500}. Measurements were performed in triplicate and the mean value was calculated. The values for AEROSIL$^®$ were obtained from batch records.

The Carr compressibility index, CC % = [(tapped density – poured density)/poured density]*100 and the Hausner ratio, HR = tapped density/bulk density, were calculated from these volume readings.

7.5.3 Particle size

The particle size distributions of Avicel[®] PH 101, Starch 1500[®] and Tablettose[®] 80 were measured by laser diffraction spectrometry (Mastersizer 2000, Malvern Instruments GmbH) using the dry-dispersing system Scirocco 2000 (Malvern Instruments GmbH). Avicel[®] PH 101 was measured using a dispersing air pressure of 3 bars, whereas no dispersing air pressure was used for Starch 1500[®] and Tablettose[®] 80. Data were collected directly by means of the system software (Malvern Instruments GmbH).

The mean values of three measurements were calculated.

7.5.4 Angle of repose

The angle of repose of the mixtures was measured using a sieve-cone-method according to DIN ISO 4324. The distance between the sieve and the metal cylinder was kept at 10 cm. 100 g of the material were sieved through an 800 µm sieve onto a metal cylinder with a radius (r) of 25 mm and the exact distance between the tip of the cone and the sieve was adjusted to 3 cm. The cylinder surface was cleaned and 100 g of the material were sieved through an 800 µm sieve onto the metal cylinder. The height (h) of the powder cone was measured with a dial high gauge (model No. 192-106, Mitutoyo Messgeraete GmbH).

The angle of repose (α) was calculated using the following equation:

$$\tan \alpha = h/r$$

The mean, the standard deviation and the 95% confidence interval of six samples were calculated.

7.5.5 Conveyor belt

The conveyor belt (Figure 7.2) consists of a circular strip of plastic material 77 cm long and 10 cm wide (Reiff-Technische Produkte GmbH). A motor (model 3557K024CR, Dr. F. Faulhaber GmbH & Co. KG) rotates the strip at a speed of 2.28 cm/s. Mixtures were passed through the funnel to the belt and conveyed to a balance (model PM 6100, Mettler Toledo GmbH). The accumulated mass of powder versus time was plotted at 0.5 or 1 second intervals. The diameter of the funnel's orifice was 1.9 cm. The gap between the funnel and the belt was set to 2 mm for Starch 1500® and Tablettose® 80 and to 3 mm for Avicel® PH 101 using a micrometer screw (0.01 mm of accuracy, Mitutoyo Messgeraete GmbH). The weight of the powder conveyed was plotted automatically (HP VEE program, version 5.0).

Mixtures 2 and 4 of Starch 1500®, Tablettose® 80 and Avicel® PH 101 were investigated for 2.5, 2 and 6 minutes, respectively. All measurements were repeated three times. In order to compare the different flow behavior of the mixtures, the slopes of the linear regression of the mass accumulated versus time curves were calculated.
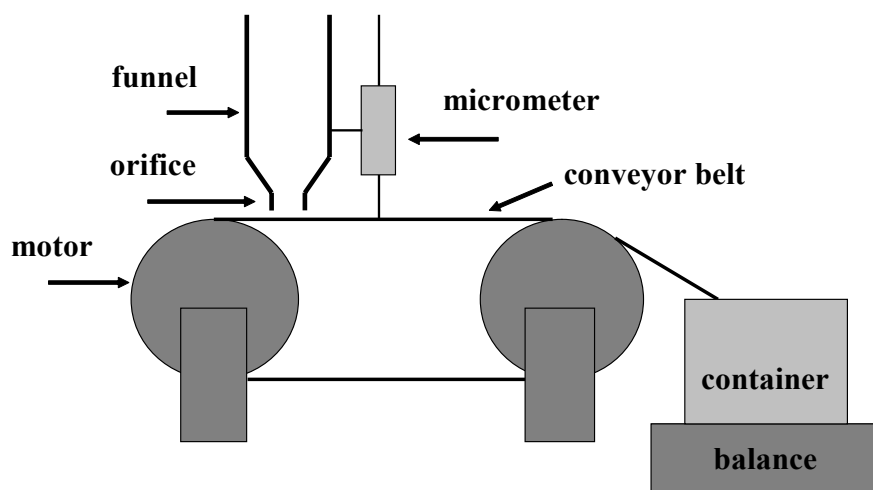
Figure 7.2   Schematic diagram of the conveyor belt.

7.5.6   Ring shear cell

The flowability factor of the mixtures was measured using an automatic ring shear tester (model RST-01.pc, Dr. Dietmar Schulze Schüttgutmesstechnik). A picture of the apparatus is shown in Figure 7.3.

Figure 7.3   Picture of the automatic ring shear tester RST-01.pc.

A set-up of the method is depicted in Figure 7.4. The powder sample was filled in an annular trough (Typ M, Dr. Dietmar Schulze Schüttgutmesstechnik) with a volume of 943 cm³, the excess of powder was carefully removed to adjust the level and the powder sample was weighed exactly (model Talent TE, Sartorius AG). A lid with a rough lower side, which was adapted to the shape of the shear cell, was placed on the sample. Normal stress (σ) was applied to the lid by the normal force (N). The normal force was adjusted via computer, which commands a motor to shift weights on a lever

arm. The force (F_A) acted as a counterweight system to compensate the weight of cover and pull roads. To shear the sample, the shear cell was rotated by a digitally controlled motor in the direction (ω) at a circumferential speed of 1 mm/min, while the lid was detained by pull roads. Shear forces F_1 and F_2 were automatically measured and the shear stress acting in the sample at a specific bulk density was calculated.
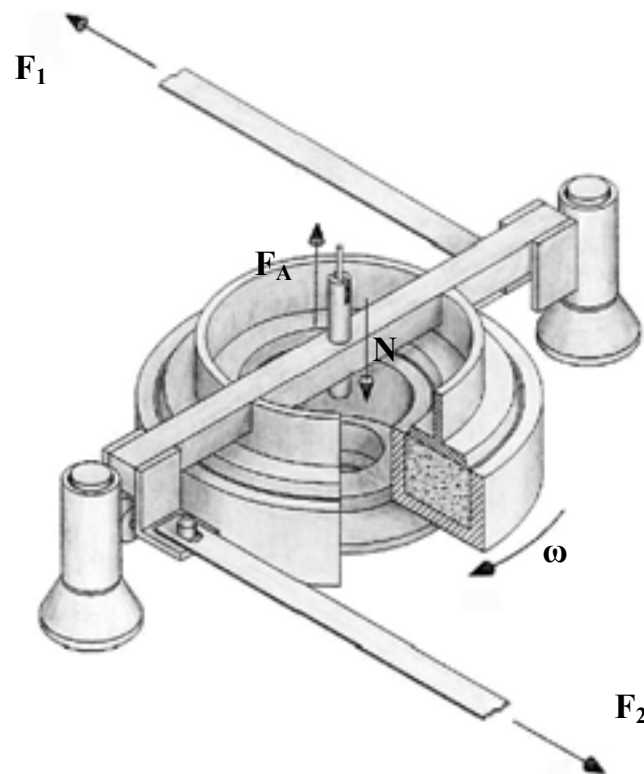
*Figure 7.4   Set-up of the automatic ring shear tester RST-01.pc.
Scheme taken from Schulze and Wittmaier (2002).*

For measurements of the unconfined failure strength, the sample was first presheared (σ_{pre}) and then sheared (σ_{sh}) to failure at three different stresses, with $\sigma_{sh} < \sigma_{pre}$. In this way, a yield locus could be determined by plotting the shear stress causing failure along a plane as a function of the normal stress on that plane for a given density of the powder. The powder density was governed by consolidation load applied during preshear. A normal stress for preshear of 2000, 3000 and 4000 Pa was adjusted for mixtures 2 and 4 of Avicel® PH 101 and a normal stress for preshear of 2000 and 4000 Pa for mixtures 2 and 4 of Starch 1500® and Tablettose® 80. For each normal stress (σ_{pre}), the measurements were repeated 3 times.

Unconfined failure strength (σ_c) and major principal stress at stationary flow or consolidation stress (σ_1) can be calculated by drawing Mohr semicircles tangential to the yield locus (Schwedes 1968). The flowability factor (ff_c) was then calculated according to the equation:

$$ff_c = \sigma_1 / \sigma_c$$

7.5.7   Scanning electron microscopy (SEM)

The powder mixture was examined by scanning electron microscopy using a Zeiss DSM 940 A instrument (Carl Zeiss). The pictures were taken with a camera (model Contax M 167 MT, Yashica-Kyocera) and were digitalized using the Orion system (Orion 5, E.L.I. sprl). Each mixture was fixed on an aluminum pin using double-adhesive tape (Tempfix) and then coated with a thin gold layer prior to examination using a Sputter Coater (model E 1500, Bio-Rad). The samples were sputtered four times for 60 s and exposed to 20 mA current and 2.1 kV acceleration voltage at a vacuum of 0.02-0.03 mbar. The micrographs were taken at 5 kV and 10 kV and at magnifications between 5000 and 20000.

7.5.8   X-Ray photoelectron spectroscopy (XPS)

The samples were measured as loose powders without any pretreatment such as compressing. They were supported by a tantalum sample container and were transferred into the XPS instrument by means of a differential pumping stage. After evacuation, a sample was transferred into the main spectrometer chamber and was measured at about $5 \cdot 10^{-8}$ mbar. Broad area XPS conditions were adjusted to obtain information on the surface properties of about 0.5 cm^2 of the material in a single spectrum. The XPS measurements were performed using MgK_α radiation at a power of 150 W. The electron energy analyzer (model EA11A, Leybold) was operated at a pass-energy of 75 eV in the fixed analyzer transmission mode. Additional details are given by Albers et al. (1998).

The spectra were treated as follows: subtraction of the X-Ray satellites, smoothing by polynomial fits, Shirley-type background subtraction (Shirley 1972), peak integration and correction by sensitivity factors according to the elemental ionization cross sections and the transmission function of the electron energy analyzer. The elemental sensitivity factors for the quantitative evaluation were: Si 2p 0.4, O 1s 0.78 and C 1s 0.34. The binding energy scale of the spectrometer was referenced to the Au $4f_{7/2}$ signal at 84.0 eV.

7.5.9   Specific surface area by gas absorption

The specific surface area of the pure material was determined using nitrogen gas adsorption at a temperature of 77 K based on the Brunauer, Emmett and Teller (BET) method according to the European Pharmacopeia 5th Edition. A quantity of test powder, that provides a surface area of at least 1 m^2, was accurately weighed (model AT 261 Delta range, Mettler Toledo GmbH).

AEROSIL® samples were dried at 105°C overnight and degassed for 1 hour at 200°C in vacuo before analysis using the volumetric method (model ASAP 2400, Micromeritics, Norcross GA). Six data points were recorded for 0.05 < p/p_0 < 0.22. Samples of Avicel® PH 101, Starch 1500® and Tablettose® 80 were degassed in vacuo for 3 hours at 90°C, for 1 hour at 90°C and for 1 hour at 50°C, respectively. The analysis was then performed using the volumetric method (model SA 3100, Coulter, Beckmann Coulter GmbH) and the specific surface area was calculated using the Coulter software (Version 2.12, Beckmann Coulter GmbH). The measurements were repeated 6 times with different sample quantities.

7.5.10 Atomic force microscopy (AFM)

Powder sample preparation

Samples of bulk Avicel® PH 101 and mixtures 2 and 4 containing AEROSIL® 200, AEROSIL® 200 VV and AEROSIL® R 972 V were immobilized on an AFM stub using doubled-sided adhesive tape. Excess loose powder was removed before measurement. Powder samples for adhesion measurements were prepared immediately before use.

Cantilever spring constant

The cantilever spring constant was determined using a dynamic method as described by Cleveland et al. (1993). A glass sphere of known density (ρ = 2500 kg/m^3) was attached to the apex of an oxide-sharpened silicon nitride cantilever (type NP-20, Digital Instruments, Veeco Inst.) under optical microscope control (Ergolux, Ernst Leitz), as depicted in Figure 7.5. The glass sphere adhered and could be easily removed before using the cantilever, rendering the method non-destructive. The diameter of the glass sphere was determined to 30 µm using a stage microscope.
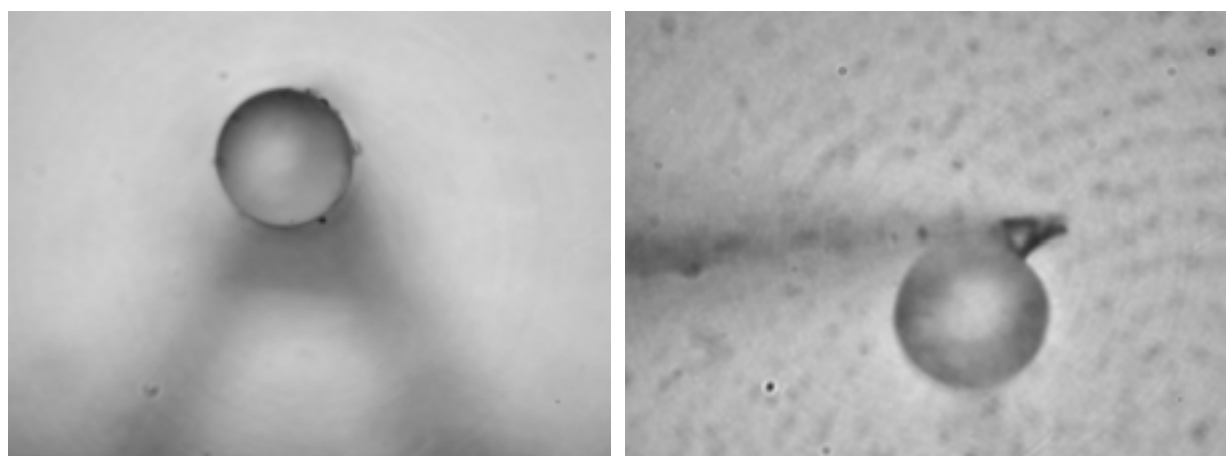
Figure 7.5   Pictures of the loaded cantilever. Left: top view; Right: side view (glass sphere adhered at the cantilever tip).

The change in resonance frequency of the cantilever with and without an added end mass was then measured using an atomic force microscope (Multimode SPM, Digital Instruments, Veeco Inst.). The unloaded and loaded resonance frequencies were measured and the spring constant was calculated using the following equation:

$$k = \frac{\frac{2}{3}\pi^3 \rho\left(-d_0^3\right)}{\frac{1}{f_0^2} - \frac{1}{f_1^2}}$$

where,   k: the spring constant (N/m)

ρ: density of the glass sphere (kg/cm³)

f_0: loaded resonance frequency (Hz)

f_1: unloaded resonance frequency (Hz)

d_0: diameter of the glass sphere (m)

Cantilever preparation

A selected small and almost isometric Avicel® PH 101 particle (10 µm in size determined using a stage microscope) was attached to the apex of a cantilever with a small quantity of epoxy resin (UHU plus endfest 300, UHU GmbH & Co. KG) under an optical microscope (Figure 7.6).
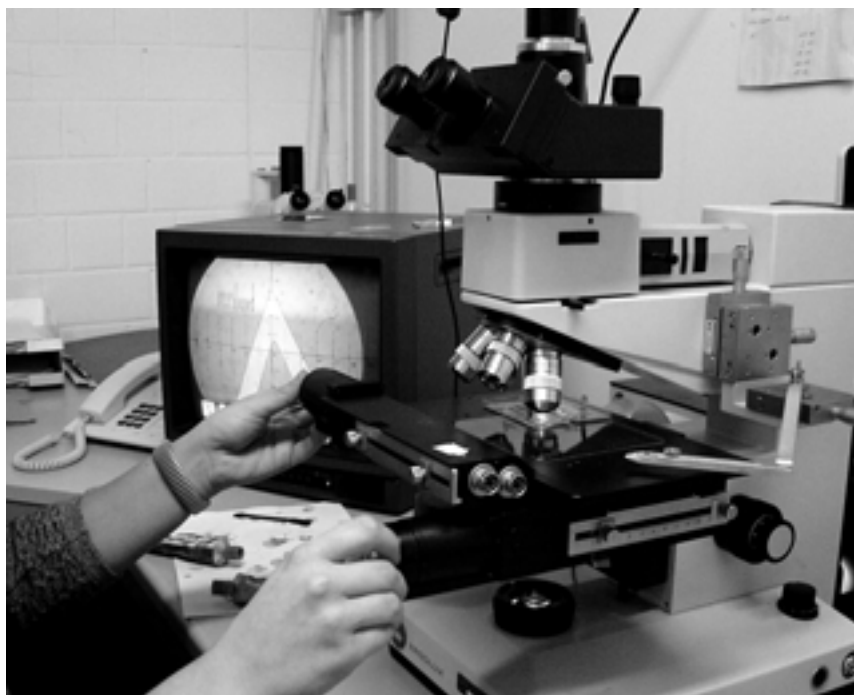
Figure 7.6   Picture of the optical microscope.

Care was taken to prevent the spreading of epoxy resin around the cantilever and the particle. The Avicel® PH 101 functionalized cantilever ("Avicel® PH 101 probe") was examined under an optical microscope after drying overnight to ensure the successful attachment of the Avicel® PH 101 particle and also after each measurement to ensure the particle integrity (Figure 7.7).
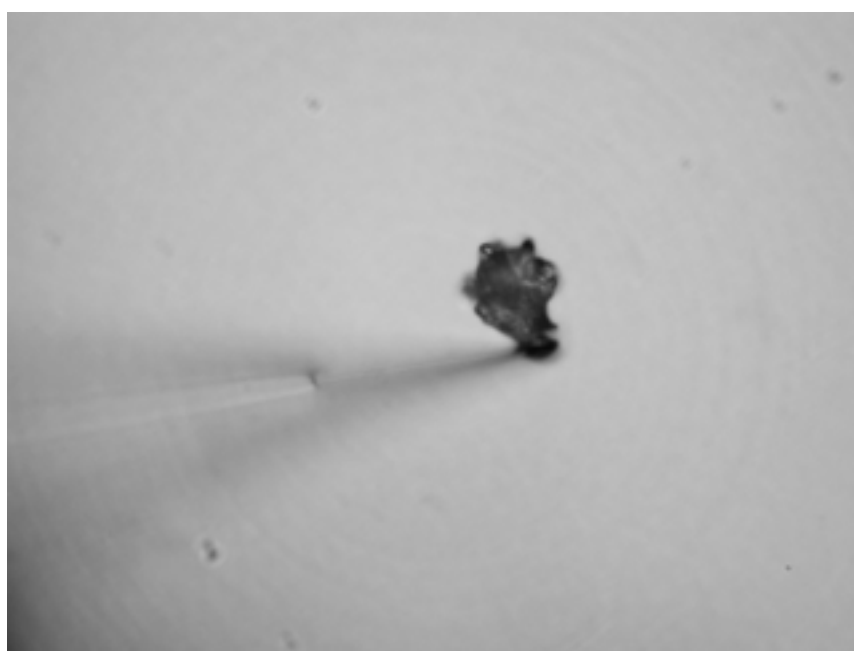
Figure 7.7   Avicel® PH 101 particle mounted onto a silicon nitride cantilever.

Adhesion force measurements

Adhesion force measurements were performed in air at room temperature (20-25°C) and ambient relative humidity (40-50% r.H.) using an atomic force microscope (Figure 7.8). All force-distance measurements were recorded with the following settings: 6μm approach-retraction cycle and 1Hz cycle rate. A digital camera (Coolpix 990, Nikon) was used to locate the Avicel® PH 101 functionalized cantilever on top of a well-defined individual Avicel® PH 101 particle of the sample. The adhesion force distribution was obtained from adhesion measurements of at least 50 individual sites for mixtures 2 and 4 and 30 sites for Avicel® PH 101. Ten force plots were captured at each site.

Figure 7.8   Experimental set-up. Left: force distance plot of the AFM measurement. Center: computer monitor showing the functionalized cantilever and the top of the Avicel®PH 101 sample. Right: atomic force microscope.

The force-distance plot of the atomic force microscope is well-described in the literature and depicted in Figure 7.9 (Agache et al. 2002, Ibrahim et al. 2000 and Young 2002). The adhesion force (F) was calculated according to Hook´s law, $F = kx$, where k is the spring constant and x is the vertical displacement of the cantilever. For an accurate adhesion force calculation, the vertical displacement was recorded using a piezoscanner that measures the difference in distance (Δz) between the point at which

the probe, in contact with the surface, crossed the zero deflection line and the point at which the probe pulled free from the surface (Willing et al. 2000).
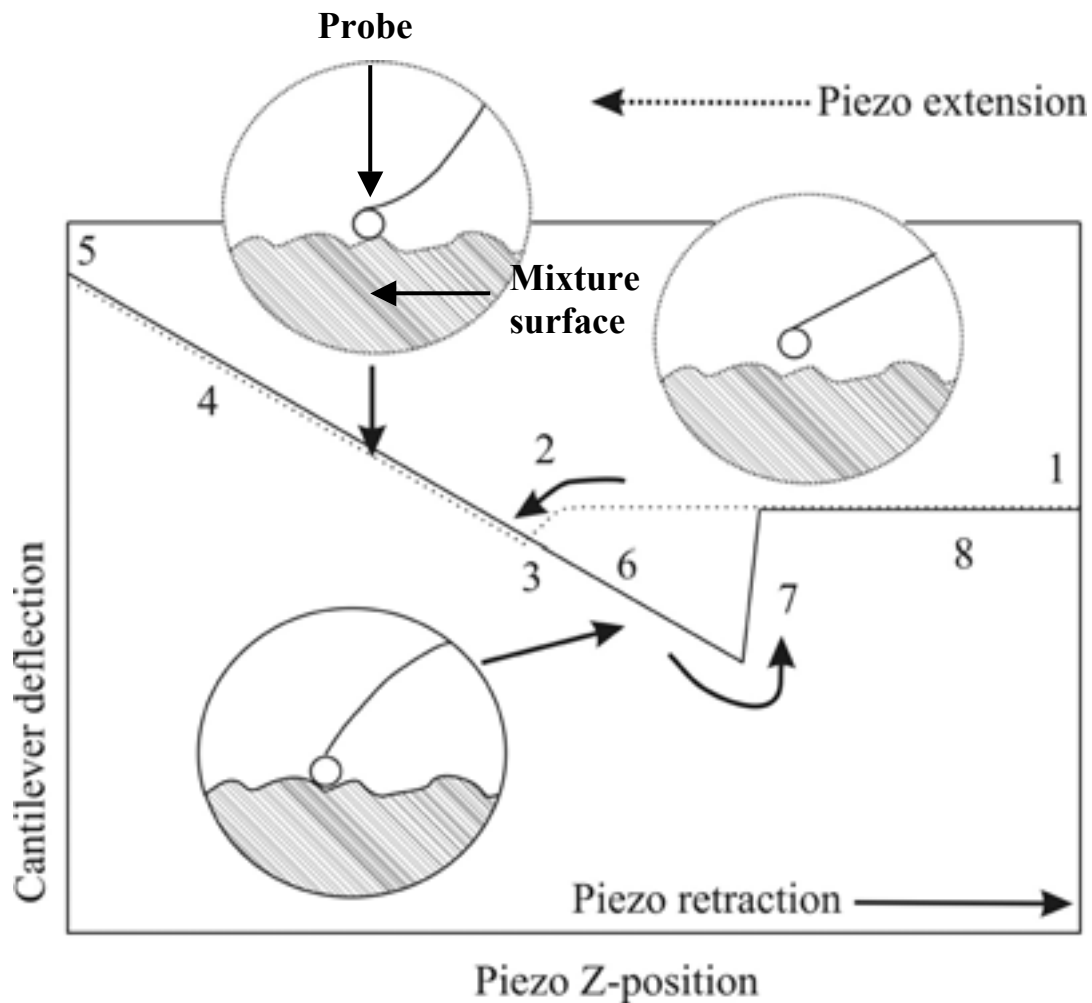
Figure 7.9   Diagram of a typical force vs. distance curve. (1) The sample surface approaches the probe (zero deflection line or baseline) (2) At close proximity, the short-range van der Waals forces produce attraction, resulting in a small downward deflection and contact between the probe and the sample (the jump-in point). (3) Contact point. (4) Upward deflection of the cantilever as the sample still moves towards the probe. (5) The piezoscanner, which supports the sample, retracts. (6) As the sample returns to its original non-contact position (retraction curve), the adhesion between the probe and the sample produces a hysteresis observed as a downward deflection past the initial contact point. (7) The spring force of the bent cantilever overcomes the adhesion forces and the cantilever pulls off sharply upward to its origin position. (8) The probe returns to the baseline.

7.6   *Preparation of the tablets*

7.6.1   Tablet press and instrumentation

Tablets were compressed on an instrumented single punch tablet press Korsch EK II (Korsch Pressen) using round flat tooling of 10 mm (d) in diameter. Compaction pressure was measured by a full Wheatstone bridge circuit of strain gauges (type 6/120 LY 11, Hottinger Baldwin Messtechnik (HBM)) at the upper punch holder and by a piezo-electric load washer (type 9041, Kistler) mounted directly below the lower punch (Herzog 1991). The measurement range was from 1.5 to 32 kN and from 1.6 to 22.5 kN for the upper and the lower punches, respectively. For the measurement of residual and ejection forces, a camshaft switch was installed on the drive shaft of the tablet press. The camshaft switched on, as soon as the lower punch started to eject the tablet and allowed a precise measurement of the forces in the Newton range.

To measure the displacement, a support made out of brass was mounted at the upper punch. The upper punch displacement was transmitted to a digital incremental displacement transducer (model MT 2571, Heidenhain) providing a precision of 0.2 μm and a resolution of 0.4 μm. The displacement error caused by distortion of tooling and frame of the machine was obtained from 10 punch to punch compressions at increasing compressional forces, which led to a linear function giving the displacement versus force correction curve. This function was implemented into the data acquisition software, thus correcting displacement according to the compression force applied. Details of the instrumentation and calibration of the machine are given by Dressler (2002) and Dressler et al. (2001)

7.6.2   Data acquisition and calculation of the compression parameters

Data were acquired using the MGC Plus system including a ML 10 B voltage amplifier (HBM) and the Catman software (HBM) according to the scheme presented in Figure 7.10. Initially, the system was set to zero. The upper punch was manually pressed onto the lower punch at a force of 300 N. The displacement transducer was also set to zero, corresponding to a tablet height of 0 μm. To acquire a second bench

mark, the upper punch was brought out of the die and a slip gauge with a height of 5 mm (± 0.12μm) was placed on the upper surface of the tablet die. The slip gauge was touched by the upper punch at a contact force of 300 N. The Catman program calculated the displacement difference between the zero point and the upper face of the slip gauge, and then subtracted the height of the slip gauge to determine the filling height of the die. The result was archived as a variable and used for further calculations. The compression cycle was recorded using a sample rate of 192000 data points per second. A dynamic data reduction was automatically carried out by the Catman script. Calculations were performed after manual input of the tablet mass using the reduced data.
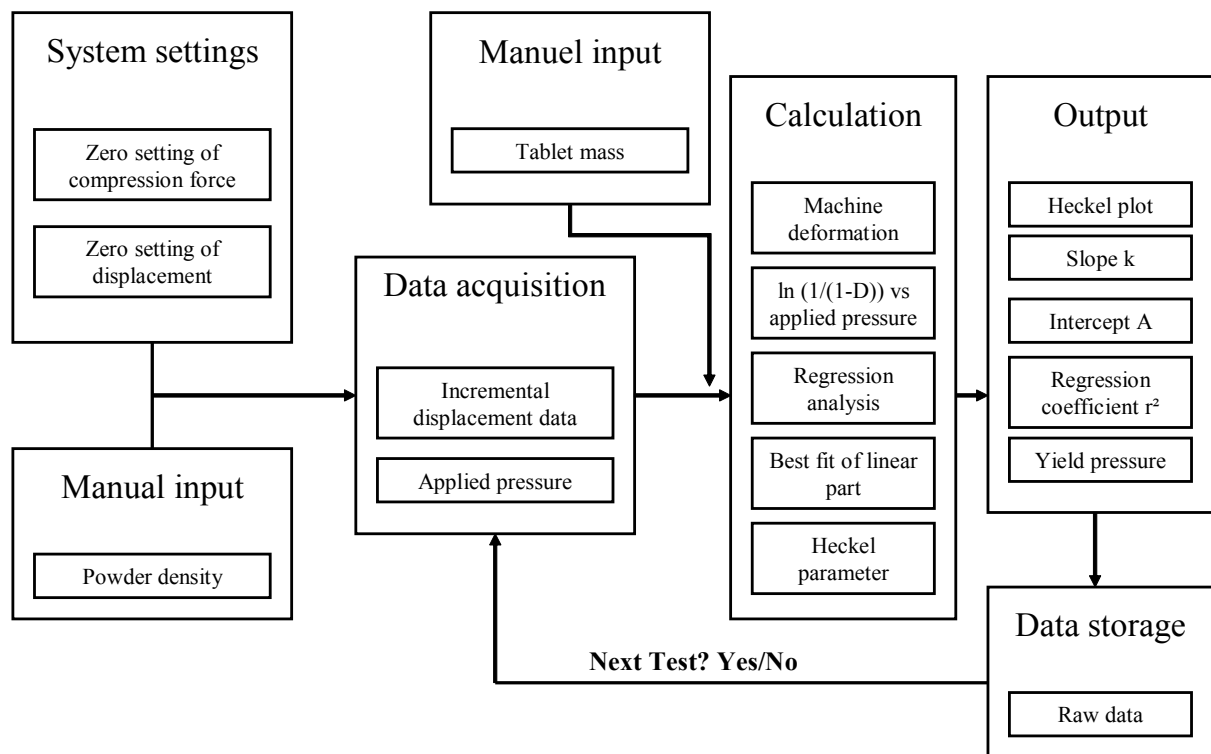
Figure 7.10   *Scheme of data acquisition, calculation of the Heckel parameters and the output of the system using the Catman script.*
Scheme adapted from Dressler (2002).

Heckel plots

The Heckel equation (Heckel 1961) is based on the assumption that powder compression follows first-order kinetics and describes the change of relative density in a powder column as a function of the applied pressure using the following equation:

$$\ln\frac{1}{1-D} = kP + A$$

where   D: relative density of a powder column at the pressure P

               P: pressure

               k: constant, indicating the plasticity of a compressed material

               A: constant, related to the die filling and particle rearrangement before deformation and bonding of discrete particles.

Heckel plots were calculated using the corrected upper punch displacement data. All parameters were calculated for each plot. The results are represented as an average value of ten single plots. The slope of the linear compression part of each Heckel plot and the yield pressure (its reciprocal value) were determined using a stepwise linear regression from 300 data points, which gave the best fit for the linear part of the curve.

R-values

R-values represent the maximum force ratio of lower to upper punch compression force (n = 10).

Residual and ejection forces

An impulse commutation from the camshaft switch was amplified and indicated the start of the ejection phase. The residual force was then immediately measured by the lower punch sensor by mean of 250 values collected in a short time. The ejection force was determined as the highest value measured by the lower punch sensor after the impulse commutation.

7.6.3 Tableting parameters and procedures

Table 7.4   Tableting parameters

Mixtures	Compression load interval [MPa]	Tablet mass [mg]
Avicel® PH 101	25-150	400
Starch 1500®	100-200	450
Tablettose® 80	100-250	450

Mixtures 2 with and without magnesium stearate and mixture 4 of each excipient were investigated. The tableting mixture was filled into the feeder, the filling depth was adjusted to produce tablets of 400 or 450 mg, the desired compression load was set and fifty tablets were compressed (Table 7.4). The script was activated and the true density of the powder was entered. After compressing one tablet, the weight of the tablet was determined (model AE 200, Mettler Toledo GmbH). The Heckel parameters were automatically calculated and stored together with the raw data. Ten tablets were investigated from each mixture at each compression level. Tablettose® 80 mixtures without magnesium stearate were compressed under extern die lubrication using oleic acid.

7.7 *Characterization of the tablets*

7.7.1 Crushing strength

The thickness (0.01-mm micrometer, Mitutoyo Messgeraete GmbH), the diameter (TBH-30 tester, Erweka GmbH) and the crushing strength (TBH-30 tester) of ten tablets were measured 24 hours after tableting. The radial tensile strength (S) was calculated from the thickness (H), diameter (D), and crushing strength (F_c) using the following equation (Frocht 1945):

$$S = 2F_c / \pi \, DH$$

7.7.2 Porosity

The porosity of the tablets was calculated from the true density (ρ_t) and the apparent density (ρ_a) of the material:

$$\varepsilon = 1 - \rho_a / \rho_t \quad \text{with} \quad \rho_a = m / \left(H\pi (D/2)^2 \right)$$

where   H: thickness out of die ρ_t: true density

m: weight of the tablet ρ_a: apparent density

D: diameter of the tablet

7.7.3 Bonding capacity

A Ryshkewitch-Duckworth relation between the radial tensile strength and the porosity was determined for every mixture according to equation (Duckworth 1953):

$$\ln \left(S/S_0 \right) = -k\varepsilon$$

where S is the radial tensile strength, S_0 is the radial tensile strength at zero porosity, ϵ is the porosity of the tablet and k is a constant, which refers to as bonding capacity indicating the effect of a change in porosity on the radial tensile strength. From the Ryshkewitch-Duckworth relation, the radial tensile strength was calculated for every mixture at 20% porosity for Avicel® PH 101 and Starch 1500® and at 10% porosity for Tablettose® 80.

7.7.4 Friability

The tablet friability was measured according to the European Pharmacopeia 5th Edition. 20 tablets were tested using a friability tester (type PTF1, Pharmatest Apparatebau) for 4 minutes at 25 rpm. Loose dust particles were removed from the tablets with air pressure before and after the test. The tablet friability was calculated from the loss of mass and expressed as the percentage of the initial mass.

7.8   Moisture studies

7.8.1 Preparation of the humidity chambers

Pyrex desiccators containing appropriate saturated salt solutions (Table 7.5) in distilled water were prepared to create chambers with different levels of relative humidity. All desiccators were kept at $20 \pm 0.5°C$ in a drying oven (model T5050, Heraeus Holding GmbH) to maintain the desired relative humidity level.

Table 7.5   Saturated salt solutions used for different relative humidity levels

Saturated salt solution	Relative Humidity at 20°C (%)
Sodium Hydroxide	7
Potassium acetate	20
Magnesium chloride	33
Potassium carbonate	44
Sodium bromide	59
Sodium nitrite	65
Sodium chloride	75
Potassium chloride	85
Potassium nitrate	93

7.8.2 Moisture study of the powders

Mixture 4 of each excipient without AEROSIL® or containing 0.5% AEROSIL® 200 VV or AEROSIL® R 972 V were placed in eight different desiccators at a relative humidity of 20, 30, 44, 59, 65, 75, 85 and 93% for 18 days (24 samples in total). The study was divided into two parts: water uptake and flowability. For the water uptake, 90 ml samples of each mixture were accurately weighed (model PG 5002-S, Mettler Toledo GmbH) into 14 cm diameter Petri dishes and then placed in the dessicators. After 3, 7, 12 and 18 days, the samples were accurately weighed again. The water uptake was calculated and expressed in %. For the flowability, the angle of repose was measured before and after 18 days storage in the dessicators. For Starch 1500®, the experiment was performed three times in order to evaluate the reproducibility.

7.8.3 Moisture study of the tablets

Mixture 2 from each excipient without AEROSIL® or containing 0.5% AEROSIL® 200 VV or AEROSIL® R 972 V, was compressed at 100 MPa for Avicel® PH 101 and at 200 MPa for Starch 1500® and Tablettose® 80. Ten tablets from each group were placed in the seven different desiccators at a relative humidity of 7, 20, 30, 44, 65, 75, and 85% for 7 days. The weight, thickness and radial tensile strength of the tablets were accurately measured after the storage period. The changes were calculated and expressed as percentages.

7.9   Statistical analysis

7.9.1 Analysis of variance

In order to compare the flowability of the different mixtures, one-way analysis of variance of angle of repose means was carried out. The procedure will be explained using Avicel PH® 101 mixtures containing AEROSIL® 200, AEROSIL® 200 VV, AEROSIL® R 972 V and no glidant under mixing condition 4 as an example. Table 7.6 shows the results of the measurements of the angle of repose and indicates means and standard deviations.

Table 7.6   Angle of repose results of Avicel PH® 101 mixtures

	Avicel PH® 101 AEROSIL® 200	Avicel PH® 101 AEROSIL® 200 VV	Avicel PH® 101 AEROSIL® R972V	Pure Avicel PH® 101
	39.1	35.75	36.5	47.7
	40.2	36.5	35.75	46.7
	39.4	36.5	35.75	47.2
	38.8	35.75	33.4	47.4
	40.3	35.75	35.75	47.0
	40.0	37.2	35.75	47.7
X	39.63	36.25	35.75	47.29
s. d.	0.62	0.60	0.47	0.42

The null hypothesis of equal angle of repose means was tested at the 5% level of significance. If the null hypothesis of equal treatment means is true, the distribution of the mean square between methods/mean square within methods ratio (BMS/WMS) is described by the F distribution.

Table 7.7   Analysis of variance of the data shown in Table 7.6

Source	*Sum of squares*	*Degrees of freedom*	*Mean square*	*F*
Between methods	523.56	3	174.52	3.10
Within methods	10.21	20	0.51	
Total	533.77	23		

The ratio BMS/WMS = 174.52/0.51 = 341.5 is higher than the critical F-value (3.10), indicating that at least two of the angle of repose means are different (Table 7.7).

However a significant ANOVA test does not indicate which of the multiple mixtures tested differ. Therefore a multiple comparison procedure should be undertaken. The Newman-Keuls test is a multiple comparison test using the multiple range factor Q in a sequential fashion. First the means to be compared are arranged in increasing order of magnitude. Then, the differences needed for the comparison of 2, 3 and 4 means were calculated as:

$$Q\sqrt{S^2/N}$$

where   Q: multiple range factor based on the tables of studentized range at 5% level.

S^2: mean square within methods in the one-way ANOVA analysis

N: sample size.

Thus, the differences required for 2, 3 and 4 means to be considered significant are represented as follows:

Number of mixtures	2	3	4
Critical differences	0.86	1.05	1.16

The results of the Newman-Keuls test for the 4 mixtures are depicted in Table 7.8. Any two means connected by the same underscored line are not significantly different. Two means not connected by the underscored line are significantly different. Only one difference of angle of repose means fell below the critical value and was therefore not statistically significant. This was the difference between the two means for Avicel PH$^{®}$ 101/AEROSIL$^{®}$ R972V and Avicel PH$^{®}$ 101/AEROSIL$^{®}$ 200 VV (36.25-35.75 = 0.5, this value is lower than 0.86, the critical difference for 2 mixtures).

Table 7.8   Analysis of results of the Newman-Keuls test performed on the angle of repose means of Avicel PH$^{®}$ 101 mixtures containing AEROSIL$^{®}$ 200, AEROSIL$^{®}$ 200 VV, AEROSIL$^{®}$ R 972 V and no glidant under mixing condition 4

Avicel PH$^{®}$ 101 AEROSIL$^{®}$ R972V	*Avicel PH$^{®}$ 101 AEROSIL$^{®}$ 200 VV*	*Avicel PH$^{®}$ 101 AEROSIL$^{®}$ 200*	*Avicel PH$^{®}$ 101 no glidant*
35.75	36.25	39.63	47.29

7.9.2 Test of normal distribution

The cumulative distributions Q_0 of the adhesion forces were tested to a log-normal distribution. The following term $\hat{\chi}^2$ was calculated for every distribution according to Sachs (1999):

$$\hat{\chi}^2 = (B - E)^2 / E$$

where,   B: observed frequency   E: expected frequency.

If $\hat{\chi}^2$ was lower than $\chi^2_{v;0.10}$ (v = k-1-a), then the distribution followed a normal distribution. An equivalent method was described by Croxton and Cowden.

7.9.3 Kruskal-Wallis test

The Kruskal-Wallis test is a nonparametric test that compares three or more unpaired groups. First, the observations are pooled and ranked, without regard to which group each value belongs. If two values are the same, then they are both awarded the average of the two ranks which they tie. The smallest number is given a rank of 1. The largest number is given a rank of N, where N is the total number of values in all the groups. After ranking, the observations are returned to their respective groups and are replaced by their corresponding ranks. The ranks of each group are then added together.

The Kruskal-Wallis test is approximately distributed as chi-square with k-1 degrees of freedom, where k is the number of groups in the experiment. The computation of the chi-square statistic follows:

$$\chi^2_{k-1} = \frac{12}{N(N+1)}\left(\sum \frac{R_i^2}{n_i}\right) - 3(N+1)$$

where,   N: total number of observations in all groups combined

R$_i$: sum of ranks in ith group

n$_i$: number of observation in ith group

If χ^2_{k-1} is higher than the value of chi-square with k-1 degrees of freedom, then the average of the group differs for at least two of the k groups at the 5% level of significance. To know which group differs, the Kruskal-Wallis test is followed by a Dunn´s post test, which compares the differences in the sum of ranks between two columns with the expected average difference. Two groups differ at the 5% level of significance if:

$$\left| \frac{R_i}{n_i} - \frac{R_{i'}}{n_{i'}} \right| \geq \sqrt{\chi^2_{k-1;0.05}\left(\frac{N(N+1)}{12}\right)\left(\frac{1}{n_i} + \frac{1}{n_{i'}}\right)}$$

CHAPTER 8

CONCLUSION

In this study, the influence of different AEROSIL® types on the flowability and tableting properties of typical filler/binders was investigated. Besides the non compacted hydrophilic and hydrophobic standard products, new compacted types were used in combination with the three well known filler/binders namely microcrystalline cellulose, Avicel® PH 101, pregelatinzed starch, Starch 1500® and α-lactose-monohydrate, Tablettose® 80. The investigations were carried out on a microscopic and macroscopic level to get a better understanding of the mechanisms of glidant action.

The first part of the study evaluates the flowability of the filler/binders upon addition of 0.5% compacted and non-compacted AEROSIL®, respectively, under different mixing conditions. Flowability studies, including angle of repose measurements, conveyor belt and ring shear methods, showed that the novel compacted types (AEROSIL® R 972 V and AEROSIL® 200 VV) are efficient glidants. Besides their handling advantages, they are even superior to the non-compacted AEROSIL® 200 in their glidant action. Among the colloidal silicon dioxide types investigated, AEROSIL® R 972 V is the most efficient glidant; gentle mixing conditions are sufficient to achieve high flowability. On the contrary, the increase in flowability obtained with hydrophilic AEROSIL® 200 VV and AEROSIL® 200 strongly depends on the mixing conditions. In general, the flowability of Avicel® PH 101 and Starch 1500® mixtures containing hydrophilic colloidal silicon dioxide increases with increasing mixing time and energy.

To evaluate the importance of the chemical nature of AEROSIL®, complementary flowability measurements (angle of repose and tapped density) were performed with AEROSIL® R 974 V and AEROSIL® 130 V. Although AEROSIL® R 974 V and

AEROSIL[®] 130 V possess identical physical properties to AEROSIL[®] 200 VV and AEROSIL[®] R 972 V, respectively, they show different flow properties. Compared to hydrophilic AEROSIL[®], their hydrophobic analogues are able to improve the flowability of Avicel[®] PH 101 faster and more intensively and seem to be unaffected by the mixing conditions.

Hydrophobic and hydrophilic AEROSIL[®] were tested under different relative humidities. The study was divided into two parts: moisture uptake and flowability. The water uptake is characteristic for each excipient and not altered by the addition of AEROSIL[®]. However, after equilibrating at high relative humidity levels, all excipient mixtures containing AEROSIL[®] maintain good flowability, while the flowability of the pure excipients is decreased. This proves that the compacted colloidal silicon dioxide types are at least as efficient anti-caking agents as their non-compacted counterparts.

The results of the first part of the study indicate that compacted AEROSIL[®] types are efficient glidants and anti-caking agents and that the chemical nature of AEROSIL[®] plays a crucial role in the flow-enhancement. The primary particle size, surface area and tapped density of the colloidal silicon dioxide type can not be held responsible for the better flow enhancement. Other factors such as surface chemistry may influence the glidant properties of different colloidal silicon dioxide types. Furthermore, the angle of repose results concur with the mass accumulation curves obtained by the conveyor belt method and the flowability factor obtained by the ring shear tester, showing that the three methods are equivalent tools to describe the flow properties of powders and that the measurement of the angle of repose is a simple and sensitive method in powder flow measurements.

The second part of the study is based on microscopic investigations designed to analyze and elucidate the differences between the AEROSIL[®] types on powder flow enhancement and to better understand the glidant mechanism. Scanning electron microscopy and X-ray photoelectron spectroscopy analyses reveal that the coverage of Avicel[®] PH 101 is less extensive and the distribution is less homogeneous for mixtures

containing hydrophilic AEROSIL$^®$ 200 and AEROSIL$^®$ 200 VV, when compared to hydrophobic AEROSIL$^®$ R 972 V under gentle mixing conditions. Higher mixing energy is necessary to achieve a homogeneous distribution of hydrophilic AEROSIL$^®$ particles. The degree and uniformity of coverage of the colloidal silicon dioxide particles on the excipient's surface correlates well with the flow enhancement exerted by the glidant. In this, the extent of surface coverage is the crucial factor determining flowability. The hydrophobic treatment proves to be effective with short blending time. Due to lower silanol groups on its surface, hydrophobic agglomerates are easily broken up and a higher number of adsorbable agglomerates is available to act as glidant.

Furthermore, the angle of repose and XPS investigation of Starch 1500$^®$ mixtures containing different concentration of AEROSIL$^®$ 200 VV reveal that the size of the agglomerates plays a key role in the flow-enhancement. When the extent of coverage is identical, smaller agglomerates lead to a better flowability. A comparison between Starch 1500$^®$ and Avicel$^®$ PH 101 based on XPS and specific surface area results shows that the excipient's surface influences the action of the glidant.

The measurement of interparticulate forces within Avicel$^®$ PH 101 mixtures using an atomic force microscope shows that colloidal silicon dioxide reduces the adhesion force between the Avicel$^®$ PH 101 particles. The experimental findings are in agreement with the sphere-sphere model, describing the position of a small particle between two larger spheres. The small particle increases the distance between the two larger excipient particles and reduces the van der Waals forces between them. The reduction of the adhesion force is influenced by the AEROSIL$^®$ type. A rapid breaking up of the hydrophobic agglomerates in AEROSIL$^®$ R 972 V allows a high degree of coverage. Consequently, a higher number of hydrophobic agglomerates are available to act as a spacer between the Avicel$^®$ PH 101 particles and to reduce the adhesion forces between them. Moreover, the adhesion force measurements correlate with the angle of repose and confirm that adhesion force between glidants and pharmaceutical filler dominates flowability.

Finally, the last part of the study deals with the influence of hydrophobic and hydrophilic colloidal silicon dioxide on the compression into tablets and tablet parameters of Avicel® PH 101, Starch 1500® and Tablettose® 80. The Heckel plots are characteristic for each excipient and independent of the addition of colloidal silicon dioxide. Addition of AEROSIL® increases the residual and ejection forces for Avicel® PH 101 and Starch 1500® and has no influence on Tablettose® 80 tablets. However, the residual and ejection forces remain in acceptable ranges for the production of tablets. The hydrophobic and hydrophilic natures of AEROSIL® and the compaction characteristics of the excipients influence the strength of the tablets. The differences can be explained by the Ryshkewitch-Duckworth relationship, describing the relationship between radial tensile strength and porosity. For Avicel® PH 101, hydrophilic colloidal silicon dioxide types reduce the radial tensile strength of the tablets slightly (-10%), whereas the hydrophobic types lead to a larger reduction (-30%). For Starch 1500®, hydrophilic colloidal silicon dioxides increase the tablet strength while hydrophobic colloidal silicon dioxides lead to a strong decrease. Compared to Tablettose® 80 without colloidal silicon dioxide, tablets compressed from colloidal silicon dioxide and Tablettose® 80 show a slight decrease in the radial tensile strength and no differences between colloidal silicon dioxide types are observed.

After seven days storage at various relative humidities, the tablet properties of Avicel® PH 101, Starch 1500® and Tablettose® 80 were not influenced by addition of hydrophobic or hydrophilic colloidal silicon dioxide types.

Moreover, the influence of different colloidal silicon dioxides on the film formation of magnesium stearate was investigated. Addition of AEROSIL® to the excipient prior to mixing with magnesium stearate reduces the deleterious effect of magnesium stearate on the bonding properties of excipient particles, while still retaining its lubricating properties. Hydrophobic AEROSIL® interferes with magnesium stearate to the same extent as hydrophilic types.

In addition, the tableting investigations show that AEROSIL® 200 VV and AEROSIL® 200 behave identically as far as tablet strength, moisture uptake and magnesium stearate film formation are concerned, indicating that the densification process of AEROSIL® has no effect on tablet properties.

The flowability studies and the tableting investigations show that the compaction process and the modification of the structure through hydrophobic treatment influence the properties of AEROSIL®. Firstly, hydrophilic compacted colloidal silicon dioxide types are more efficient excipients compared to their non-compacted counterparts. They are easier to handle and show better flow enhancement and identical tableting properties. Secondly, hydrophobic colloidal silicon dioxide types show better flow enhancing properties compared to their hydrophilic counterparts because the agglomerates are easier to degrade during mixing. The rapid break up of the agglomerates allows a high degree of coverage of AEROSIL® on the excipient, which leads to a greater reduction of the interparticulate forces within the powder mixture. However, hydrophobic AEROSIL® significantly reduces the tablet strength of poorly binding materials such as Starch 1500®. Nevertheless, they present a good alternative to hydrophilic types for plastically deforming materials (e.g. Avicel® PH 101) and for fragmenting excipients (e.g. Tablettose® 80).

All experiments carried out in this study indicate that AEROSIL® acts as a spacer between the excipient's particles, which reduces the van der Waals forces. Two major factors are responsible for its effect: the degree of coverage of the AEROSIL® agglomerates on the excipient's surface and the size of the AEROSIL® agglomerates adhering to the excipient's surface. These factors depend on the surface chemistry and the particle size of the products.

CHAPTER 9

REFERENCES

Agache, V.; Legrand, B.; Collard, D. and Buchaillot, L.
"Adhesive forces investigation on a silicon tip by contact-mode atomic force microscope"
Appl. Adv. Phys. **81**, 2623-2625 (2002)

Albers, P.; Seibold, K.; Haas, T.; Prescher, G. and Hölderich, W. F.
"SIMS/XPS Study on the Deactivation and Reactivation of B-MFI Catalysts Used in the Vapour-Phase Beckmann Rearrangement"
J. Catal. **176**, 561-568 (1998)

Amidon, G. E.; Ausburger, L. L.; Brittain, H. G.; Byrn, S. R.; Fox, C. D.; Peck, G. E. and Wurster D. E.
"Physical Test Methods for Powder Flow Characterization of Pharmaceutical Materials: A Review of Methods"
Pharmacopeial Forum **25**, 8298-8308 (1999)

Ammon, P.T.
"Hunnius Pharmazeutisches Wörterbuch 9. Auflage"
W. de Gruyter, New York and Berlin (2004) 82-84.

Barthel, H
"Surface interactions of dimethylsiloxy group-modified fumed silica"
Colloids Surf. A **101**, 217-26 (1995)

Beamson, G. and Briggs, D.
"High Resolution XPS of Organic Polymers"
John Wiley & Sons, Chichester (1992), 158

Begat, P.; Morton, D. A. V.; Staniforth, J. N. and Price, R.

"The cohesive-adhesive balances in dry powder inhaler formulations I: Direct quantification by atomic force microscopy"

Pharm. Res. **21**, 1591-1597 (2004)

Begat, P.; Young, P. M.; Edge, S. Kaerger, S. and Price, R.

"The effect of mechanical processing on surface stability of pharmaceutical powders: visualization by atomic force microscopy"

J. Pharm. Sci. **92**, 611-620 (2003)

Bérard, V. ; Lesniewska, E. ; Andrès, C. ; Pertuy, D.; Laroche, C. and Pourcelot, Y.

"Dry powder inhaler: influence of humidity on topology and adhesion studied by AFM"

Int. J. Pharm. **232**, 213-224 (2002)

Bhattachar, S. N.; Hedden, D. B.; Olofsky, A. M.; Qu, X.; Wen-Yaw, C. and Canter, K. G.

"Evaluation of the vibratory feeder method for assessment of powder flow properties"

Int. J. Pharm. **269**, 385-392 (2004)

Binning, G.; Quate, C. F. and Gerber, C.

"Atomic force microscope"

Phys. Rew. Lett. **56**, 930-933 (1986)

Bolhuis, G. and Chowan, Z. T.

"Materials for direct compaction"

in: Alderborn, G. and Nyström, C. "Pharmaceutical powder compaction technology"

Marcel Dekker, New York (1996) 428-440

Bolhuis, G. K. and Hölzer, A. W.

"Lubricant sensitivity"

in: Alderborn, G. and Nyström, C. "Pharmaceutical powder compaction technology"

Marcel Dekker, New York (1996) 519-560

Bolton, S.
"Pharmaceutical statistics"
Marcel Dekker, New York (1990) 262-307

Carr, R. L.
"Evaluating Flow properties of Solids"
Chem. Eng. **18**, 163-168 (1965)

Chang, R. K.; Leonzio, M. and Hussain, M. A.
"Effect of Colloidal Silicon Dioxide on Flowing and Tableting Properties of an Experimental, Crosslinked Polyalkylammonium Polymer"
Pharm. Dev. Technol., **4,** 285-289 (1999)

Cleveland, J. P.; Manne, S.; Bocek, D. and Hansma, P. K.
"A non-destructive method for determining the spring constant of cantilevers for scanning force microscopy"
Rev. Sci. Instrum. **64**, 403-405 (1993)

Crooks, M.; Ho, R. and Bagster, D. F.
"Tensile and shear testing of some pharmaceutical powders"
Drug Dev. Ind. Pharm. **3**, 291-308 (1977)

Czetsch-Lindenwald, H.
"Der neue Füllstoff R 972"
Pharm. Ind. **27**, 300-301 (1965)

Czetsch-Lindenwald, H. and Asker, A. F.
"Der neue Füllstoff R 972"
Pharm. Ind. **28**, 614-616 (1966)

de Villiers, M. M. and van der Waat, J. K.
"The measurement of mixture homogeneity and dissolution to predict the degree of drug agglomerate breakdown achieved through powder mixing"
Pharm. Res. **11**, 1557-1561 (1994)

DIN ISO 4324

"Pulver und Granulate, Bestimmung des Schüttwinkels"

(1983) 1-4

Dressler, J. A.

"Vergleichende Untersuchung pharmazeutischer Hilfsstoffe unter Einsatz eines inkrementalen Weggebers zur präzisen Wegmessung an einer Exzenter-Tablettenpresse"

Ph.D. Thesis, Tübingen, Germany 2002

Dressler, J. A.; Wagner, K. G.; Wahl, M. A. and Schmidt P. C.

"Comparison of incremental and inductive displacement transducers on an eccentric tablet press"

Pharm. Ind. **63**, 886-893 (2001)

Duberg, M. and Nystroem, C.

"Studies on direct compression of tablets. XVII. Porosity-pressure curves for the characterization of volume reduction mechanisms in powder compression"

Powder Technol. **43**, 67-75 (1986)

Duckworth, W.H.

"Discussion of Ryskewitch paper by Winston Duckworth"

J. Am. Ceram. Soc. **36**, 68 (1953)

European Pharmacopoeia 5th edition

"Apparent volume"

Council of Europe, Strasbourg (2005), 241-242

European Pharmacopoeia 5th edition

"Friability of uncoated tablets"

Council of Europe, Strasbourg (2005), 234-235

European Pharmacopoeia 5th edition

"Specific surface area by gas absorption"

Council of Europe, Strasbourg (2005), 260-263

Eve, J. K.; Patel, N.; Luk, S. Y.; Ebbens, S. J. and Roberts, C. J.
"A study of single drug particle adhesion interactions using atomic force microscopy"
Int. J. Pharm. **232**, 213-224 (2002)

Feng, S. and Huang, G.
"Effects of emulsifiers on the controlled release of paclitaxel (Taxol) from nanospheres of biodegradable polymers"
J. Contr. Rel. **71**, 53-69 (2001)

Fiedler, H. P.
"Lexikon der Hilsstoffe für Pharmazie, Kosmetik und angrenzende Gebiete 5. Auflage"
Editio-Cantor-Verl., Aulendorf (2002) 115-117

Finot, E.; Lesniewska, E.; Mutin, J. C. and Goudonnet, J. P.
"Investigations of surface forces between gypsum crystals in electrolytic solutions using microcantilevers"
J. Chem. Phys. **111**, 6590-6598 (1999)

Freeman, R.
"Predicting flowability and characterizing powders"
Pharm. Technol. **16**, 41-43 (2004)

Frocht, M. M.
"Photoelasticity"
John Wiley & Sons, New York (1945), 116-157

Fuji, M.; Machida, K.; Takei, T.; Watanabe, T. and Chikazawa, M.
"Effect of wettability on adhesion force between silica particles evaluated by atomic force microscopy measurement as a function of relative humidity"
Langmuir **15**, 4584-4589 (1999)

Gillies, G.; Prestidge, C. A. and Attard, P.
"An AFM study on the deformation and nanorheology of cross-linked PDMS droplets"
Langmuir **18**, 1674-1679 (2002)

Gstirner, F. and Pick, C.
"Der Einfluß von AEROSIL® und „Füllstoff R 972" auf die Fließeigenschaft von Zinkoxid"
Arch. Pharmaz. **6**, 757-765 (1967)

Gstirner, F. and Pick, C.
"Einfluß von AEROSIL® und AEROSIL® R 972 auf das Wasseraufnahmevermögen von Puderrohstoffen"
Arch. Pharmaz. **8**, 590-604 (1969)

Gustafsson, C.; Lennholm, H.; Iversen, T. and Nyström, C.
"Evaluation of surface and bulk characteristics of cellulose I powders in relation to compaction behaviour and tablet properties"
Drug Dev. Ind. Pharm. **29**, 1095-1107 (2003)

Hausner, H. H.
"Friction conditions in a mass of metal powder"
Int. J. Powd. Metall. **3**, 7-13 (1967)

Heckel, R. W.
"Density-Pressure relationships in powder compaction"
Trans. Metall. Soc. Aime **221**, 671-675 (1961)

Heng, P. W. S.; Chan, L. W. and Lim, L. T.
"Quantification of the surface morphologies of lactose carriers and their effect on the in vitro deposition of salbutamol sulphate"
Chem. Pharm. Bull. **48**, 393-398 (2000)

Herzog, R.
"Calciumphosphate in der Tablettierung"
Ph.D. Thesis, Tübingen, Germany 1991

Ibrahim, T. H.; Burk, T. R.; Etzler, F. M. and Neuman, R. D.
"Direct adhesion measurements of pharmaceutical particles to gelatine capsule surfaces"
J. Adhesion Sci. Technol. **14**, 1225-1242 (2000)

Ilkka, J. and Paronen, P.

"Prediction of the compression behaviour of powder mixtures by Heckel equation"

Int. J. Pharm. **94**, 181-187 (1993)

Jenike, A. W.

"Storage and flow of solids"

Utah Eng. Exp. Stn. Bull. **123**, 1-194 (1964)

Lam, K. K. and Newton, J. M.

"Investigation of applied compression on the adhesion of powders to a substrate surface"

Powder Technol. **65**, 167-175 (1991)

Lavoie, F.; Cartilier, L. and Thibert, R.

"New methods characterizing avalanche behaviour to determine powder flow"

Pharm. Res. **19**, 887-893 (2002)

Lee, Y. S. L.; Poynter, R.; Podczeck, F. and Newton, J. M.

"Development of a dual approach to assess powder flow from avalanching behaviour"

AAPS PharmSciTech. **1**, article 21 (2000)

Lerk, C. F. and Bolhuis, G. K.

"Interaction of lubricants and colloidal silica during mixing with excipients. II. Its effect onwettability and dissolution velocity"

Pharm. Acta Helv. **52**, 39-44 (1977)

Lerk, C. F.; Bolhuis, G. K. and Smedema, S.S.

"Interaction of lubricants and colloidal silica during mixing with excipients. I. Its effect on tabletting"

Pharm. Acta Helv. **52**, 33-39 (1977)

Leuenberger, H and Rohera, B. D.

"Fundamentals of powder compression. I. The compactibility and compressibility of pharmaceutical powders"

Pharm. Res. **3**, 12-22 (1986)

Lieberman H. A. and Lachman L.
"Pharmaceutical Dosage Forms: Tablets, Vol. 1, 2nd Ed."
Marcel Dekker, Inc., New York (1989), 141-143.

List, P. H. and Müller, B. W.
"Untersuchungen über den FST-Komplex"
Pharm. Ind. **34**, 963-972 (1972)

Louey, M.D.; Mulvaney, P. and Stewart, P. J.
"Characterisation of adhesional properties of lactose carriers using atomic force microscopy"
J. Pharm. Anal. **25**, 559-567 (2001)

Lüdde, K. H. and Kawakita, K.
"Die Pulverkompression"
Pharmazie **21**, 393-403 (1966)

Mattsson, S. and Nyström, C.
"Evaluation of critical binder properties affecting the compactibility of binary mixtures"
Drug Dev. Ind. Pharm. **27**, 181-194 (2001)

Meyer, K. and Zimmermann, I.
"Effect of glidants in binary powder mixtures"
Powder Technol. **139**, 40-54 (2004)

Nürnberg, E.
"Experimentelle Prüfungen von direct verpreßten Tablettengrundlagen"
Pharm. Ind. **34**, 193-206 (1972)

Nyqvist, H. and Nicklasson, M.
"Flow properties of compressible lactose containing small quantities of drug substances"
Drug Dev. Ind. Pharm. **11**, 745-59 (1985)

Nyström, C.; Alderborn, G.; Duberg, M. and Karehill, P.-G.

"Bonding surface area and bonding mechanism – two important factors for the understanding of powder compactability"

Drug Dev. Ind. Pharm. **19**, 2143-2196 (1993)

Ohta, K. M.; Fuji; M. and Chikazawa, M.

"Effect of geometric structure of flow promoting agents on the flow properties of pharmaceutical powder mixture"

Pharm. Res. **20**, 804-809 (2003)

Ohta, K. M. and Toyoshima, K.

"Mechanism of enhancing flowability and tablet hardness by glidants in pharmaceutical powder mixtures- effects of geometric structure and surface wettability-"

Hyomen Kagaku **24**, (2003) (abstract)

Ohta, K. M.; Toyoshima, K.; Fuji, M.; Takei, T. and Chikazawa, M.

"Evaluation of pharmaceutical glidant with atomic force microscope and mechanism of flowability enhancement"

Funtai Kogaku Kaishi **41**, (2004) (abstract)

Otsuka, A.

"Adhesive properties and related phenomena for powdered pharmaceuticals"

Yakugaka Zasshi **118**, (1998) (abstract)

Otsuka, M.; Gao, J. and Matsuda, Y.

"Effect of mixer and mixing time on the pharmaceutical properties of theophylline tablets containing various kinds of lactose as diluents"

Drug Dev. Ind. Pharm. **19**, 333-348 (1993)

Paronen, P. and Ilkka, J.

"Porosity-pressure functions"

in: Alderborn, G. and Nyström, C. "Pharmaceutical powder compaction technology"

Marcel Dekker, New York (1996) 428-440

Podczeck, F.

"Particle-particle Adhesion in Pharmaceutical Powder Handling"

Imperial College Press, London (1998), 111-114.

Podczeck, F and Lee-Amies, G

"The bulk volume changes of powders by granulation and compression with respect to capsule filling"

Int. J. Pharm. **142**, 97-102 (1996)

Podczeck, F. and Newton, J. M.

"Development of an ultracentrifuge technique to determine the adhesion and friction properties between particles and surfaces"

J. Pharm. Sci. **84**, 1067-1071 (1995)

Poux, M.; Fayolle, P.; Bertrand, J.; Bridoux, D. and Bousquet, J.

"Powder mixing: Some practical rules applied to agitated systems"

Powder Technol. **68**, 213-234 (1991)

Räsänen, E.; Antikainen, O. and Yliruusi, J.

"A new method to predict flowability using a microscale fluid bed"

AAPS PharmSciTech. **4**, article 53 (2003)

Ragnarsson, G.; Hölzer, A. W. and Sjögren, J.

"The influence of mixing time and colloidal silica on the lubricating properties of magnesium stearate"

Int. J. Pharm. **3**, 127-131 (1979)

Ramachandruni, H. and Hoag, S.W.

"Design and validation of an annular shear cell for pharmaceutical powder testing"

J. Pharm. Sci. **90**, 531-540 (2001)

Rees, J. E. and Rue, P. J.

"Time-dependant deformation of some direct compression excipients"

J. Pharm. Pharmacol. **30**, 601-607 (1978)

Rey, H.

"Uniformity of multiunit tablets under pilot plant conditions as a function of unit size and filler composition"

Ph.D. Thesis, Tübingen, Germany 2003

Ritschel, W. A. and Bauer-Brandl, A.

"Die Tablette"

Editio-Cantor-Verlag, Aulendorf (2002), 144-146.

Rowe, R. C.

"Interactions in the ternary powder system microcrystalline cellulose, magnesium stearate and colloidal silica – a solubility parameter approach"

Int. J. Pharm. **45**, 259-261 (1988)

Rumpf, H.

"Die Wissenschaft des Agglomierens"

Chem.-Ing.-Tech. 46, 1-11 (1974)

Sachs, L.

"Angewandte Statistik 10. Auflage"

Springer-Verlag, Berlin (2002) 396-399

Schubert, H.

"Haftung zwischen Feststoffteilchen aufgrund von Flüssigkeitsbrücken"

Chem.-Ing.-Tech. **46**, 333-334 (1974)

Schulze, D.

"The automatic ring shear tester RST-01.pc"

www.dietmar-schulze.com (2005)

Schulze, D.

"Zur Fließfähigkeit von Schüttgüttern – Definition und Meßverfahren"

Chem.-Ing.-Tech. **67**, 60-68 (1995) 195-207

Schulze, D. and Wittmaier, A.

"Messung der Fließfähigkeit hochdisperser Schüttgüter bei sehr kleinen Verfestigungsspannungen"

Chem.-Ing.-Tech. **74**, 1144-1148 (2002)

Schwedes, J.

"Fließverhalten von Schüttgütern in Bunkern"

Verlag Chemie, GmbH, Weinheim (1968)

Schwedes, J.

"Measurement of flow properties of bulk solids"

Powder Technol. **88**, 285-290 (1996)

Schweiger, A.; Sindel, U. and Zimmermann, I.

"Determination of the optimum mixing time for a mixture of lactose and corn starch"

Pharm. Ind. **59**, 985-988 (1997)

Shirley D. A.

"High-resolution x-ray photoemission spectrum of the valence bands of gold"

Phys. Rev. B **5**, 4709-14 (1972)

Siegbahn, K.

"Photoelectron spectroscopy: retrospects and prospects"

Math. Phys. Eng. Sci. **318**, 3-36 (1986)

Sindel, U. and Zimmermann, I.

"Measurement of interaction forces between individual powder particles using an atomic force microscopy"

Powder Technol. **117**, 247-254 (2001)

Staniforth, J. N. and Ahmed, H. A.

"Influence of ternary components on compressibility of microcrystalline cellulose following blending with magnesium stearate"

J. Pharm. Pharmacol. **38**, 50P (1986)

Staniforth, J. N. and Ahmed, H. A.

"Influence of ternary components on lubrication of microcrystalline cellulose following blending with magnesium stearate"

J. Pharm. Pharmacol. **39**, 68P (1987)

Stephenson, P. L. and Thiel, W. J.

"The Effect of humidity on the Production of Ordered Mixtures"

Powder Technol. **25**, 115-119 (1980)

Tänzer, W

"Biologisch abbaubare Polymere"

Wiley-VCH, Stuttgart (2000) 56-73.

Tan, S. B. and Newton, J. M.

"Powder flowability as an indication of capsule filling performance"

Int. J. Pharm. **61**, 145-155 (1990)

Tawashi, R.

"Der Einfluss von Aerosil auf die Packungseigenschaften von Pulver"

Pharm. Ind. **25**, 655-685 (1963)

Taylor, M. K.; Ginsburg, J.; Hickey, A. J. and Gheyas, F.

"Composite method to quantify powder flow as a screening method in early tablet or capsule formulation development"

AAPS PharmSciTech **1**, article 18 (2000)

Technical bulletin fine particles no. 11.

"Basic characteristic of AEROSIL®"

Degussa, Düsseldorf (2003) 12-14

Technical information no. 1237.

"AEROSIL® 200 Pharma: A versatile excipient for the pharmaceutical industry"

Degussa, Düsseldorf (2001) 4-11

Technical information no. 1247.

"*AEROSIL® 200 VV Pharma: A new excipient for the pharmaceutical industry*"

Degussa, Düsseldorf (2002) 4-12

Tsukada, M.; Irie, R.; Yonemochi, Y.; Noda, R.; Kamiya, H.; Watanabe, W. and Kauppinen, E.I.

"*Adhesion force measurement of a DPI size pharmaceutical particle by colloid probe atomic force microscopy*"

Powder Technol. **141**, 262-269 (2004)

van der Voort Maarschalk, K.; Zuurman, K.; Vromans, H.; Bolhuis, G. K. and Lerk, C. F.

"*Porosity expansion of tablets as a result of bonding and deformation of particulate solids*"

Int. J. Pharm. **140**, 185-183 (1996)

van Veen, B.; Bolhuis, G. K.; Wu, Y. S.; Zuurman, K. and Frijlink, H.W.

"*Compaction mechanism and tablet strength of unlubricated and lubricated (silicified) microcrystalline celluloser*"

Eur. J. Pharm. Biopharm. 59, 133-138 (2005)

van Veen, B.; van der Voort Maarschalk, K.; Bolhuis, G. K.; Zuurman, K. and Frijlink, H. W.

"*Tensile strength of tablets containing two materials with different compaction behaviour*"

Int. J. Pharm. **203**, 71-79 (2000)

Visser, J.

"*Particle adhesion and removal: a review*"

Part. Sci. Technol. **13**, 169-196 (1995)

Vromans, H. and Lerk, C. F.

"*Densification properties and compactibility of mixtures of pharmaceutical excipients with and without magnesium stearate*"

Int. J. Pharm. **46**, 183-192 (1988)

Wang, C. H.; Sengothi, K.; Wong, H. M. and Lee, T.
"Controlled release of human immunoglobulin G. 2. Morphological characterization"
J. Pharm. Sci. **88**, 221-228 (1999)

Wang, J.J.; Li, T.; Bateman, S. D., Erck, R. and Morris, K. R.
"Modeling of adhesion in tablet compression – I. Atomic force microscopy and molecular simulation"
J. Pharm. Sci. **92**, 798-814 (2003)

Weth, M.; Hofmann, M.; Kuhn, J. and Fricke, J.
„Measurement of attractive forces between single aerogel powder particles and the correlation with powder flow"
J. Non-Cryst Solids **285**, 236-243 (2001)

Willing, G. A.; Ibrahim, T. H.; Etzler, F.M. and Neuman, R. D.
"New approach to the study of particle-surface adhesion using atomic force microscopy"
J. Colloid. Interface Sci. **226**, 185-188 (2000)

Xie, H-Y.
"The role of interparticle forces in the fluidization of fine particles"
Powder Technol. **94**, 99-108 (1997)

York, P.
"Application of powder failure testing equipment in assessing effect of glidants on flowability of cohesive pharmaceutical powders"
J. Pharm. Sci. **64**, 1216-1221 (1975)

Young, P. M.; Price, R.; Tobyn, M. J.; Buttrum, M. and Dey, F.
"Investigation into the effect of humidity on drug-drug interactions using the atomic force microscope"
J. Pharm. Sci. **92**, 815-822 (2002)

Zhang, Y.; Law, Y. and Chakrabarti, S.

"Physical properties and compact analysis of commonly used direct compression binders"

AAPS PharmSciTech **4**, article 62 (2003)

Zimmerman, I.; Eber, M. and Meyer, K.

"Nanomaterials as flow regulators in dry powders"

Z. Phys. Chem. **218**, 51-102 (2004)

Zuurman, K.; van der Voort Maarschalk, K. and Bolhuis, G. K.

"Effect of magnesium stearate on bonding and porosity expansion of tablets produced from materials with different consolidation properties"

Int. J. Pharm. **179**, 107-115 (1999)

CHAPTER 10

APPENDIX

Index of Suppliers

Willy A. Bachofen AG, Utengasse 15-17, CH-4002 Basel

Beckmann Coulter GmbH, Europark Fichtenhain B13, D-47807 Krefeld

Beckman Instruments Inc., Frankfurter Ring 115, D-80807 München

Colorcon Ltd., Dartford, GB-Kent

Degussa AG, Bennigsenplatz 1, D-40474 Düsseldorf

Digital Instruments, Veeco Inst., CA-Santa Barbara USA

Engelsmann AG, Frankenthaler Str. 137-141, D-67059

Erweka GmbH, Ottostr. 20-22, D-63150 Heusenstamm

Dr. F. Faulhaber GmbH & Co. KG, Postfach 1146, D-71094 Schönaich

FMC Biopolymer, Wallingston, Little Island, IRL-Cork

Haraeus Holding GmbH, Haraeusstr. 12-14, D-63450 Hanau

Heidenhain GmbH, Dr.-Johannes-Heidehain-Str. 5, D-83301 Traunreut

Hosokawa Alpine, Postfach 10 11 51, D-86001 Augsburg

Hottinger-Baldwin Messgeraete GmbH, Im Tiefen See 45, D-64293 Darmstadt

Kistler Instruments GmbH, Eulachstr. 22, CH-8408 Winterthur

Korsch Pressen GmbH, Breitenbachstr. 1, D-13509 Berlin

Leitz, Ernst-Leitz-Straße 17-37, D-35578 Wetzlar

Malvern Instruments GmbH, Rigipsstr. 19, D-71083 Herrenberg

Meggle GmbH, Megglestr. 6-12, D-83512 Wasserburg

Merck KGaA, Frankfurter Str. 250, D-64293 Darmstadt

Messer Griesheim GmbH, Füttingsweg 34, D-47805 Krefeld

Mettler Toledo GmbH, Ockerweg 3, D-35396 Gießen

Micromeritics Instrument Corp., GA-Norcross USA

Microsoft Deutschland GmbH, Konrad-Zuse-Str. 1, D-85716 Unterschleißheim

Mitutoyo Messgeraete GmbH, Borisigstr. 8-10, D-41469 Neuss

Orion E.L.I. sprl, 46 avenue des jardins, B-1030 Bruxelles

Pharmatest Apparatebau, Postrfach 11 -50, D-63512 Hainburg

Reiff-Technische Produkte GmbH , Tübinger Str. 2-6, D-72762 Reutlingen

Roquette, Roquette Frères, F-62136 Lestrem

Sartorius AG, Weender Landstr. 94-108, D-37075 Göttingen

Dr. Dietmar Schulze Schüttgutmesstechnik, Am Frost 20, D-38302 Wolfenbüttel

VCH Verlagsgesellschaft, Bochstr. 12, D-69469 Weinheim

Carl-Zeiss GmbH, Carl-Zeiss-Str., D-72447 Oberkochen

My academic teachers were:

Anton, Beretz, Ferard, Gairard, Gerard, Goelner, Hasselman, Haitz, Jung, Kieffer, Kilhoffer, Lami, Landry, Laugel, Lugnier, Pabst, Pesson, Poindron, Schmidt, Spiess, Stahl, Stoclet, Vidon, Wachsman, Wehrlé, Wermuth.

CURRICULUM VITAE

15 Mai 1976	Born in Mulhouse, France
1982-1987	Primary School A. Schweitzer, Blotzheim, France
1987-1991	Secondary School at Collège de Hegenheim, France
1991-1994	Secondary School at Lycée J. Mermoz, Saint Louis, France
June 1994	Baccalauréat C in Mathematics, Physics and Chemistry
Sept. 1994-Sept.2001	Study of Pharmacy at University Louis Pasteur of Strasbourg, France
Aug. 1996-Sept. 1996	Practical Pharmacy Training Course, Blotzheim
Nov. 1999-April 2000	Clinical Training Course at University Hospital of Strasbourg, Intensive Care Service
27 March 2000	Test of English for International Communication (865/995)
Mai 2000-Sept. 2000	Research Training Course at Analysis and Research Center, Dept. of Hydrology, Strasbourg
Oct. 2000-Mar. 2001	Research Training Course at Institute of Pharmacy, Dept. of Pharmaceutical Technology, University of Tübingen, Germany
April 2001-Sept. 2001	Industrial Training Course at Novartis, Dept. of Analytical Research and Development, Basel, Switzerland
14 November 2001	Master of Industrial Pharmacy, Strasbourg
Since January 2002	Research Assistant at Institute of Pharmacy, Dept. of Pharmaceutical Technology, University of Tübingen. Begin of the Ph.D. Thesis under the supervision of Prof. Dr. P. C. Schmidt.
5 October 2002	National Pharmacist´s Diploma of France (Diplome d´Etat de Docteur en Pharmacie)
15 Mai 2003	National Pharmacist´s Diploma of Germany (Approbation als Apotheker)
23 February 2004	Test of German, Goethe Institut (Deutsches Sprachdiplom für Ausländer)